DOKUZ EYLÜL UNIVERSITY
GRADUATE SCHOOL OF NATURAL AND APPLIED SCIENCES

ESTIMATING COMPACTION CHARACTERISTICS OF ENGINEERING FILL MATERIALS BASED ON SOIL INDEX PARAMETERS USING ARTIFICIAL NEURAL NETWORKS

by
Fatih IŞIK

November, 2012
İZMİR

ESTIMATING COMPACTION CHARACTERISTICS OF ENGINEERING FILL MATERIALS BASED ON SOIL INDEX PARAMETERS USING ARTIFICIAL NEURAL NETWORKS

A Thesis Submitted to the
Graduate School of Natural and Applied Sciences of Dokuz Eylül University
In Partial Fulfillment of the Requirements for the Degree of Doctor of Philosophy in Civil Engineering, Geotechnics Program

by
Fatih IŞIK

November, 2012
İZMİR

Ph.D. THESIS EXAMINATION RESULT FORM

We have read the thesis entitled **"ESTIMATING COMPACTION CHARACTERISTICS OF ENGINEERING FILL MATERIALS BASED ON SOIL INDEX PARAMETERS USING ARTIFICIAL NEURAL NETWORKS"** completed by **FATİH IŞIK** under supervision of **ASSOC. PROF. DR. GÜRKAN ÖZDEN** and we certify that in our opinion it is fully adequate, in scope and in quality, as a thesis for the degree of Doctor of Philosophy.

Assoc. Prof. Dr. Gürkan ÖZDEN

Supervisor

Prof. Dr. Arif Şengün KAYALAR

Thesis Committee Member

Assoc. Prof. Dr. Mehmet KUNTALP

Thesis Committee Member

Prof. Dr. Hasan ÇETİN

Examining Committee Member

Assoc. Prof. Dr. M. Ayşen LAV

Examining Committee Member

Prof. Dr. Mustafa SABUNCU
Director
Graduate School of Natural and Applied Sciences

ACKNOWLEDGMENTS

I would like to express my deepest and sincere gratitude to my supervisor, Assoc. Prof. Dr. Gürkan ÖZDEN for his consistent guidance and advices throughout the period of this thesis. His support and directions have contributed to the quality of this thesis.

I would also like to thank Prof. Dr. Arif Ş. KAYALAR and Assoc. Prof. Dr. Mehmet KUNTALP for their valuable contributions to improve my thesis.

I am also grateful to my colleagues; Asst. Prof. Dr. Okan ÖNAL, Lecturer Dr. Mehmet KURUOĞLU, Rsrch. Asst. Gökhan İMAÇLI, Rsrch. Asst. Ender BAŞARI, Rsrch. Asst. Tuğçe ÖZDAMAR and Technician M. Fatih BÜYÜKTOPÇU. My special thanks are also for Asst. Prof. Dr. A. Hakan ÖREN for his undeniable support and encouragement.

A very special acknowledgement to my wife, Funda Zühal IŞIK, for her love and endless support. She has exalted my life with my daughter, Elif. At last, I would like to thank my parents for their supporting and encouragement. Also, I thank to Funda's family for their support.

Fatih IŞIK

ESTIMATING COMPACTION CHARACTERISTICS OF ENGINEERING FILL MATERIALS BASED ON SOIL INDEX PARAMETERS USING ARTIFICIAL NEURAL NETWORKS

ABSTRACT

Maximum dry unit weight and optimum water content are the two compaction characteristics obtained by means of Proctor test in the laboratory. Earth structures often need large quantities of soil and sometimes it may be difficult to obtain the desired amount from a single borrow area resulting in the determination of compaction characteristics of several types of soils. It may be preferable to determine compaction characteristics by means of prediction models instead of performing whole compaction test.

This dissertation presents artificial neural networks prediction models for estimating compaction characteristics of coarse and fine-grained soils. A total number of two hundred soil mixtures are prepared by blending different amount of gravel-sand-clay soil materials. These soil mixtures are compacted under Standard and Modified Proctor energy levels by means of an automatic soil compactor machine. The trained networks are able to accurately estimate compaction characteristics of soil mixtures. It is found that data clustering and division methodologies have a considerable effect on performance of developed networks. Multiple linear regression models are also developed.

The effect of fine content on compaction behavior is observed during the testing program. This behavior is also captured by means of computed tomography imaging technique. It is found that both maximum dry unit weight and optimum water content of the compacted soil mixtures exhibit a transitional behavior nearby a transition fine content. Prior to the transition zone, soils behave like a sand or gravel and beyond this zone fine matrix governs soil behavior. The compaction curve obtained using automatic soil compactor is also compared with that obtained by hand. It is found that the automatic soil compactor has a remarkable effect on compaction characteristics of soils compacted under Modified Proctor energy level. Regarding the Standard Proctor compaction curves, there is a slight difference between compaction characteristics of soils.

Keywords: Soil compaction, artificial neural networks, multiple linear regressions, data transformation, normalization, data division, clustering analysis.

MÜHENDİSLİK DOLGU MALZEMELERİNİN KOMPAKSİYON ÖZELLİKLERİNİN ZEMİN İNDEKS PARAMETRELERİNE BAĞLI OLARAK YAPAY SİNİR AĞLARI İLE TAHMİN EDİLMESİ

ÖZ

Maksimum kuru birim hacim ağırlık ve optimum su içeriği laboratuvarda Proctor deneyi ile elde edilen iki kompaksiyon özelliğidirler. Toprak yapılar genellikle büyük miktarlarda zemine ihtiyaç duyarlar ve bazen gerekli miktardaki zemini tek bir alandan almak zor olabilir ki bu durum birçok zemin numunesinin kompaksiyon özelliklerinin belirlenmesiyle sonuçlanabilir. Tam bir kompaksiyon deneyi yapmaktansa kompaksiyon özelliklerinin tahmin modelleri ile belirlenmesi tercih edilebirlir.

Bu tez iri ve ince-daneli zeminlerin kompaksiyon özellikleri tahmini için geliştirilen yapay sinir ağları tahmin modellerini sunmaktadır. Çakıl-kum-kil zeminlerin farklı oranlarda karıştırarak toplam iki yüz zemin karışımı hazırlanmıştır. Bu zemin karışımları otomatik kompaktör kullanılarak Standart ve Modifiye Proctor sıkılıklarında sıkıştırılmışlardır. Eğitilen ağlar, zemin karışımlarının kompaksiyon özelliklerini tam olarak tahmin edebilmektedirler. Data kümeleme ve ayırma metotlarının eğitilen ağların performansı üzerinde dikkate değer etkisinin olduğu tespit edilmiştir. Ayrıca, çoklu lineer regresyon modelleri geliştirilmiştir.

İnce dane içeriğinin kompaksiyon davranışına etkisi deneysel çalışma ile ortaya konmuştur. Bu davranış ayrıca bilgisayarlı tomografi tekniği kullanılarak ta elde edilmiştir. Sıkıştırılmış zemin karışımlarının maksimum kuru birim hakim ağırlık ve optimum su içeriğinin belirli bir ince dane oranında geçiş davranışı gösterdiği bulunmuştur. Geçiş zonunundan önce, zeminler kum veya çakıl gibi davranırken bu zonun üstünde ise ince zemin daneleri zemin davranışını kontrol etmektedir. Otomatik kompaktör ile elde edilen kompaksiyon eğrisi el ile elde edilenle karışlaştırılmıştır. Otomatik kompaktörün Modifiye Proctor enerjisi altında sıkıştırılan zeminler üzerinde dikkate değer ölçüde etki ettiği bulunmuştur. Standart

Proctor kompaksiyon eğrilerinde ise, belli belirsiz bir farklılığın olduğu tespit edilmiştir.

Anahtar sözcükler: Zemin kompaksiyonu, yapay sinir ağları, çoklu lineer regresyon, data dönüşümü, normalizasyon, data bölümü, kümeleme analizi

CONTENTS

Page

THESIS EXAMINATION RESULT FORM ii
ACKNOWLEDGEMENTS iii
ABSTRACT iv
ÖZ vi
CONTENTS viii

CHAPTER ONE – INTRODUCTION 1

1.1 Overview 1
1.2 Objectives and Scopes 3
1.3 Organization of the Dissertation 3

CHAPTER TWO – SOIL COMPACTION 5

2.1 Introduction 5
2.2 Compaction Theory 6
2.2.1 Water Films and Lubrication 6
2.2.2 Pore Water and Air Pressures 7
2.2.3 Microstructure 8
2.2.4 Effective Stress Theory 10
2.3 Factors Affecting Compaction 11
2.4 Previous Studies on Compaction Correlations 14

CHAPTER THREE – ARTIFICIAL NEURAL NETWORKS 30

3.1 Introduction 30
3.2 Structure of an Artificial Neuron 31
3.3 Artificial Neural Networks Architecture 34

3.4 Learning Algorithms 35
3.5 Pre-processing of Data 38
3.5.1 Data Transformation 39
3.5.1.1 Statistical Normalization 40
3.5.1.2 Min-Max Normalization 41
3.5.1.3 Non-linear Transformation 41
3.5.1.4 Whitening Transformation 41
3.5.2 Data Division 42
3.5.2.1 Random Division 43
3.5.2.2 Fuzzy C-Means Clustering 43
3.6 Previous ANNs Modeling Studies for Soil Compaction 44

CHAPTER FOUR – TESTING MATERIALS AND EXPERIMENTAL PROGRAM 53

4.1 Soil Materials 53
4.1.1 Sieve and Hydrometer Analysis 53
4.1.2 Specific Gravity Test 54
4.1.3 Consistency Limits Tests 54
4.2 Soil Mixtures 55
4.2.1 Grain Size Distributions of Soil Mixtures 57
4.2.2 Consistency Limits of Soil Mixtures 58
4.2.3 Compaction Tests Results of Soil Mixtures 63
4.3 Discussion of Compaction Test Results 69
4.3.1 Effect of Fine Content on Compaction Behavior 69
4.3.2 Effect of Compaction Energy 83
4.3.3 Effect of Automatic Soil Compactor 85

CHAPTER FIVE – MODELLING OF COMPACTION CHARACTERISTICS 87

5.1 Comparison of Literature Equations using Author’s Experimental Results ... 87

5.2 Multiple Linear Regression Analysis 93
5.2.1 MLR Models for Standard Proctor Compaction 94
5.2.2 MLR Models for Modified Proctor Compaction.................................... 97
5.3 Artificial Neural Networks Analysis 101
5.3.1 Standard Proctor Compaction ANN Models 111
5.3.2 Modified Proctor Compaction ANN Models 116
5.3.3 Proctor Energy ANN Models 120

CHAPTER SIX – GENERALIZATION ABILITY OF THE DEVELOPED MODELS 126

6.1 Overview 126
6.1.1 Check of Suitability of Different Data Bases Using Self-Organizing Map 126
6.2 Generalization Ability of the Developed MLR Compaction Models 130
6.3 Generalization Ability of the Developed ANN Compaction Models 132
6.4 Discussion of Effect of Automatic Soil Compactor..................................... 135

CHAPTER SEVEN – CONCLUSIONS AND RECOMMENDATOINS......... 141

7.1 Conclusions 141
7.1.1 Compaction Characteristics.. 141
7.1.2 Multiple Linear Regression Analysis 142
7.1.3 Artificial Neural Networks Analysis 143
7.2 Recommendations 145

REFERENCES.. 146

CHAPTER ONE
INTRODUCTION

1.1 Overview

Majority of man made structures are constructed on soil, supported by soil or made of soil. This means that soils are used as construction material in most civil engineering applications. In this respect, it becomes necessary to determine the characteristics of soil and its engineering properties, in order to assess the suitability of site soil for the intended purpose at hand.

In geotechnical engineering practice, the soil at a given site may not exhibit the desired properties for the intended purpose. In this case, changing location of the project site may be considered as a solution. In general, relocation of the structure is not a good solution due to economical limitations. Therefore, two kinds of solutions are developed by geotechnical engineers. The first one is the redesigning of the superstructure foundation. The second one is based on modification of the soils.

According to the alternatives at hand, soil modification may be the most appropriate solution. Soil modification is carried out by stabilization; either chemical or mechanical. Chemical stabilization includes the mixing or injection of chemical stabilization agents such as cement, lime, asphalt, calcium chloride and sodium chloride into the soil. Mechanical stabilization, also called compaction, involves densification of soil by applying mechanical energy. Compaction is also defined as the rearrangement of solids and reduction of air voids by application of mechanical energy to an unsaturated soil. During compaction process, soil particles are packed closer and air is expelled from voids while the volume of solids and the water content remains constant.

The maximum dry unit weight (γ_{dmax}) and the optimum water content (ω_{opt}) are the two compaction characteristics which are obtained by performing a whole Proctor compaction test procedure in soil mechanics laboratory. Considering that the necessity of large quantities of soils from different borrow pits to be tested for their usage in an embankment dam construction or frequently changing soils to be tested along a highway alignment, determination of compaction characteristics from laboratory Proctor test requires considerable time and effort. Sometimes, it is preferable to estimate the compaction characteristics using soil index properties due to aforementioned reasons.

Several researchers tried to correlate soil index properties with γ_{dmax} and ω_{opt} (Korfiatis and Manikopoulos, 1982; Wang and Huang, 1984; Hausmann, 1990; Pandian et al., 1997; Blotz et al., 1998; Gurtug and Sridharan, 2002; Omar et al., 2003; Gurtug and Sridharan, 2004; Sridharan and Nagaraj, 2005; Nagaraj et al., 2006; Olmez, 2007; Hortibulsuk et al., 2008; Sivrikaya et al., 2008; Sivrikaya 2008). Majority of these studies utilized common soil index properties (i.e liquid limit, plastic limit, plasticity index, mean grain size, effective grain size, and specific gravity) and targeted a rather homogeneous data set (i.e. data either from cohesive or cohesionless soils). Therefore, generalization of such models to cover c-ϕ soils is limited. Non-linear relationship between soil index properties and compaction characteristics needs the usage of a nonlinear modeling technique. Najjar et al. (1996), Basheer (2001), Abdel-Rahman (2008), Sinha and Wang (2008), Günaydın (2009), and Sivrikaya & Soycan (2010) used to capture the nonlinear relationship via artificial neural networks.

In this respect, this thesis presents results of a doctoral study concerning the development of prediction models for estimating compaction characteristics of both coarse and fine-grained soils under Standard and Modified Proctor energy levels. The linear relationship between compaction characteristics and index properties are obtained by means of multiple linear regression (MLR) method, where as the non-linear relationships are investigated using artificial neural networks (ANNs) methodology.

1.2 Objectives and Scopes

The primary objective of this study is to develop prediction models to determine the compaction characteristics of coarse and fine-grained soils without performing a laboratory Proctor test. In addition to the primary objective, the effect of fine content, compaction energy and automatic soil compactor on compaction characteristics are also investigated in this study. The scopes of the dissertation are as follows:

Laboratory tests were conducted on two hundred soil mixtures obtained by blending different amount of gravel-sand-clay soil materials. The grain size distributions of the soil mixtures were determined using weighted averages of the main soil components. Consistency indices of the forty-five soil mixtures were conducted and the remaining soil mixtures' consistency indices were determined by means of regression analyses.

Both standard and modified Proctor compaction tests were performed on all of the soil mixtures. From these tests results; optimum water content (ω_{opt}) and maximum dry unit weight (γ_{dmax}) of the soil mixture were obtained under standard and modified energy levels. The compaction test results were used to build the database of this study.

The effect of fine content on compaction characteristics was also captured visually using computed tomography (CT) images. The soil mixtures exhibited transitional behavior were compacted and then scanned by means of CT imaging technique.

1.3 Organization of the Dissertation

Chapter One of this dissertation contains an introduction of the soil compaction. The objective and scope of this study and the organization of the dissertation are also presented in this chapter.

Chapter Two gives detailed information about the soil compaction. The theory of compaction and the factors affecting compaction are briefly described. The literature review of soil compaction modeling is also presented in the second chapter.

Chapter Three provides a rather detailed description of artificial neural networks (ANNs). This chapter focuses on the general architecture of ANNs, learning algorithms and data pre-processing. A literature review of the previous applications of ANNs in geotechnical engineering area is given. Details of soil compaction modeling by means of ANNs are also provided.

Chapter Four presents characteristics of the materials and methods used in this study are explained. Laboratory studies are summarized in this chapter. The effects of fine content, compaction energy and automatic soil compactor on compaction behavior are also discussed in this chapter.

Chapter Five presents modeling studies. First of all, the requirements of new prediction models are briefly discussed. Subsequently, the prediction models developed by means of both multiple linear regressions (MLR) and artificial neural networks (ANNs) are presented.

Chapter Six evaluates the robustness of the developed prediction models. The effects of automatic soil compactor on the data and performance of the developed models against different data bases are discussed in detail. Chapter Seven includes the conclusion of this study and suggestions for future studies.

CHAPTER TWO
SOIL COMPACTION

2.1 Introduction

The principles of compaction were mostly set by Proctor (1933). In his honor, the laboratory compaction test is named as the Proctor test (Holtz and Kovacs, 1981). There are three types of laboratory compaction tests. One of them is kneading compaction test. In this test, a tamper is used to push the soil into a mold at a specified number of times and specified stress. In the static compaction test, the soil is subjected to a predetermined static stress. The last one and the most commonly used is the dynamic or the impact compaction test. This test is performed by means of a special hammer dropped from a constant height. The soil is placed layer by layer into a mold and compacted using a special hammer.

During a laboratory Proctor compaction test, several samples of the same soil are compacted at different water contents. Typically, wet unit weight and corresponding water content of each compacted sample are measured. Then the dry unit weight for each sample is calculated as following;

$$g_{dry} = \frac{g_{wet}}{1+w} \tag{2.1}$$

Dry unit weight versus water content curve, also called as the compaction curve, is plotted such as in Figure 2.1. A typical compaction curve represents different densification stages of the soil in different water contents at a constant compactive effort. It is clear from the compaction curve that as the molding water content increases, the dry unit weight of the soil increases to a peak value and then decreases. This peak point defines the compaction characteristics: maximum dry unit weight (γ_{dmax}) and the optimum water content (ω_{opt}). Soils condition can be defined according to their position on the compaction curve; dry of optimum, near or at optimum and wet of optimum (Figure 2.1).

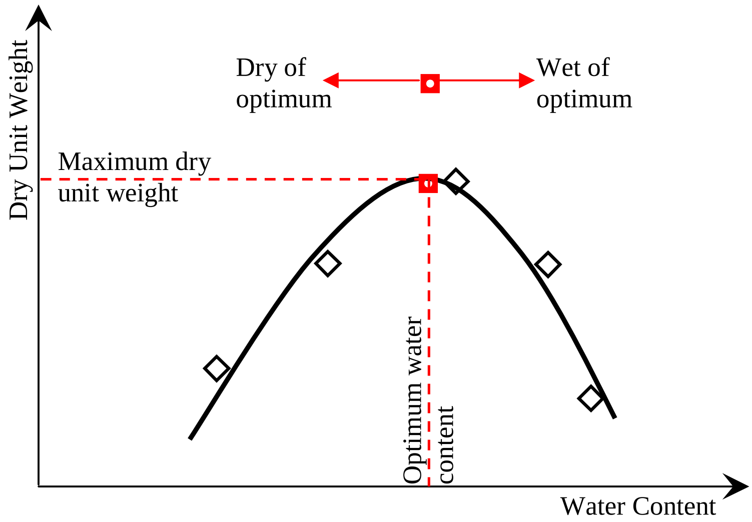

Figure 2.1 Compaction curve

2.2 Compaction Theory

In the literature, researchers have tried to explain the typical water content – dry unit weight relationship since the pioneering work of Proctor (1933). The compaction theories can be classified into four categories: (1) lubrication, (2) pore water and air pressure, (3) soil microstructure and (4) effective stress concept.

2.2.1 Water Films and Lubrication

Proctor (1933) mentioned that at a very dry side of the compaction curve, the soil particles are surrounded with a thin film held in place by surface tension forces. Where the films come in contact, the capillary force emerges by effect of surface tension. This capillary force draws the soil particles together, and causes high frictional resistance between them making compaction difficult. The capillary force decreases by adding water to the soil. Proctor (1933) thought that the addition of water lubricates the soil particles. Lubrication effect reduces the interparticle friction resistance and therefore there is a decrease in shear strength. The reduction in shear strength causes an increase in the dry unit weight because of sliding of the soil particles over each other. The soil particles rearrange their position easily and get closer together by means of lubrication. Lubrication effect continues until the specific water content (i.e. optimum water content). Beyond this point, adding more water causes soil softening and reduces the dry unit weight.

Hogentogler (1936) explained the compaction curve with lubrication concept. He represents the water content – dry unit weight relationship by four stages of wetting: (1) hydration, (2) lubrication, (3) swelling and (4) saturation (Figure 2.2). In the hydration stage, thin water films occur at the soil particle surfaces. In the lubrication stage, the remaining water except the absorbed by the soil particles is acting as a lubricant. This causes rearrangement of soil particles without displacing all the air from voids. Beyond the optimum water content, the addition of water causes the soil to swell with the amount of air remaining constant (swelling stage). Theoretically adding more water causes expulsion of all air voids and the soil becomes saturated. However, soil cannot practically become fully saturated in a compaction test.

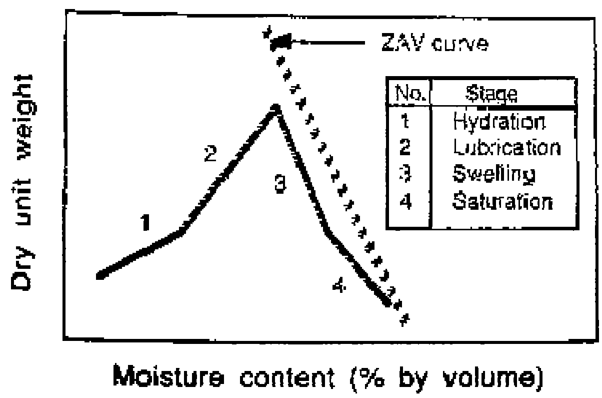

Figure 2.2 Wetting stages according to Hogentogler (1936) (after Hausman ,1990)

2.2.2 Pore Water and Air Pressures

Hausmann (1990) reviewed that the early work of Hilf (1956) employed the pore water and pore air pressures concept to relate the water content to the dry unit weight. He represented this relationship in terms of void ratio versus water void ratio (i.e. the ratio of volume of water to volume of solids), as depicted in Figure 2.3. In this figure the compaction curve is sketched by a new curve where the optimum water content corresponds to a minimum void ratio. The saturation line is used as zero air void ratio (ZAV) (i.e. the ratio of volume of air to volume of solids) line. The soil samples that have equal air void ratios plot on lines parallel to the 100% saturation or ZAV line. Hilf (1956) stated that at the dry side it is difficult to compact the soils because of high friction that is forced by capillary pressures. Also, air can be expelled quickly due to presence of large air voids at this side. Addition of water decreases the capillary tension and reduces friction resulting in better densification until a minimum void ratio is reached. Beyond this point, less effective compaction is attributed to the trapping of air and the building up of pore air pressures.

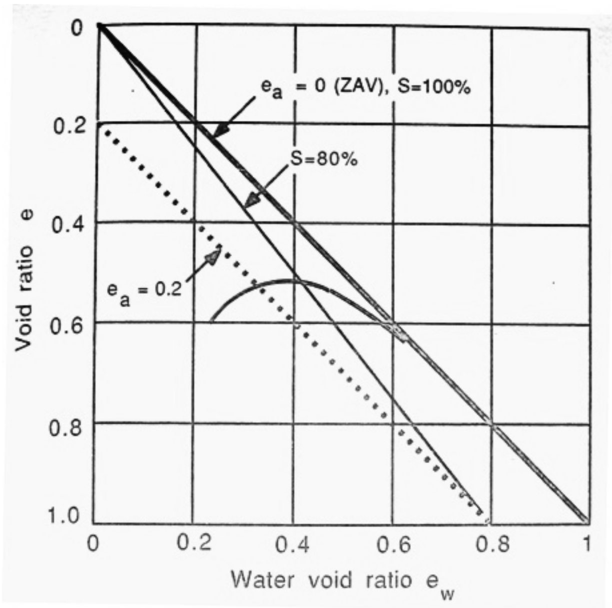

Figure 2.3 Compaction curve relationship as proposed by Hilf (1956) (after Hausmann, 1990)

2.2.3 Microstructure

Lambe (1958) conducted a study to investigate structural composition and arrangement of particles in compacted clayey soils. According to his physicochemical interpretation, the clayey soils tend to be more flocculated on the dry side as compared to the wet side at a constant compactive effort. In this case, the attractive forces between clay particles control soil behavior; positively charged particle edges are in contact with negatively charged faces, which are causing low density. The addition of water content increases the inter-particle repulsion resulting in parallel orientation of soil particles. If the addition of water continues, more parallel structures named as the dispersed structure takes place (Figure 2.4). At constant water content, increasing compactive effort tends to disperse soil particles, especially on the wet of optimum.

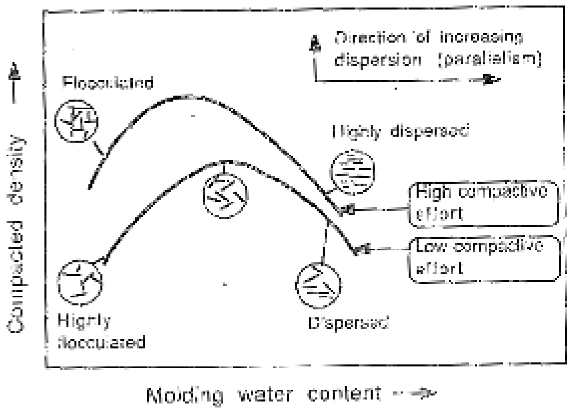

Figure 2.4 Effect of compaction on soil structure according to Lambe (1958) (after Hausmann, 1990)

Recent study of Çetin et al. (2007) aimed to understand soil structure change during compaction. In order to measure elongation of soil particles, they prepared soil specimens by mixing a natural clay with platy muscovite mica sand. By compacting this soil mixture at eight different water contents, they obtained standard Proctor compaction curves. The researchers examined the orientation of soil particles by means of thin sections trimmed from each compacted specimen. They found that at the dry side of optimum the orientation of soil particles is nearly random. The randomly oriented voids are large. They mentioned that the average angles to the horizontal decrease and the percentages of the orientation measurements between 0° and 10° increase until the optimum water content. Figure 2.5 presents the average angles and the percentages of the orientation measurements. It is evident that, an increase in water content causes a decrease in the average angles to the horizontal up to optimum water content, and then starts to increase steadily (Figure 2.5.a). From Figure 2.5.b, it can be seen that the orientation measurements between 0° and 10° increase up to 14% water content and starts to increase beyond the optimum water content. By addition of water, edge to edge contacts between the soil particles first become mainly edge to face and face to face contacts near the optimum water content. In opposite with Lambe (1958), they mentioned that beyond the optimum water content the average angles to the horizontal start to increase and orientations start to decrease again (Figure 2.5). At the wet side of optimum, the compaction hammer starts to penetrate greater than the dry side. This causes large shear strains and produces more oriented soil particles.

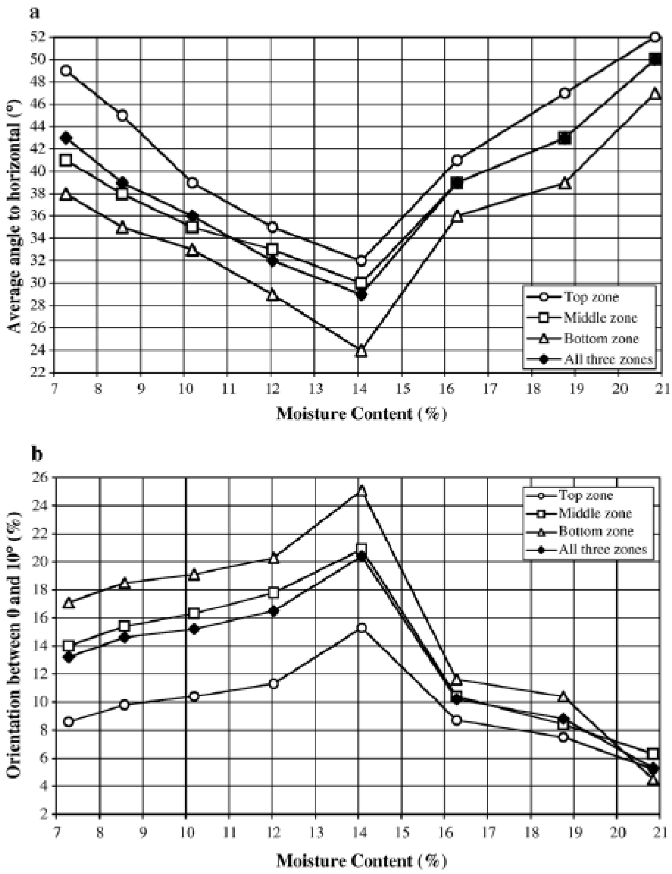

Figure 2.5 Changes of average angles and orientations at different water contents (after Çetin et al., 2007)

2.2.4 Effective Stress Theory

Olson (1963) tried to explain water content – dry unit weight relationship with effective stress concept. At first, one should take notice that the effective stress theory pertains only to fine grained soils. It is also noteworthy that this compaction theory was developed using kneading compaction procedure. Olson (1963) mentioned that this theory applies directly to kneading compaction, but with minor modifications, it could be applied to other compaction procedures as well.

Before application of compaction, the soil is in a loose state and has low shearing strength. When the compaction pressure is applied, the shearing stresses developed among the soils particles. The soil particles resist to the compaction pressure by means of the shearing strength developed at the contact surfaces of the soil particles. If the contact yields, the soil particles slide over each other which cause an increase in soil density. During the compaction pressure application, both the total stresses and the pore pressures increase. However, the increment of the pore pressures is less than the total stresses due to low value of B-coefficient. Hence, the effective stresses among the particles increase as the compaction pressure is being applied. Yielding of the contacts continues until the soil particles reach sufficient shearing strength. The hammer is pulled out releasing the compaction pressure thus completing one full "blow" cycle.

Olson (1963) mentioned that the relative deformation of the soil particles continues until increasing effective stresses provide the soil with sufficient shearing strength to resist the compaction pressure. By applying repeated "blows", the shearing strength of the soil increases, at this point there is no further deformation occurrence. In this case, it is accepted that the soil reach its maximum dry density. Olson (1963) mentioned that the effective stress theory of compaction will demonstrate why an increase in water content causes an increase in dry density at the dry of optimum. At the wet side of optimum, however, the effective stress theory remains inapplicable. In his own words, he said "It is apparent that additional, and perhaps different, variables must be taken into account" for the wet side of optimum.

2.3 Factors Affecting Compaction

It is well known that molding water content, compaction energy and soil type are the main factors affecting compaction behavior of soils. The soil type has a great influence on compaction behavior of soils. In Figure 2.6, some typical compaction curves for different types of soils are shown.

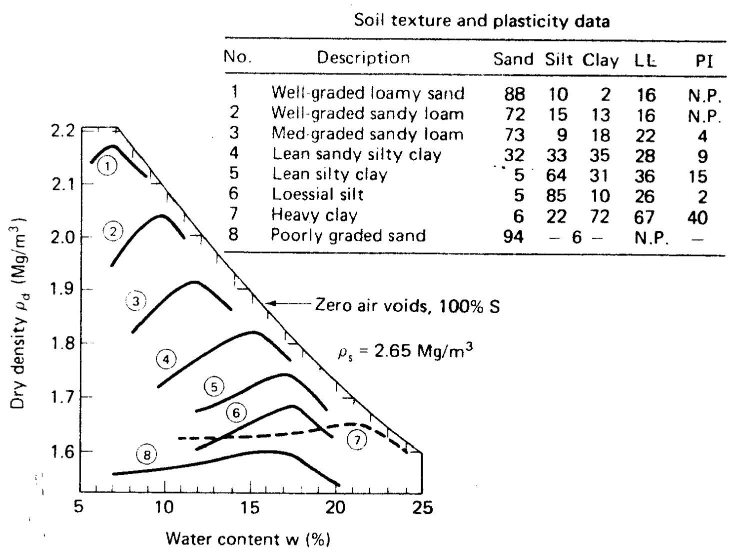

Figure 2.6 Compaction curves of eight different soils (after Holtz and Kovacs, 1981)

It is clear from Figure 2.6 that well graded sandy or gravelly soils have a higher maximum dry unit weight when compared with poorly graded sandy or clayey soils. For clayey soils, maximum dry unit weight decreases with increasing plasticity. Also, it is inferred from Figure 2.6 that fine-grained soils need more water to reach to the optimum point whereas coarse-grained soils need less water.

Another affecting factor is the molding water content. This effect can be explained by means of Figure 2.7. On the dry side of optimum, soil particles are covered with larger and larger water films by adding more and more water into soil. The aforementioned lubrication mechanism makes soil particles easier to be arranged and step by step gets them to a denser condition until the optimum water content. Beyond the optimum point, there is no further increase in dry unit weight because of replacement of water with soil particles in the mold. The addition of water causes a decrease in the compaction curve as depicted in Figure 2.7.

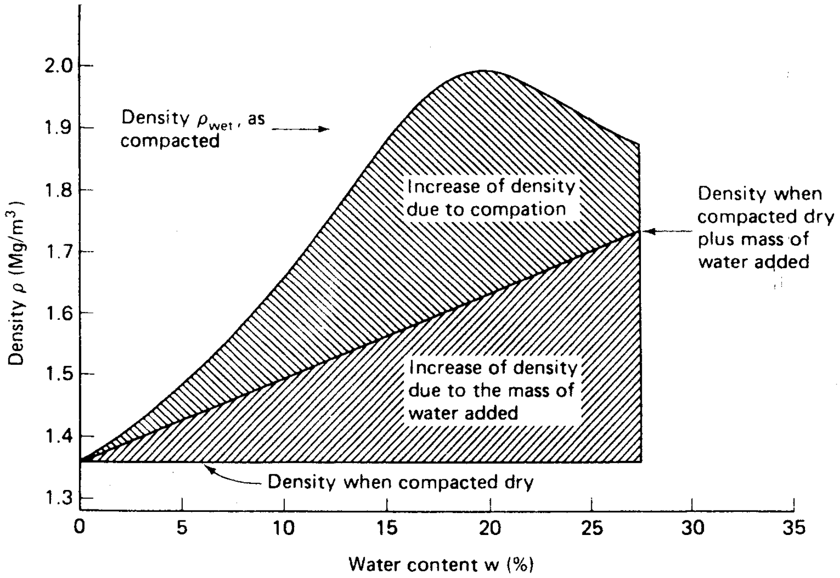

Figure 2.7 Water content – dry unit weight relationship (after Holtz and Kovacs, 1981)

One of the most important factors is the compaction energy, also known as the compactive effort. The compaction energy is a function of the mechanical energy applied to soil mass. The compaction energy per unit volume (E) is given in Equation 2.1.

$$Compaction\ Energy = \frac{\begin{pmatrix} Mass\ of \\ Hammer \end{pmatrix}\begin{pmatrix} Gravitational \\ Acceleration \end{pmatrix}\begin{pmatrix} Height\ of \\ Drop \end{pmatrix}\begin{pmatrix} Number \\ of\ Layers \end{pmatrix}\begin{pmatrix} Number\ of \\ Blows\ per\ Layer \end{pmatrix}}{Volume\ of\ Mold} \quad (2.1)$$

There are generally two types of compaction tests; Standard Proctor and Modified Proctor. In the Standard Proctor test, a 2.495 kg hammer falling from 0.305 m is used. The soil is placed in 3 layers in a 944 cm^3 mold and 25 blows are applied per layer. The compaction energy of the Standard Proctor test is calculated using Equation 2.1:

$$Standard\ Comp.\ Energy = \frac{(2.495\,kg)\left(9.81\,m/s^2\right)(0.3048\,m)(3)(25)}{0.944\times10^{-3}\,m^3} = 592.7\ kJ/m^3$$

The Modified Proctor test was developed due to requirements of airfields serving to heavy airplanes in World War II. There are two major differences between Standard and Modified Proctor test: (1) 4.536 kg hammer dropped from 0.457 m height and (2) soil is tamped in 5 layers. By using Equation 2.1, the Modified Proctor energy is determined as 2693.0 kJ/m^3. Compaction curves of Standard and Modified Proctor tests are illustrated in Figure 2.8. It has been long known that with an increase in the compaction energy causes an increase in maximum unit weight and a decrease in optimum water content. It is clear from Figure 2.8 that the modified compaction curve shifts upward and left side of the standard compaction curve.

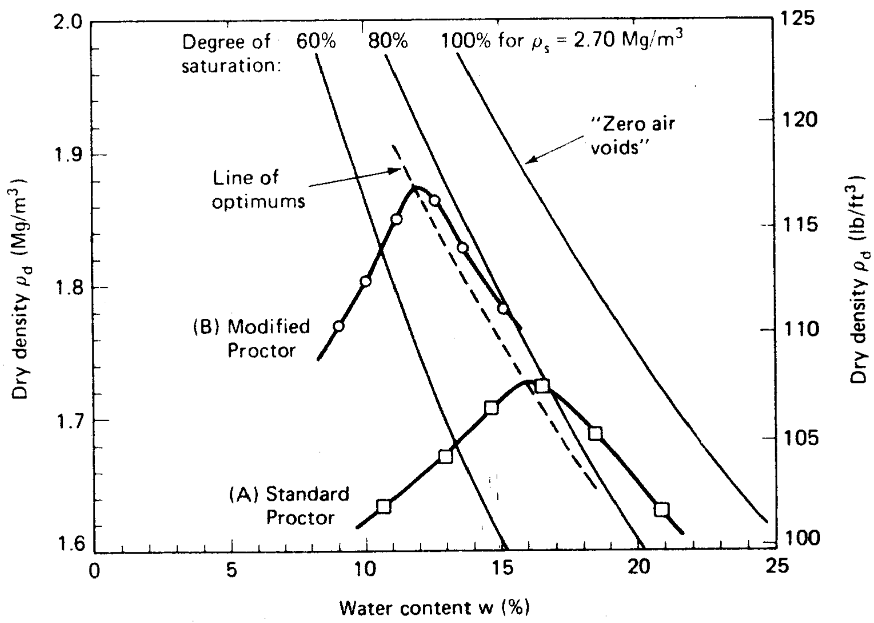

Figure 2.8 Standard and Modified Proctor curves (after Holtz and Kovacs, 1981)

2.4 Previous Studies on Compaction Correlations

Attempts have been made by many researches to determine the compaction characteristics of soils. On the other hand, several researchers have tried to correlate the soil compaction characteristics to basic soil index parameters.

The first category of researchers focused on obtaining the soil compaction characteristics of both cohesive and cohesionless soils.

Garga and Madureira (1985) performed field and laboratory tests to investigate compaction characteristics of a river terrace gravel soil. They investigated the effects of gravel content on compaction characteristics of gravelly soils. They prepared the soil samples at 0%, 30%, 40%, 50%, 60% and 70% gravel content. They mentioned that the percentage of gravel fraction is probably the most important factor influencing γ_{dmax} of gravelly soils. As expected, γ_{dmax} increases while gravel content increases and an increase of gravel content causes a decrease in ω_{opt}. The influence of compaction effort was also examined by the authors. Therefore, they compacted the soil samples at three different energy levels: Standard (592.7 kJ/m^3), Intermediate (1196.7 kJ/m^3), and Modified Proctor (2693.0 kJ/m^3). It was observed that with an increase in the compactive effort γ_{dmax} increased accompanied by a decrease in ω_{opt}. The effect of equipment size was investigated by authors and they concluded that mould diameter equal to six to eight times the maximum gravel size is acceptable. They also examined the effect of absorbed water content on γ_{dmax}. The results indicated that the variation in absorbed water content of the gravel fraction does not influence the γ_{dmax} values.

Omotosho (1993) investigated the influence of multi-cyclic compaction on γ_{dmax} and ω_{opt} of some deltaic lateritic soils. They conducted two distinct Proctor tests. One of them is “Standard Proctor” compaction test. In this method, a single batch of soil sample is used for obtaining a whole compaction curve. The other one is “Break-up Proctor” compaction test. This method covers usage of a fresh batch of soil each time. From this study, they observed that the Standard Proctor test underestimates γ_{dmax} values. For ω_{opt} values, there was no clear relationship (Table 2.1).

Table 2.1 Compaction test results (after Omotosho, 1993).

Sample	Depth (m)	Standard Proctor		Break-up Proctor		DMDD*	DOWC**
		MDD (kg/m^3)	OMC (%)	MDD (kg/m^3)	OMC (%)	(kg/m^3)	(%)
A	2.0	1710	16.0	1754	16.8	44	0.8
B	2.0	1700	16.6	1795	17.3	95	0.7
C	2.75	1660	19.7	1700	20.6	40	0.9
D	3.5	1645	19.5	1670	19.75	25	0.25
E	5.5	1765	18.0	1789	17.6	24	-0.4
F	5.5	1864	17.2	1890	16.5	26	-0.7
G	7.5	1810	16.0	1816	14.75	6	-1.25

*$\Delta MDD = MDD_{breakup} - MDD_{standard}$
**$\Delta OWC = OWC_{breakup} - OWC_{standard}$

The effects of clayey soil type, curing period, and mixing procedure on laboratory compaction were all examined by Howell et al. (1997). They used three different sand-clay mixtures: sand-attapulgite clay (S-AC), sand-granular bentonite (S-GB), and sand-powdered bentonite (S-PB). They conducted compaction tests at 10, 15, and 20% clay contents. After a series of compaction tests, they found that the S-AC mixture obeyed to expected trends of increasing ω_{opt} and decreasing γ_{dmax} with increasing clay contents, as depicted in Figure 2.9. However, an increase in clay content causes a decrease in ω_{opt} for both S-GB and S-PB mixtures. On the other hand, the γ_{dmax} of the S-PB mixture increases with the increase in clay content whereas the γ_{dmax} of the S-GB mixture remains relatively constant while clay content increases (Figure 2.9).

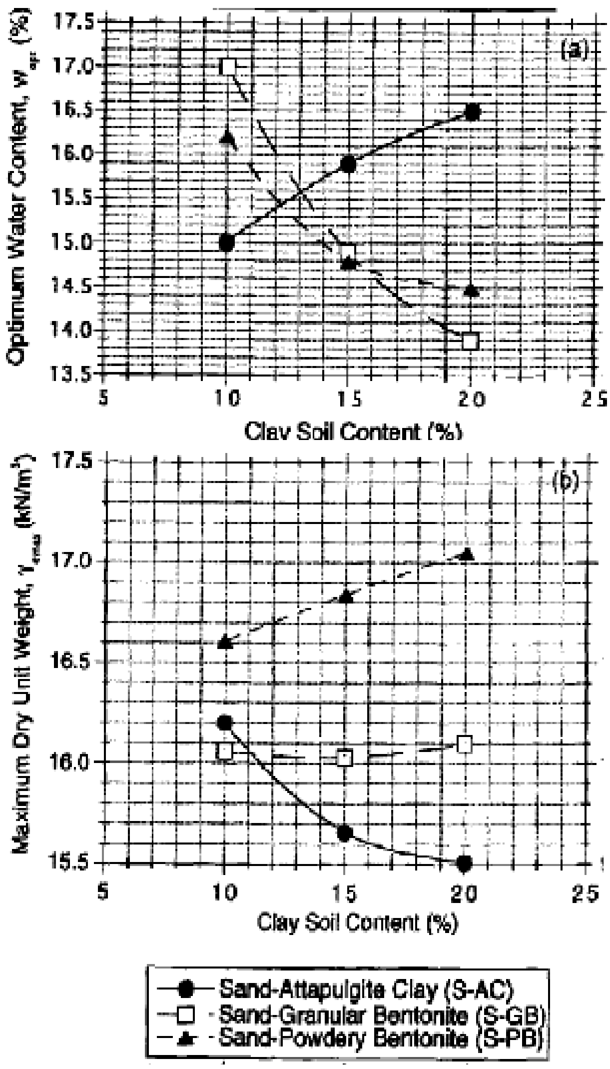

Figure 2.9 Influence of clay soil content on (a) ω_{opt} and (b) γ_{dmax} for a one-day curing period and Mixing Procedure 1 (after Howell et al., 1997)

In order to determine the curing period effect, the S-GB and the S-PB mixtures and Mixing Procedure 1 were used by the authors. They cured the mixtures for one day and for seven days. They found that, in general, the two different curing periods had a small effect on the ω_{opt} and γ_{dmax} for the S-GB and the S-PB mixtures at the same clay contents and for the same mixing procedure (Figure 2.10).

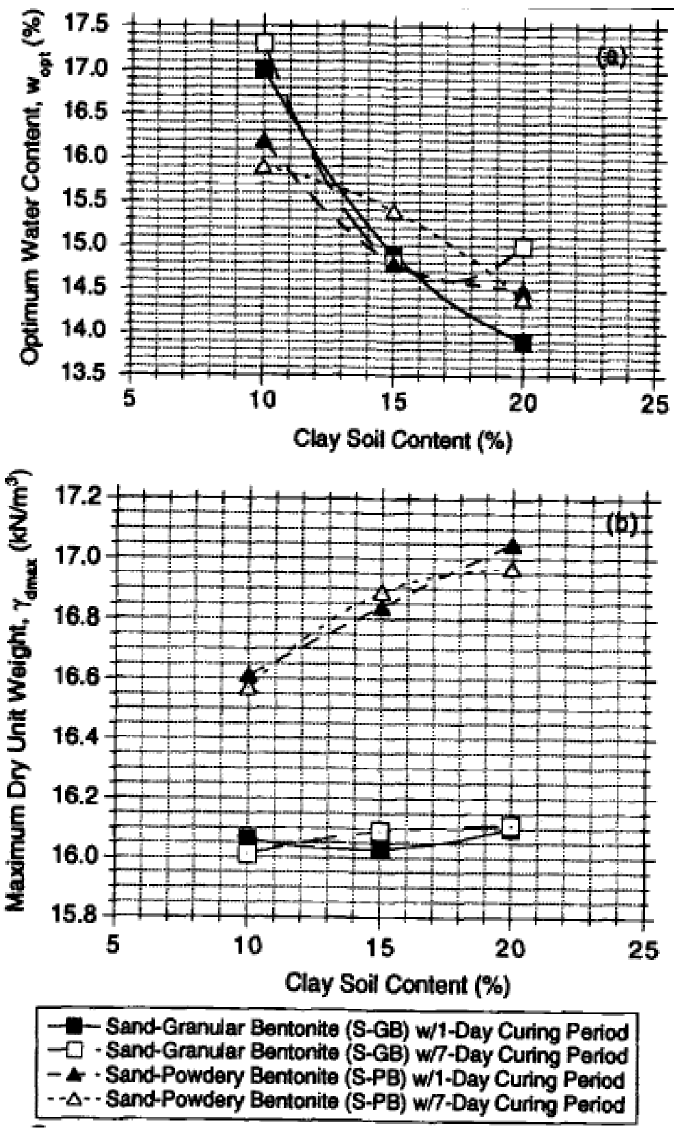

Figure 2.10 Influence of bentonite content on (a) ω_{opt} and (b) γ_{dmax} for Mixing Procedure 1 and two curing periods (after Howell et al., 1997)

Howell et al. (1997) used two mixing procedures to evaluate the effect of mixing on compaction. Mixing Procedure 1 consisted of mixing the sand with water before adding the clay in stages and thoroughly mixing by hand using spoon after each addition of clay soil. Mixing Procedure 2 involved mixing the dry sand and clay soil before adding appropriate amount of water with a spray bottle and mixing frequently by hand using a spoon. For this research, again the S-GB and the S-PB mixtures were used and seven-days curing period was performed. As a result, mixing the sand and bentonite in a dry condition before adding water consistently resulted in greater ω_{opt}

and γ_{dmax} than mixing the sand with appropriate amount of water before adding the bentonite (Figure 2.11).

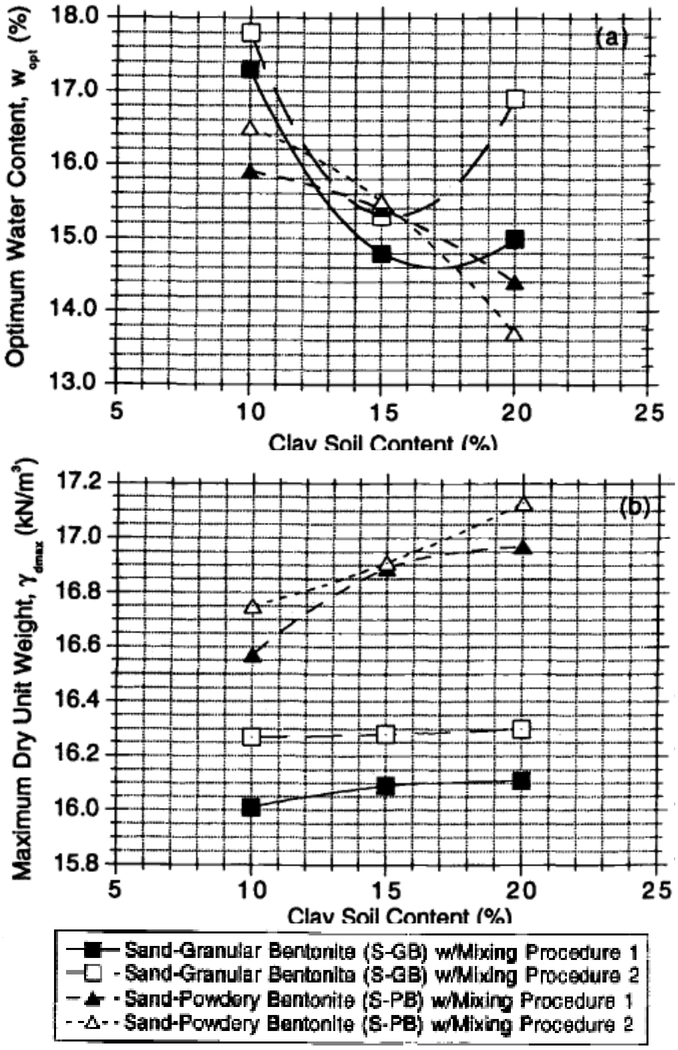

Figure 2.11 Influence of bentonite content on (a) ω_{opt} and (b) γ_{dmax} for a seven day curing period and two mixing procedures (after Howell et al., 1997)

The second category of researchers tried to model the soil compaction characteristics with basic soil parameters. In this manner, two different modeling techniques were used; the first kind of compaction modeling aimed to estimate the compaction characteristics (i.e. ω_{opt} and γ_{dmax}). On the other hand, some of the researchers tried to model the whole compaction curve. Many attempts were made to correlate compaction characteristics with soil index properties. There are numerous correlation equations for both cohesive and cohesionless soils.

Wang and Huang (1984) correlated specific gravity, fineness modulus, plastic limit, uniformity coefficient, bentonite content, and particle diameters corresponding to 10% and 50% passing with compaction characteristics of mixed soils.

Al-Khafaji (1987) investigated the role of the liquid limit and clay content on standard Proctor test parameters of the fine-grained soils of Iraq. He developed three types of correlation equations: The first one includes only liquid limit, the second one includes only clay content and the last one includes liquid limit and clay content as given below;

$$\omega_{opt} = 8.7 + 0.26 \cdot \omega_L \tag{2.2}$$

$$\omega_{opt} = 11.07 + 0.26 \cdot C \tag{2.3}$$

$$\omega_{opt} = 0.5 + 0.26 \cdot (\omega_L + C) \tag{2.4}$$

where ω_{opt}, ω_L and C are in percentages.

$$\gamma_{dmax} = 2.05 - 0.84 \cdot \omega_L \tag{2.5}$$

$$\gamma_{dmax} = 1.966 - 0.814 \cdot C \tag{2.6}$$

$$\gamma_{dmax} = 2.31 - 0.84 \cdot \omega_L - 0.81 \cdot C \tag{2.7}$$

where ω_L and C are expressed as decimal, and γ_{dmax} in t/m^3.

Korfiatis and Manikopoulos (1982) used percent fines and slope of the grain size distribution curve in order to predict Modified Proctor γ_{dmax} for granular soils.

Blotz et al. (1998) developed prediction equations to estimate ω_{opt} and γ_{dmax} using liquid limit (ω_L) and compaction energy. A linear relationship between γ_{dmax} and the base 10 logarithm of compaction energy (log E) was described by Blotz et al. (1998). The same relation is valid for ω_{opt} - log E as well. They used Proctor compaction data from 22 clayey soils, which were compacted at three different compacting efforts including reduced Proctor, standard Proctor, and modified Proctor to develop the relationships:

$$\gamma_{dmax.E} = (2.27 \log \omega_L - 0.94) \log E - 0.16\, \omega_L + 17.02 \tag{2.8}$$

$$\omega_{opt.E} = (12.39 - 12.21 \log \omega_L) \log E + 0.67\, \omega_L + 9.21 \tag{2.9}$$

where, E : compactive effort, and expressed in kJ / m^3. $\omega_{opt.}$ and ω_L are expressed in percentage and γ_{dmax} is in kN/m^3 unit. This method should currently be limited to be used with clayey soils where ω_L varies between 17 and 70.

Another predictive model was developed by Gurtug and Sridharan (2002) who used four different clayey soils and performed Standard Proctor test only. Apart from their own results, the authors have also used results published in the literature. They correlated ω_{opt} with plastic limit (ω_P) and γ_{dmax} with dry unit weight at plastic limit, $\gamma_{dry,\omega p}$, (Figure 2.12).

$$w_{opt} = 0.92 \cdot w_P \tag{2.10}$$

$$g_{d\max} = 0.98 \cdot g_{dw_P} \tag{2.11}$$

The dry unit weight at plastic limit was given by:

$$g_{dry,wp} = \frac{G_s g_w}{1 + w_p G_s} \tag{2.12}$$

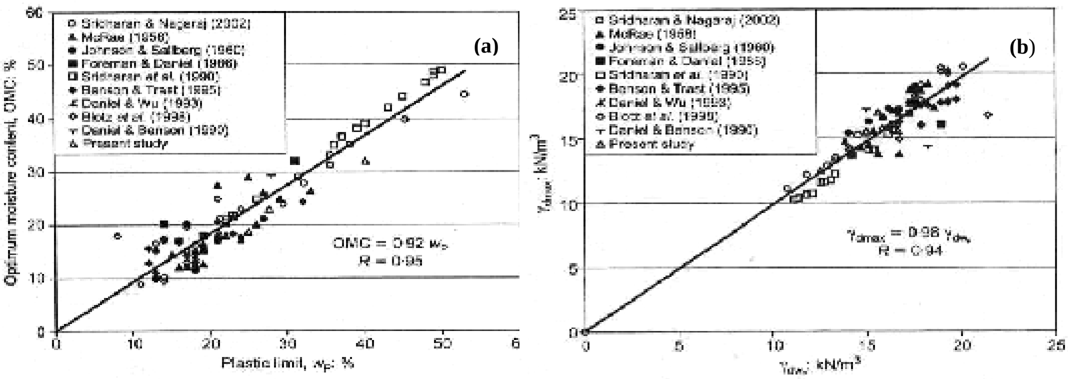

Figure 2.12 Relationship (a) between ω_{opt} and ωp, and (b) between γ_{dmax} and $\gamma_{dry,\omega p}$ (Gurtug and Sridharan, 2002).

Engin (2003) tried to correlate both Standard and Modified Proctor compaction characteristics with soil index parameters. He developed correlation equations using different combinations of plasticity index (I_P), specific gravity (G_s), percent passing No.4 sieve (-No.4), percent retained on No.200 sieve (+No.200) and loose dry unit weight ($\gamma_{dry,loose}$) as independent variables. However, correlation equations which include -No.4 and +No.200 parameters were found to be as the most consistent;

for Standard Proctor

$$\omega_{opt} = 0.2108 + 0.0227\cdot(\text{-No.4}) - 0.1470\cdot(\text{+No.200}) \tag{2.13}$$

$$\gamma_{dmax} = 1.6148 - 0.1329\cdot(\text{-No.4}) + 0.5576\cdot(\text{+No.200}) \tag{2.14}$$

for modified Proctor

$$\omega_{opt} = 0.1589 + 0.0212\cdot(\text{-No.4}) - 0.1118\cdot(\text{+No.200}) \tag{2.15}$$

$$\gamma_{dmax} = 1.9300 - 0.1940\cdot(\text{-No.4}) + 0.4166\cdot(\text{+No.200}) \tag{2.16}$$

where ω_{opt}, -No.4,+No.200 are expressed in percentages and γ_{dmax} is in t/m^3. He also correlated modified ω_{opt} and γ_{dmax} with standard ω_{opt} and γ_{dmax} as below,

$$\omega_{opt,modified} = 0.7735\cdot\omega_{opt,standard} + 0.0008 \tag{2.17}$$

$$\gamma_{dmax,modified} = 0.8377\cdot\gamma_{dmax,standard} + 0.4568 \tag{2.18}$$

Gurtug and Sridharan (2004) generalized their previous study (Gurtug and Sridharan, 2002) considering compaction energy. They performed Reduced Proctor (RP), Standard Proctor (SP), Reduced Modified Proctor (RMP) and Modified Proctor (MP) tests on five different soils and they also used other researchers' results. They modified the relationship between ω_{opt} and ω_P as;

$$\omega_{opt} = k_1\omega_p \tag{2.19}$$

Also, they modified γ_{dmax} as;

$$\gamma_{dmax} = k_2\ \gamma_{dry,\omega p} \tag{2.20}$$

where k_1 and k_2 constants are determined by;

$$k_1 = -0.344 \cdot \log E + 1.88 \tag{2.21}$$

$$k_2 = -0.145 \cdot \log E + 0.57 \tag{2.22}$$

Gurtug and Sridharan (2004) also developed a prediction model that correlates γ_{dmax} with ω_{opt}. They presented the linear relationship as;

$$g_{d\max} = 22.26 - 0.28 \cdot w_{opt} \tag{2.23}$$

and the curvilinear relationship as;

$$g_{d\max} = 22.68 e^{-0.0183 \cdot w_{opt}} \tag{2.24}$$

Sridharan and Nagaraj (2005) presented correlation to predict the compaction characteristics of fine-grained soils at Standard Proctor compaction effort. They showed that the plastic limit (ω_P) is well correlated with the compaction characteristics. In order to determine the effect of plasticity characteristics on compaction behavior, they selected soil samples having the same liquid limit values but different plastic limit values. Although, the liquid limit values of both soils is almost the same, lower plastic limit causes lower optimum water content and higher maximum dry unit weight and vice versa for high plastic soils. They predicted the compaction characteristics as follows:

$$\omega_{opt} = 0.92 \cdot (\omega_P) \tag{2.25}$$

$$\gamma_{dmax} = 0.23 \cdot (93.3 - \omega_P) \tag{2.26}$$

where ω_{opt} and ω_P are expressed in percentages and γ_{dmax} is in kN/m^3.

Ölmez (2007) conducted a laboratory work to estimate the compaction characteristics of coarse-grained soils. He performed a total number of 77 Standard Proctor tests and a total number of 32 Modified Proctor tests. Using the multiple linear regressions modeling technique, he developed several different kinds of regression models. He used liquid limit (ω_L), plastic limit (ω_P), plasticity index (I_P), gravel content (G), sand content (S), and fine content (FC) as input variables in his regression models. He preferred the following correlation equation to predict the compaction characteristics.

for Standard Proctor

$$\omega_{opt} = 0.618 \cdot \omega_P - 0.453 \cdot I_P \tag{2.27}$$

$$\gamma_{dmax} = 0.223 \cdot G + 0.411 \cdot FC \tag{2.28}$$

and for Modified Proctor

$$\omega_{opt} = 0.284 \cdot \omega_L \tag{2.29}$$

$$\gamma_{dmax} = 0.234 \cdot G + 0.233 \cdot S + 0.055 \cdot FC \tag{2.30}$$

where ω_L, ω_P, I_P, G, S, FC and ω_{opt} are expressed in percentages and γ_{dmax} is in kN/m^3.

Sivrikaya (2008) performed multiple linear regression analyses to estimate the compaction characteristics of a liner system. The author developed prediction models and tried to find out which index property correlated better with the compaction characteristics of fine-grained soils at the Standard Proctor compaction effort. Besides liquid limit and plasticity index, plastic limit presents a good agreement with γ_{dmax} and ω_{opt} (Sivrikaya, 2008). He also correlated γ_{dmax} with ω_{opt}:

$$\omega_{opt} = 0.92 \cdot (\omega_P) \tag{2.31}$$

$$\gamma_{dmax} = 0.21 \cdot (99.52 - \omega_P) \tag{2.32}$$

$$\gamma_{dmax} = 21.84 - 0.27 \cdot \omega_{opt} \tag{2.33}$$

where ω_{opt} and ω_P are substituted into equations in percent, and the unit of γ_{dmax} is in kN/m^3.

Sivrikaya et al. (2008) developed correlation equations in order to estimate compaction characteristics of fine-grained soils by means of index properties under Modified Proctor compaction effort. They performed multiple linear regression analyses using their own data and that gathered from the literature. In addition, they developed correlation equations for different compaction energy levels. They found that optimum water content could be predicted well using plastic limit. They recommended the following two equations to predict ω_{opt} of fine-grained soils;

$$\omega_{opt} = 0.94 \cdot \omega_P \qquad \text{(for Modified compaction)} \qquad (2.34)$$

$$\omega_{opt} = (1.99 - 0.165 \cdot \mathit{ln}\ E) \cdot \omega_P \qquad \text{(for all compaction energy levels)} \qquad (2.35)$$

where the unit of ω_{opt} and ω_p are in percent and E is in kJ/m^3. On the other hand, they correlated maximum dry unit weight (γ_{dmax}) with optimum water content (ω_{opt}) for estimating Modified γ_{dmax} and estimating γ_{dmax} considering compaction energy;

$$\gamma_{dmax} = 23.78 - 0.38 \cdot \omega_{opt} \qquad \text{(for Modified compaction)} \qquad (2.36)$$

$$\gamma_{dmax} = (14.34 - 0.195 \cdot \mathit{ln}\ E) - (0.073 \cdot \mathit{ln}\ E - 0.19) \cdot \omega_{opt} \qquad \text{(for all compaction energy levels)} \qquad (2.37)$$

where γ_{dmax}, ω_{opt} and E are in kN/m^3, percent and kJ/m^3, respectively.

Gunaydin (2009) performed both simple and multiple linear regression analyses to estimate the compaction characteristics of soils. From simple regression analysis, he developed;

$$\omega_{opt} = 0.3802 \cdot \omega_L + 2.4513 \qquad (2.38)$$

$$\gamma_{dmax} = -0.1008 \cdot \omega_L + 21.16 \qquad (2.39)$$

where γ_{dmax} is in kN/m^3 and ω_{opt} and ω_L are in percent. Günaydin (2009) also developed MLR equations as given below;

$$\omega_{opt} = 0.323 \cdot \omega_L + 0.157 \cdot \omega_P \quad (2.40)$$

$$\gamma_{dmax} = -\ 0.078 \cdot \omega_L - 0.062 \cdot \omega_P \quad (2.41)$$

An early study was realized by Joslin (1959) to determine the whole compaction curve of soils. He developed 26 typical Standard Proctor compaction curves using the Ohio Department of Highways research data base. These compaction curves, which were known as the Ohio's curves, were used as a way for evaluating soils' compaction curves. These curves were not only used to evaluate the field compaction curve in place where the soil type changed so rapidly but also used to determine the complete laboratory compaction curve performing one point compaction test. Joslin (1959) mentioned that the Ohio's curves have proven most helpful both for the laboratory and field use. Using one point test, it is capable of testing more samples in the laboratory. In the field, the uses of the Ohio's curves have resulted in more uniform, more rapid and more efficient control of compacted soils.

Pandian et al. (1997) suggested a model that can draw compaction path for fine-grained soils separately for the dry and the wet sides of optimum based on liquid limit (ω_L) and degree of saturation (S_r). However, this model was only developed for the standard Proctor compaction effort. They mentioned that knowing just one point of the density-water content data and the liquid limit value, the entire path of compaction could be confirmed. They sketched a whole compaction curve in two portions; for the dry of optimum and for the wet of optimum as follows;

$$\frac{w}{\sqrt{S_r}} = 9.46 + 0.258 \cdot w_L \qquad \text{for the dry side of optimum} \quad (2.42)$$

$$\frac{w}{S_r^2} = 10.61 + 0.362 \cdot w_L \qquad \text{for the wet side of optimum} \quad (2.43)$$

where ω and ω_L are expressed as percentages and S_r is in decimal. From their experimental study, the optimum degree of saturation (i.e. degree of saturation at optimum water content) was determined as 80%. Pandian et al. (1997) mentioned that using different values of degree of saturation (i.e. 50% < S_r < 85%) in Equation 2.42, the water content can be calculated and hence the dry density and the compaction path on the dry side of optimum point. Similarly, the compaction path on the wet side of optimum can be drawn using different values of degree of saturation in the range of 85% < Sr < 95% in Equation 2.43. However, these two curves intersect to form a sharp angle at the optimum compaction point. Thus, the curve is an inverted V shape, not the well known bell shape.

Nagaraj et al. (2006) developed a pore model to sketch up the entire compaction curve of fine-grained soils both on the dry and the wet sides of optimum under different compaction energies. They mentioned that the air-water interface is formed by menisci that bridge the space between two clay clusters around the air pore. As the degree of saturation increases, the continuity in the air phase is lost and air would tend to be in the form of occluded air bubbles, leaving behind only continuity of the water phase. They related molding water content with liquid limit (ω_L), saturation degree (S_r) and compaction energy (E) both for the dry and the wet sides of optimum water content.

$$\frac{w}{w_L \cdot \sqrt{S_r}} = 1.24 - 0.18 \cdot \log(E) \qquad \text{for the dry side of optimum} \qquad (2.44)$$

$$\frac{w}{w_L \cdot S_r^2} = 1.79 - 0.28 \cdot \log(E) \qquad \text{for the wet side of optimum} \qquad (2.45)$$

where ω and ω_L are expressed in percentages, and S_r and E are in decimal and ft·lb/ft^3, respectively.

Horpibulsuk et al. (2008) introduced a new prediction model for rapid estimation of compaction curves for fine-grained soils under different compaction energies. They related water content with degree of saturation at both the dry and the wet sides of optimum by means of two power functions;

$$w = A_d S_r^{B_d} \text{ for the dry side of optimum} \quad (2.46)$$

$$w = A_w S_r^{B_w} \text{ for the wet side of optimum} \quad (2.47)$$

where A_d, A_w, B_d, and B_w are constants. The ω and S_r are expressed in percentage and decimal, respectively. These parameters are mainly dependent upon the soil type. They stated that for a particular clay and constant compaction energy level the parameters A_d and A_w control the values of dry unit weight. They revealed that γ_{dmax} increases with decreasing values of A_d and A_w while the values of B_d and B_w remain constant (Figure 2.13.a). The degree of water sensitivity (i.e. slope of compaction path) is controlled by B_d parameter on the dry side and B_w parameter on the wet side of the compaction curve. As depicted in Figure 2.13.b, the lower the value of B_d and the higher the value of B_w causes the greater the degree of water sensitivity. They found that a decrease in compaction energy causes an increase in A_d and A_w values whereas there is no considerable change in B_d, and B_w values when compaction energy changes. With a known compaction curve determined under specific compaction energy, Horpibulsuk et al. (2008) tried to sketch up whole compaction curve of fine-grained soils under any compaction effort. This approach consists of determining A_d, A_w, B_d and B_w values and the compaction characteristics using Equation 2.46 and 2.47. Then water content values can be determined for both the dry and the wet sides of optimum at different values of degree of saturation using Equation 2.46 and 2.47, respectively, and hence the dry unit weight values. Consequently, the compaction curve can be drawn using obtained water contents and corresponding dry unit weights. The details of this approach are given in Horpibulsuk et al. (2008)'s study.

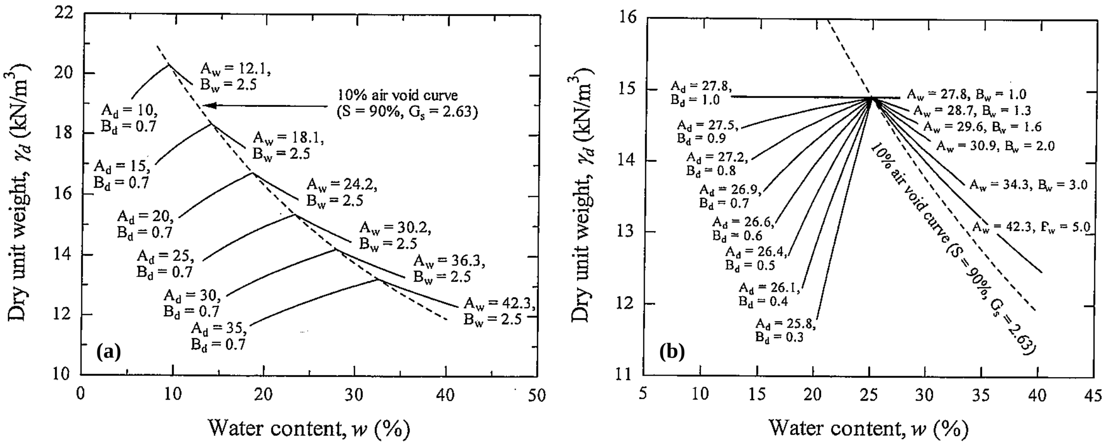

Figure 2.13 Effect of (a) A_d and A_w, (b) B_d and B_w on compaction curves (after Horpibulsuk et al. 2008)

Blotz et al. (1998) and Gurtug & Sridharan (2004) showed that the optimum water content (OWC) has a linear relationship with logarithm of compaction energy (E). On this base, Horpibulsuk et al. (2008) developed a new correlation equation which can be used to assess the OWC of fine-grained soils compacted under any compaction effort when the optimum water content at Standard Proctor (OWC_{st}) energy is known;

$$\frac{OWC}{OWC_{st}} = 2.02 - 0.37 \log E \tag{2.48}$$

where OWC and OWC_{st} are expressed in percentage and E is in the range of 296.3 to 2693.3 kJ/m^3. With known optimum degree of saturation, the maximum dry unit weight is also calculated.

CHAPTER THREE
ARTIFICIAL NEURAL NETWORKS

Artificial neural networks are used to predict the compaction parameters of both coarse and fine-grained soils in the present research. For completeness of the study, artificial neural networks methodology is introduced in this chapter.

3.1 Introduction

Artificial neural networks (ANNs) have emerged in the last decade and attracted attention of researchers due to its capability in modeling the complex real world problems. ANNs are artificial intelligence technique which tries to mimic the human nervous system by means of it structure. Biological neural networks are composed of basic structural and functional units known as *neurons* or *nodes* (Figure 3.1). A neuron consists of four elements: *dendrites, synapses, cell body,* and *axon*. Dendrites are the units that transmit information coming into the neuron from another neuron. Synapses are the connection units that serve as links with the other neurons. The cell body of the neuron is where most of the processing takes place. The axon is responsible for transmitting the output of the neuron.

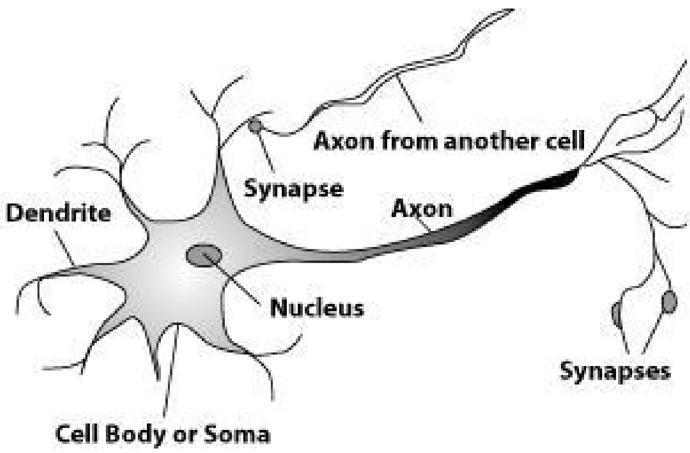

Figure 3.1 Schematic diagram of a biological neuron

Although ANNs mimic the nervous system, the main aim of their usage is not to duplicate the structure of biological nervous system, but to make use of the knowledge of functionality and the capability of the biological network for the solution of complex problems. The advantages of ANNs are;

- An ANN works in parallel like in biological counterparts. This structure is capable of solving complex problem with its own previous experience.
- Most importantly, ANNs have ability in modeling nonlinearity, where most of the real-world problems are considered as non-linear.

3.2 Structure of an Artificial Neuron

The artificial neuron is the basic processing unit of an ANN. It is a simplified version of a biological neuron. The structure of an artificial neuron is illustrated in Figure 3.2.

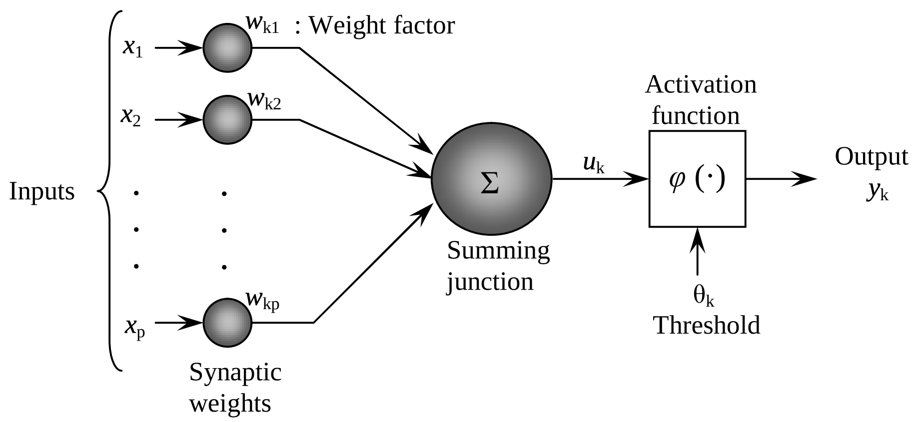

Figure 3.2 Simple structure of an artificial neuron

Each input represents the output of another neuron. These inputs are multiplied by corresponding weights, which symbolize synaptic strength. All weighted inputs are then added by the cell body and processed by an activation function to calculate the output of the neuron. The following equations describe mathematical statement of the above mentioned model.

$$u_k = \sum_{j=1}^{p} w_{kj} \cdot x_j \tag{3.1}$$

$$y_k = j\left(u_k - q_k\right) \tag{3.2}$$

$$u_k = u_k - q_k \tag{3.3}$$

where x_1, x_2, … $\mathbf{x}_p$ are the inputs; w_{k1}, w_{k2},…, w_{kp} are the synaptic weights of neuron k; u_k is the linear combiner output (summing result); θ_k is the threshold; $\varphi(\cdot)$ is the activation function; ν_k activation potential; and y_k is the output of the neuron. The threshold has an effect of lowering the net input of the activation function (Haykin, 1994). In contrast, bias may be used to increase the net input of the activation function. Figure 3.3 presents the architectural layout of an artificial neuron as an alternative to the neuron depicted in Figure 3.2. The bias is the opposite of the threshold. These two terms are represented in the structure of a neuron by;

- If the threshold is used, there should be adding a new input fixed to -1 (x_0 = -1) and adding a new synaptic weight equal to the threshold ($w_{k0} = \theta_k$).
- If the bias is used, there should be adding a new input fixed to +1 (x_0 = +1) and adding a new synaptic weight equal to the bias ($w_{k0} = b_k$).

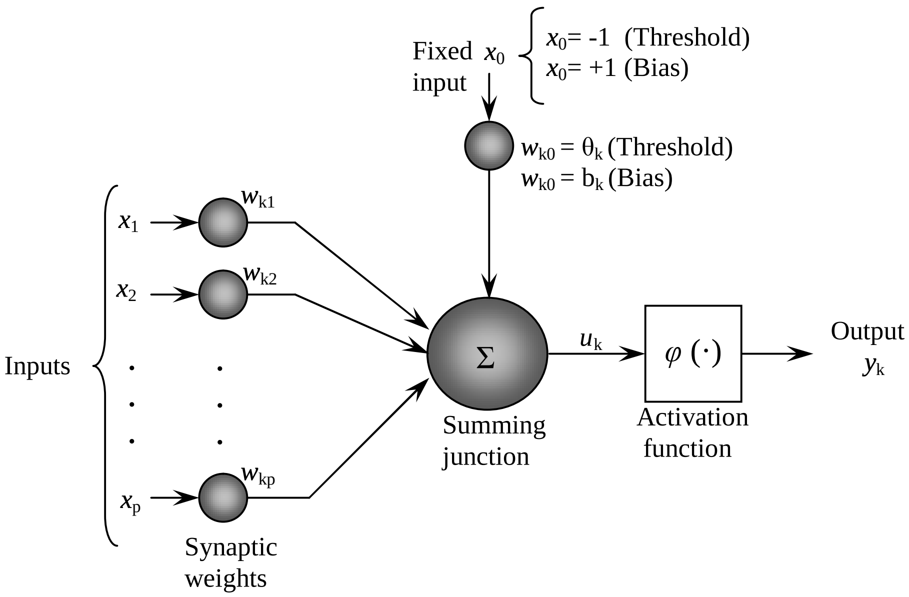

Figure 3.3 Alternative architecture of an artificial neuron

Figure 3.4 illustrates generally used activation functions. The hard-limit function, also known as threshold function, limits the output of the neuron to either 0, if the net input argument *x* is less than 0, or 1, if *x* is greater than or equal to 0. The sigmoid function, which is the most common form of activation function used to build an ANN, squashes the output into a range of 0 to 1. The sigmoid function is defined by;

$$y = \frac{1}{1 + \exp(-a \cdot x)} \tag{3.4}$$

where α is the slope parameter of the sigmoid function. Usually, it is equal to unity. One of the commonly used activation functions is the hyperbolic tangent sigmoid function, which forces the outputs to vary between -1 and +1. It is defined by;

$$y = \frac{1 - \exp(-2 \cdot x)}{1 + \exp(-2 \cdot x)} = \frac{2}{1 + \exp(-2 \cdot x)} - 1 \tag{3.5}$$

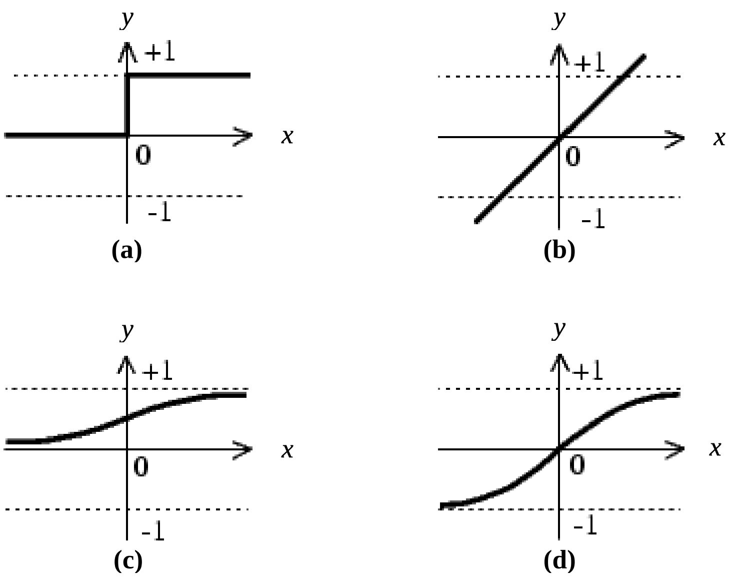

Figure 3.4 Generally used (a) hard-limit, (b) linear, (c) sigmoid and (d) hyperbolic tangent sigmoid transfer functions

3.3 Artificial Neural Networks Architecture

Although there are many different types of ANNs, only the feedforward networks are used in this study. Information about this network is given below.

Feedforward ANNs are composed of two layers (i.e. single-layer feedforward networks) or more layers (i.e. multi-layer feedforward networks) of neurons. While a single-layer feedforward network consists of an input and an output layer, a multi-layer feedforward network has one or more hidden layers between input and output layers. Figure 3.5 shows a multi-layer feedforward network with one hidden layer. Each layer only receives inputs from its previous layer. In other words the information flows only in forward direction (i.e. from input layer to the output layer). Each neuron in a layer computes its own output independently and sends the computed outputs to the next layer.

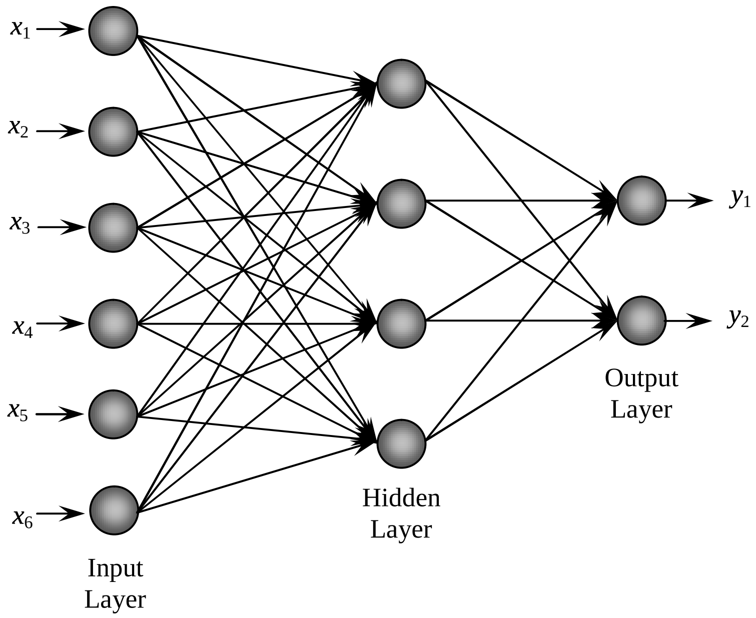

Figure 3.5 Fully connected feedforward network with one hidden layer

For such networks, each neuron in the input layer multiplies the input value by a weight and passes them to the hidden layer. Hidden neurons sum up these weighted inputs gathered from input layer neurons and fix the bias term, and then process them all with a transfer function. The output received from the hidden layer passes through the same procedure described above at the output layer where the network output is determined.

3.4 Learning Algorithms

The process by which the networks' free parameters (i.e. synaptic weights and biases) are adjusted through an iteration procedure to improve the network performance is called learning. There are many types of learning algorithms for ANNs. Details of these algorithms can be found in Haykin (1994), Hagan et al. (1996) and Ham & Kostanic (2001) in detail. The supervised back-propagation learning algorithm was used to modify the network weights and biases in this study. Brief information about this learning algorithm is given below.

The supervised learning can be represented by the concept of "teacher-student relationship". The teacher represents network targets where the student is the network. As the input is applied to the network, its output is compared with the targets. By this control process, the error between the output and the corresponding target is minimized. Figure 3.6 depicts a block diagram of supervised learning.

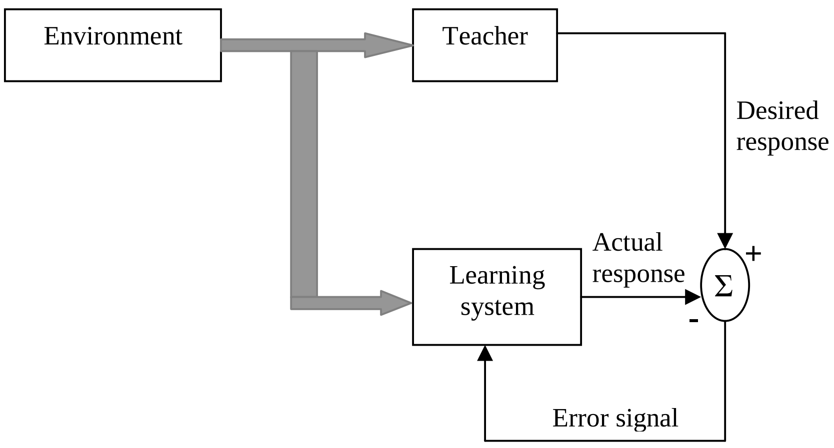

Figure 3.6 Block diagram of supervised learning (after Haykin, 1994)

The back-propagation algorithm is one of the commonly used types of supervised learning procedures. The name of back-propagation comes from the fact that error terms in the algorithm are back-propagated through the network from output to the input layer. The error at the output neuron j is defined by;

$$e_j = d_j - y_j \tag{3.6}$$

where e_j refers the error at the output neuron j, d_j is the desired response for neuron j and y_j refers to the function result at the output of neuron j. The back-propagation algorithm is based on the gradient descent method, also known as conjugate-gradient method, applied to minimize an energy function (i.e. performance function) representing the instantaneous sum of squared errors as below;

$$E = \frac{1}{2}\Sigma e_j^2 \tag{3.7}$$

The correction term for a weight in any one of the network layers is defined by the *delta rule*

$$\Delta w_{ji} = -h \frac{\partial E}{\partial w_{ji}} \tag{3.8}$$

where η is a constant which is called as the *learning rate parameter* of the back-propagation algorithm. By differentiating the gradient term of Equation 3.8 (i.e. $\partial E / \partial w_{ji}$), the gradient can be expressed as

$$d_j = \frac{\partial E}{\partial w_{ji}} = -e_j \cdot j'_j(u_j) \cdot y_i \tag{3.9}$$

where $j'_j(u_j)$ is the first derivative of the activation function. The term of d_j defined in Equation 3.9 is known as *local gradient*. The delta rule equation can be written as combining Equation 3.8 and Equation 3.9,

$$\Delta w_{ji} = h \cdot d_j \cdot y_i \tag{3.10}$$

The adjusted weight is defined as

$$w_{ji}(k+1) = w_{ji}(k) + \Delta w_{ji} = w_{ji}(k) + h \cdot d_j \cdot y_i \tag{3.11}$$

One should take notice that the local gradient term in Equation 3.9 is determined for the output layer of the network. In this regard, two distinct cases can be defined depending on where neuron j is located. In the first case, neuron j is an output neuron whereas it is located in the hidden layer for Case 2. The local gradient is defined as below for Case 2:

$$d_j = j'_j(u_j) \cdot \sum_k d_k \cdot w_{kj} \tag{3.12}$$

where $\sum_k d_k \cdot w_{kj}$ term is the weighted sum of the local gradients computed for the neurons in the next hidden or output layer that are connected to neuron j. Equation 3.13 summarizes the delta rule derived for the back-propagation algorithm.

$$\begin{pmatrix} \text{Weight} \\ \text{correction} \\ \Delta w_{ji} \end{pmatrix} = \begin{pmatrix} \text{Learning} \\ \text{rate} \\ h \end{pmatrix} \cdot \begin{pmatrix} \text{Local} \\ \text{gradient} \\ d_j \end{pmatrix} \cdot \begin{pmatrix} \text{Input signal} \\ \text{of neuron } j \\ y_i \end{pmatrix} \tag{3.13}$$

The local gradient should be calculated by means of Equation 3.9 if the neuron is located in the output layer. In contrast, Equation 3.12 is used to compute the local gradient if the neuron is a hidden layer one. The gradient steps get smaller as the error decreases. This causes to slow down the network convergence. Although there are several methods used to speed up the back-propagation algorithm, the Levenberg-Marquardt technique is generally preferred over. The Levenberg-Marquardt back-propagation (LMBP) algorithm is a simplified version of Newton's method without having to compute the Hessian matrix. When approaching the minimum of the energy function, the Hessian matrix can be closely approximated by

$$H \approx J^T \cdot J \tag{3.14}$$

and the gradient can be computed as

$$d_j = J^T \cdot e \tag{3.15}$$

where **J** is the Jacobian matrix, which contains first derivatives of the network errors with respect to the weights and biases, and **e** is a vector of network errors. The LMBP algorithm uses the following update rule as

$$\Delta w_{ji} = \left(J^T \cdot J + m \cdot I\right)^{-1} \cdot J^T \cdot e \tag{3.16}$$

where μ is the scalar and **I** is the identity unit matrix. Also the updated weight is expressed as

$$w(k+1) = w(k) - \left(J_k^T \cdot J_k + m_k \cdot I\right)^{-1} \cdot J_k^T \cdot e_k \tag{3.17}$$

Equation 3.17 becomes the Newton’s equation when μ is zero. On the other hand, if μ is very large, it approximates the gradient descent method. Thus, μ is decreased if the error increases, and it is increased while the error gets smaller. By this way, the energy function will always be reduced at each iteration. Limited information about the LMBP algorithm is being given in this study. Detailed information can be found in Haykin (1994) and Ham & Kostanic (2001).

3.5 Pre-processing of Data

It is well known that the performance of the artificial neural networks is often improved by transforming the raw data. Due to the requirements of the ANN modeling technique, the raw data set is usually normalized into non-dimensional scale of [0, 1] or [-1, 1] intervals through data transformation.

The relationship between input and output variables is explored during training process. Training of ANNs includes the iterative adaptation of the connection weights in order to generate the desired output. At the end of the training process, the associated trained weights of the model are tested with a separate set of data, which is known as the testing set. According to the present knowledge, the network size and the number of training cycles are the two important issues at training process of network. If training cycles are insufficient, the network will not learn the relation between input and output (underfitting). In contrast, if training cycles are too excessive, the network will memorize the training data. This reduces the generalization capability of the network. Moreover, an oversized network tends to learn the noise and overfit the data (Figure 3.7). Overfitting problem can be accomplished using cross-validation technique. In this technique, the main data set is divided into three subsets; training, testing and validation. The training subset is used to adjust the connection weights. The validation subset is used to control the trained network at each step in order to stop the training process if it attempts to overfit the training data. After network convergence, the testing subset is used to evaluate the performance of the model on data it was not trained on. Routinely, the data are divided into training, testing and validation subsets on a randomly basis. However, importance of data division methodology on performance of ANN models was investigated by Shahin et al. (2004).

3.5.1 Data Transformation

In order to build the ANN prediction models which are insensitive to units, all input variables and sometimes target(s), are normalized. Normalization is a transformation performed on a single data input to scale it into an acceptable range for the network. Learning time of an ANNs model can cause faster convergence due to using same scale inputs. Data normalization is especially useful for modeling applications where inputs are generally on widely different scales. For instance, if an input variable has large magnitude on scale basis, the network will perceive it having greater influence on the output. Thus, the network will assign it larger weights values that cause to reduce the importance of other inputs. By data normalization each input variable has an equal opportunity to convey its own effect on the output. In this study, the input variables are transformed using four different normalization methods: (*i*) statistical normalization, (*ii*) min-max normalization, (*iii*) non-linear transformation, and (*iv*) whitening transformation. The details of these normalization methods are described below.

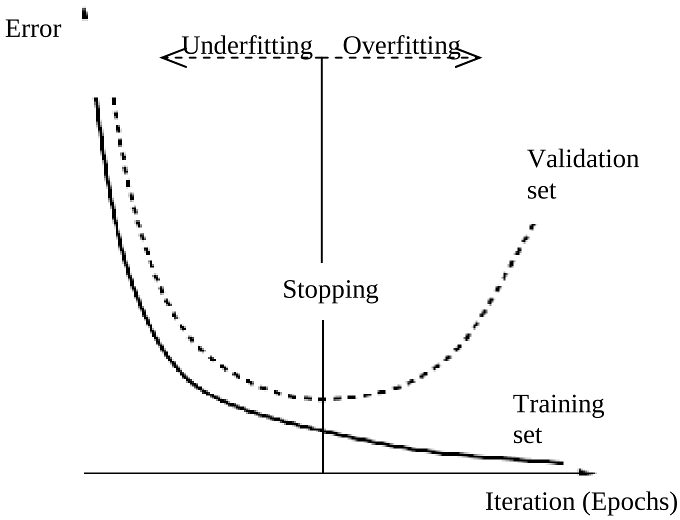

Figure 3.7 Schematic representation of early stopping

3.5.1.1 Statistical Normalization

The statistical normalization technique uses the mean (μ) and the standard deviation (σ) for each variable. This transformation produces a dataset such that each variable has a zero mean and a unit variance.

$$y_i = \left[\frac{x_i - m}{s} \right] \tag{3.18}$$

where x_i is the original raw data, y_i is the transformed data, μ is the mean and σ is the standard deviation of the i^{th} variable of the training data set.

3.5.1.2 Min-Max Normalization

Min-Max normalization is a process where inputs or output(s) from one range of values are rescaled to a new range of values. Generally, the variables are rescaled to lie within a range of 0 to 1 or from -1 to 1. The rescaling is executed by,

$$y_i = (x_{target,\max} - x_{target,\min}) \times \left[\frac{x_i - x_{\min}}{x_{\max} - x_{\min}} \right] + x_{target,\min} \tag{3.19}$$

where $x_{target,max}$ and $x_{target,min}$ are the maximum and the minimum target values in the normalized set, respectively. The x_{min} and the x_{max} are the minimum and the maximum value of the raw data set. y_i is the transformed data and x_i is the raw data.

3.5.1.3 Non-Linear Transformation

Non-linear transformation is another process used to transform the data from its original value into a new range. In this study, log-sigmoid function is used as

$$y_i = \frac{1}{1 + e^{-x_i}} \tag{3.20}$$

where y_i is the transformed data and x_i is the original data.

3.5.1.4 Whitening Transformation

The whitening transformation is a linear transformation method that converts the covariance matrix of a set of data into the identity matrix. The whitening transformation transforms x_i to y_i by the following equations:

$$y_i = V \cdot x_i \tag{3.21}$$

where y_i is the transformed data matrix, x_i is the original data matrix and V is a transformation matrix calculated by

$$V = D^{-1/2} \cdot E^T \tag{3.22}$$

where D is the diagonal matrix of eigenvalues and E is the eigenvectors of the covariance matrix.

3.5.2 Data Division

In general, performance of an ANNs model increases if it does not try to extrapolate beyond the extreme values of the data used for training (Shahin et al., 2004). This means that the training subset should cover all pattern ranges contained in the main data set. Similarly, the validation subset should be representative of the training subset since it is used to stop the learning process. Ideally, it is expected that training data are evenly distributed over the entire space.

There are numerous studies that compared different clustering methods (i.e. hierarchical clustering, K-means clustering, self organizing map, fuzzy clustering etc.) for a given classification problem in the literature. In recent years, the fuzzy clustering method has successfully been applied to a wide variety of civil engineering applications (Shi, 2002; Shahin et al., 2004; Goktepe and Sezer, 2005; Budayan et al., 2009; Das and Basudhar, 2009).

In this study, the data set was divided into training, testing and validation subsets using two different methodologies. One of the methods is the well known random data division approach. The second method is the fuzzy c-means clustering division of the main data set following more systematic procedures in order to avoid shortcomings of the random division technique.

3.5.2.1 Random Division

In majority of the published literature, the main data set was divided into training, testing and validation subsets on a randomly base with no consideration about statistical consistency of the subsets' data. Consequently, the validity and generalization ability of the ANN models is extremely dependent on whether the training subset covers all pattern ranges in the main data set. If it does not cover, generalization ability the developed model will decrease. On the other hand, the modeler decides which proportion of the main data set is used for training, testing and validation subsets. There is not a standard with respect to selecting the percentages of subsets. Generally, the modeler chooses the proportions for these three subsets.

3.5.2.2 Fuzzy C-Means Clustering

Fuzzy c-means (FCM) algorithm proposed by Bezdek (1981) is a data clustering method. It allows each data belongs to two or more clusters by calculating a membership grade to each data point corresponding to each cluster center. The total membership value of any data should be equal to unity. The purpose of FCM is to minimize the following objective function;

$$J_m(U,v) = \sum_{i=1}^{n}\sum_{j=1}^{c} u_{ij}^{m}\left\|x_i - v_j\right\|^2 \quad , \quad 1 \le m < \infty \tag{3.23}$$

where u_{ij} represents the membership value of ith data to jth cluster center, x_i is the ith data, v_j is the jth center of the cluster, m is the fuzziness index greater than 1, and $||x_i - v_j||$ is any norm expressing the similarity between ith data and jth cluster center (Dulyakarn and Rangsenseri, 2001). An iterative procedure is followed to minimize the objective function. At the beginning, the number of clusters and the fuzziness index value are determined. Then, the u_{ij} matrix is initialized. At each step, the cluster centers (v_j) are calculated and the membership is updated by;

$$u_{ij} = \frac{1}{\sum_{k=1}^{c}\left(\frac{\|x_i - v_j\|}{\|x_i - v_k\|}\right)^{\frac{2}{m-1}}} \tag{3.24}$$

$$v_j = \frac{\sum_{i=1}^{n} u_{ij}^m \cdot x_i}{\sum_{i=1}^{n} u_{ij}^m} \tag{3.25}$$

The iteration process will stop when $\max_{ij}\{\left|u_{ij}^{(k+1)} - u_{ij}^{(k)}\right|\} < e$, where ε is a termination criterion between 0 and 1, and k represents the iteration steps. Detailed algorithm of FCM method was proposed by Bezdek (1981).

3.6 Previous ANNs Modeling Studies for Soil Compaction

Many civil engineers tried to overcome the problems in civil engineering by means of artificial neural networks (ANNs). In these studies, ANNs were mostly used as a powerful tool for design automation and optimization, structural system identification, structural condition assessment and monitoring, structural material characterization and modeling, construction scheduling and management, construction cost estimation, etc. A comprehensive list of the applications of ANNs in civil engineering was summarized by Adeli (2001). A summary on published articles about ANNs in civil engineering was made by Flood (2006). Flood (2006) also gave a critical point of view about the next generation ANNs for civil engineering.

In recent years, ANNs have been successfully applied several problems in geotechnical engineering. ANNs were used for predicting the bearing capacity of piles (Chan et al., 1995; Lee & Lee, 1996; and Kiefa, 1998). Najjar and Basheer (1996) demonstrated potential application of ANNs for evaluating the permeability of compacted clay liners. Juang and Chen (1999) used ANNs to predict the liquefaction potential of sandy soils. Applicability of ANNs to predict the collapse potential of soils was discovered by Juang et al. (1999). Pradeep et al. (2002) used ANN models for estimating the overconsolidation ratio of clays from piezocone penetration tests (PCPT). Shahin et al. (2002) predicted shallow foundations settlement on granular soils using ANNs. Wang et al. (2005) dealt with slope stability evaluation using back propagation neural networks. Ashayeri and Yasrebi (2009) presented ANN models to predict free-swell percent and swelling pressure of a soil sample. A brief overview of ANN applications in geotechnical engineering were made by Toll (1996), Shahin et al. (2001) and Shahin et al. (2009).

Najjar et al. (1996) developed an ANN model to predict both γ_{dmax} and ω_{opt} from given geotechnical parameters. In this study two different databases were used: data pertaining to synthetic and natural soils were acquired from the literature. They only modeled Standard Proctor test data. They used three-layered feed-forward error-backpropagation network for their models. The authors trained several ANN models with varying number and type of input variables (Table 3.1). Among the 11 independent variable, some or all were used as the input of the networks. On the other hand, γ_{dmax} and ω_{opt} were the two targets. The authors modeled the networks that had multi-output or single-output. They examined the ANN model for its prediction accuracy after the network convergence. Therefore, they developed a comparison criterion. The authors named this criterion using the percentage "Absolute value of the Relative Error" (ARE) given as;

$$ARE = \left| \left(\frac{X_{pred} - X_{actual}}{X_{actual}} \right) \times 100 \right| \tag{3.26}$$

Table 3.1 ANNs models trained by Najjar et al. (after Najjar et al., 1996).

Net#	*#Inputs*	*Input variables*	*#Output*	*Outputs*	*HN*	*% MARE*
(1) Synthetic soils						*OMC/MDD*
A1	11	C,S,Sd,Gr,G_s,LL,PL,FM,U,D_{50},D_{10}	2	OMC,MDD	6	8.10/3.70
A2	9	C,S,Sd,Gr,G_s,LL, PL, FM,U	2	OMC,MDD	2	11.00/2.97
A3	7	C,S,Sd,Gr,G_s,LL,PL	2	OMC,MDD	2	10.50/2.69
A4	6	C,S,Sd,G_s,LL,PL	2	OMC,MDD	4	11.49/2.51
A5	6	LL,PL,FM,U,D_{50},D_{10}	2	OMC,MDD	1	14.80/1.02
A6	3	Gs,LL,PL	2	OMC,MDD	1	15.10/5.28
A7	1	LL	2	OMC,MDD	5	24.80/5.70
						MDD
B1	11	C,S,Sd,Gr,G_s,LL,PL,FM,U,D_{50},D_{10}	1	MDD	1	1.97
B2	4	G_s,PL,FM,D_{10}	1	MDD	5	1.01
B3	4	C,G_s,FM,U	1	MDD	1	1.41
B4	3	G_s,LL,PL	1	MDD	1	4.36
B5	2	LL,PL	1	MDD	1	4.98
B6	1	LL	1	MDD	4	5.70
						OMC
C1	11	C,S,Sd,Gr,G_s,LL,PL,FM,U,D_{50},D_{10}	1	OMC	1	8.66
C2	3	G_s,LL,PL	1	OMC	1	14.00
C3	3	PL,FM,U	1	OMC	3	16.50
C4	3	C,FM,D_{50}	1	OMC	12	11.60
C5	2	LL,PL	1	OMC	1	20.40
C6	1	LL	1	OMC	8	24.00
						LL/PL
D1	4	C,S,Sd,G_s	2	LL,PL	5	2.92/5.01
(2) Natural soils						*OMC/MDD*
E1	3	LL,PL,G_s	2	OMC,MDD	1	6.26/2.52
E2	1	LL	2	OMC,MDD	3	7.15/2.48

where HN: number of hidden nodes, C: bentonite content (%), S: silt content (%), Sd: sand content (%), Gr: gravel content (%), FM: fineness modulus. The authors used the mean of ARE (i.e. MARE) for selecting the best network. For the synthetic soils, it is evident from Table 3.1 that as the number of input variables increases lower MARE values are obtained. The authors mentioned that network A1 yielded the best performance for γ_{dmax} and ω_{opt}. However, A1 impractical because of using 11 input variables. They mentioned that network A4 may be used for practical use without any decrease of accuracy. On the other hand, network E1 with one hidden node could be used for natural soils.

A study has been carried out by Basheer (2001) to model the compaction curves of cohesive soils based on basic soil parameters and compaction energy. The author developed this model using both conventional statistical regression and ANN techniques. In this study, a total of 82 compaction curves were used by the author. From each compaction curve he extracted seven water content-dry density data points (ω, DD) including the optimum water content and dry density. He followed a normalization process in order to developed unit free models. A nondimensional dry density parameter (N3D) was used (i.e. N3D=DD_{soil} / D_{water}) The author also converted compaction energy into a nondimensional form dividing by the standard Proctor energy (E_{std}), that is, $E^*=E_x/E_{std}$ where E_x is the energy for the x^{th} compaction procedure. In addition, the author defined a deviatoric water content ω^*, that is, $\omega^* = \omega - \omega_{opt}$. This parameter represents mutual difference (in percent) of water content from ω_{opt}. If it is negative, this means that the point is on the dry side of optimum. If it is positive, this indicates the point is on the wet side. Also, $\omega^* = 0$ refers to optimum.

The author expressed the general compaction model as N3D = $\psi(\omega^*, E^*$, soil physical properties), where ψ is a function to be determined by a prediction model. In ANNs models the author used three-layered feed-forward network with a single hidden layer. He partitioned 82 compaction curves into 60 training curves representing 420 (ω^*, N3D) data points, and 11 both for test and for validation curves representing 77 data points. Several N3D models have been developed and examined for their accuracy by the author. In Table 3.2, the developed networks by the author and their statistical features were summarized.

Table 3.2 Statistical features obtained for N3D ANN model (after Basheer, 2001).

			Coefficient of determination (R^2) and sum of squared error (SSE) for the agreement between ANN output and correct solution			
ANN No.	Model inputs	Best topology[a]	Training data	Test data	Validation data	All data[b]
1	w^*, LL, PL, G_s, E^*	5–3–1 (4200)	0.789, 2.900	0.624, 0.837	0.601, 0.525	0.742, 4.262 (0.84)
2	w^*, LL, PL, G_s, E^*, OWC	6–4–1 (5000)	0.982, 0.252	0.981, 0.031	0.939, 0.008	0.978, 0.363 (0.25)
3	w^*, LL, PL, E^*, OWC	5–4–1 (2200)	0.970, 0.408	0.965, 0.056	0.812, 0.246	0.957, 0.710 (0.34)
4	w^*, LL, G_s, E^*, OWC	5–5–1 (5000)	0.975, 0.345	0.977, 0.036	0.944, 0.007	0.973, 0.455 (0.27)
5	w^*, LL, E^*, OWC	4–4–1 (4200)	0.968, 0.445	0.971, 0.057	0.883, 0.154	0.960, 0.656 (0.33)

[a]Number of training cycles is given in parentheses.
[b]Standard error in kN/m^3 is given in parentheses.

It is clear from Table 3.2 that the ANN-1 model is the best predictive network when considering only five-input model. The author developed a new network model considering ω_{opt} as an input variable, and defined the compaction model as N3D = $\psi(\omega^*, E^*, \omega_L, \omega_P, G_s, \omega_{opt})$. In Figure 3.8, the author compared ANN-1 model with ANN-2 model.

The author mentioned that by his own words "at first glance, the inclusion of ω_{opt} in N3D models may seem irrational because one usually does not know a priori the ω_{opt} of the soil unless an experimental compaction curve is available or a correlation equation is used to estimate it from known soil properties". However, the presence of ω_{opt} as input variable in the model increases the predictability of the model. Thus he developed a secondary model to determine the ω_{opt}. Various ω_{opt} models were developed and examined for their accuracy. As a result, he determined the best network that had four inputs (i.e. ω_L, ω_P, G_s, E^*) and 12 hidden nodes (4-12-1 ANN).

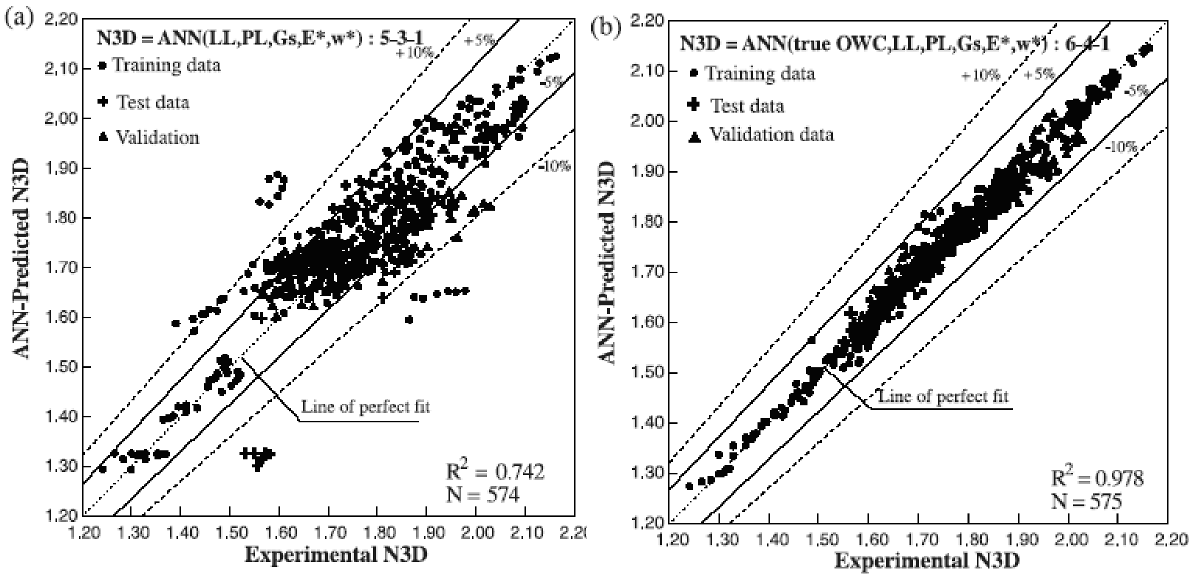

Figure 3.8 The results of (a) Ann-1 model and (b) Ann-2 model (after Basheer, 2001).

In order to develop a comprehensive simulation of compaction curves, these two models were combined and named as "Compaction curve module" by the author. In Figure 3.9, a schematic diagram of the compaction curve module is given. This module works as; firstly, the ω_{opt} model estimates ω_{opt}, and then the N3D model is activated in order to determine N3D values at all the predetermined ω^* values. Determination of compaction curve was fallowed by transforming ω^* and N3D values into actual water content and dry density.

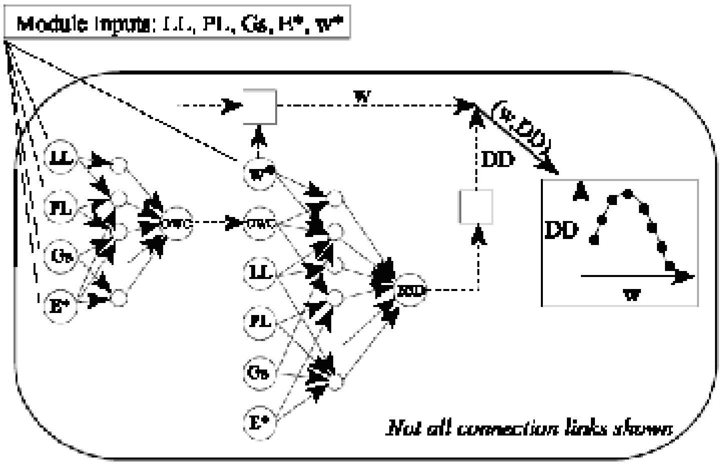

Figure 3.9 A schematic illustration of compaction curve module (after Basheer, 2001).

ANN models were developed for predicting compaction characteristics of cohesionless soils by Abdel-Rahman (2008). He estimated the γ_{dmax} and ω_{opt} only at modified Proctor compaction energy level. In this study, a total number of 175 test results from numerous projects in Egypt were collected by the author. The author separated 150 data for training set and the remaining 25 data for testing set on a random basis. He used the percent passings through 3/4″, No.4, No.10, No.40, and No.200 sieves as inputs in his ANN model. The author developed a three layers feedforward back-propagation neural network for estimating compaction characteristics. He concluded that the ANN models designed in this study predicted the γ_{dmax} and ω_{opt} with a coefficient of regression (R^2) of 0.99 and 0.89, respectively. He explained the reason of lower R^2 values for of ω_{opt} as the variance in the input values of ω_{opt} was much higher than for γ_{dmax}. It should be mentioned that the author did not provide a normalization procedure for the inputs and the targets.

Sinha and Wang (2008) presented ANN models which related γ_{dmax} and ω_{opt} with soil index properties. A total number of 55 soil mixtures were prepared by blending different proportions of bentonite, limestone dust, sand and gravel and compacted at Standard Proctor energy level. Two separate ANN models were developed for γ_{dmax} and ω_{opt} by the authors. They used feedforward neural network with back-propagation learning algorithm. They used the density of solid phase (γ_s), fineness modulus (F_m), effective grain size (D_{10}), plastic limit (ω_P), and liquid limit (ω_L) as inputs for prediction of γ_{dmax}. They determined the best ANN structure by means of trial-error approach. A hidden layer with three neurons was determined as the best topology for estimating γ_{dmax} (Figure 3.10a). The fineness modulus (F_m), uniformity coefficient (U) and plastic limit (ω_P) were used as input variables to estimate ω_{opt} by the authors. They mentioned that a hidden layer with two neurons was the best network (Figure 3.10b).

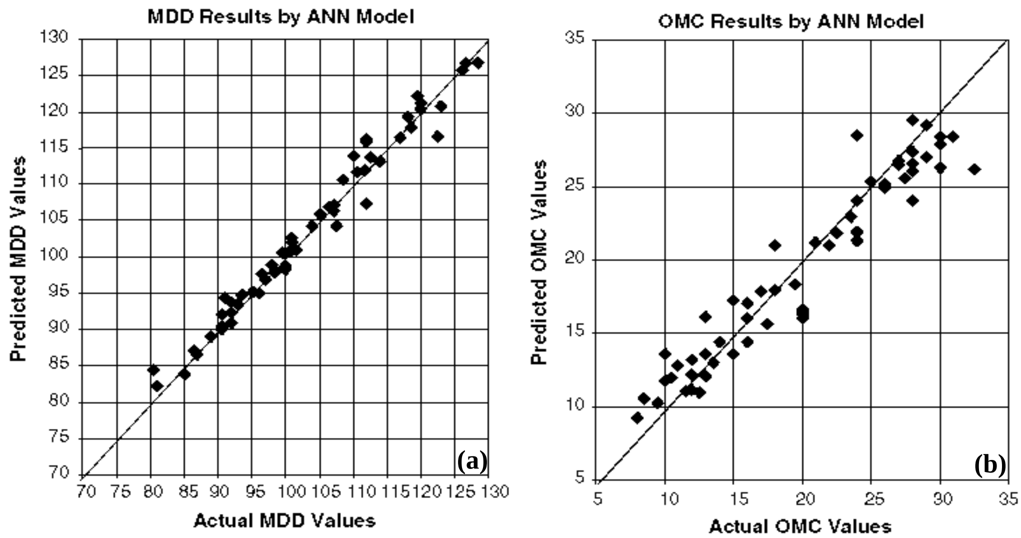

Figure 3.10 ANN prediction results for (a) γ_{dmax} and for (b) ω_{opt} (after Sinha & Wang, 2008)

Günaydın (2009) used multi-layer feedforward neural network for predicting compaction characteristics. The author divided the data randomly into training (i.e 103 data) and testing (i.e. 23 data) sets. The data were scaled between 0 and 1 using min-max normalization method. The author used fine-grained (FG,%), sand (S,%) gravel (G,%), specific gravity (G_s), liquid limit (ω_L,%), plastic limit (ω_P,%), and soil type (ST) as inputs in ANN models. By changing the number of input parameters, five different ANN models were employed in the analysis (Table 3.3). In order to evaluate the ANN models, the author compared the estimated and the corresponding measured values of γ_{dmax} and ω_{opt} by means of statistical features of coefficient of regression (R^2) and standard error (SE). The author decided that Model II was the best model in terms of R^2 and SE. He calculated R^2 values of Model II as 0.893 and 0.836 for ω_{opt} and γ_{dmax}, respectively. Also, SE values were 0.079 and 0.081 for ω_{opt} and γ_{dmax}, respectively.

Table 3.3 The ANN models information of Günaydın (2009)

Model	Inputs	Structure	Transfer function
I	FG, *S*, *G*, G_s, w_L, w_P, ST	7-3-2	tan sig–log sig
II	FG, *S*, *G*, w_L, w_P	5-3-2	tan sig–tan sig
III	FG, *S*, *G*	3-3-2	tan sig–log sig
IV	w_L, w_P	2-6-2	tan sig–log sig
V	w_L, w_P	2-3-1	tan sig–log sig

A recent study by Sivrikaya and Soycan (2010) estimated the compaction characteristics of fine-grained soils as a function of compaction energy using ANNs. The data used in analysis were gathered from the literature. In this study, a total number of 190 and 215 data were used to estimate ω_{opt} and γ_{dmax}, respectively. The authors mentioned that half of the data were randomly selected for training and the remaining were used for testing. In order to estimate ω_{opt}, they used compaction energy (E) and plastic limit (ω_P) as input parameters. They also related γ_{dmax} with compaction energy (E) and optimum water content (ω_{opt}) in the ANN analysis. In this study, the authors employed a feedforward neural network trained by back-propagation algorithm. They developed different types of ANN models by changing number of hidden layers and number of neurons in that layer in order to determine the best ANN topology. The authors tabulated that the best topology for estimating ω_{opt} was one hidden layer with three neurons and for estimating γ_{dmax} it was one hidden layer with one neuron. They graphically compared their estimations with corresponding measured values of ω_{opt} and γ_{dmax} (Figure 3.11). They used the correlation coefficient (R) and the standard error (SE) of the correlations as statistical verification tools. The statistical features of ANN prediction models were summarized as R=0.93 and SE=±2.8% for ω_{opt} and R=0.98 and SE=±0.5kN/m^3 for γ_{dmax} estimations.

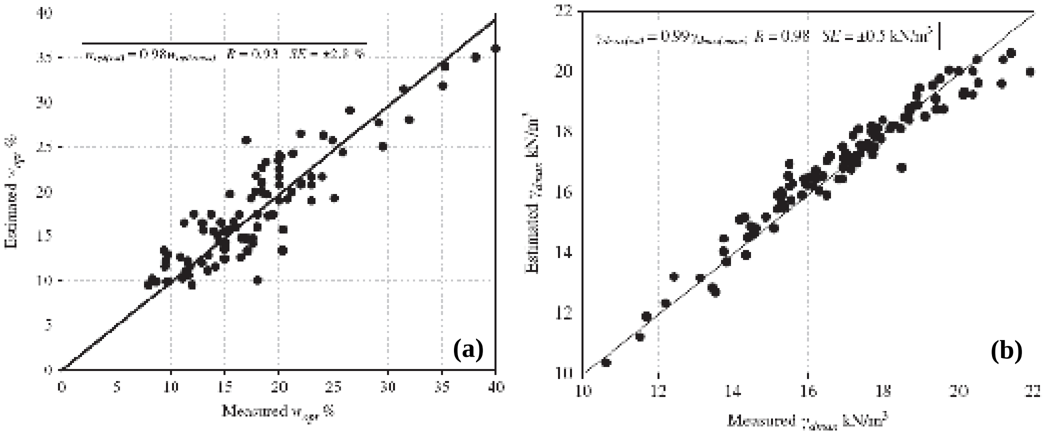

Figure 3.11 ANN models prediction results for (a) ω_{opt} and for (b) γ_{dmax} (after Sivrikaya and Soycan, 2010)

CHAPTER FOUR
TESTING MATERIALS AND EXPERIMENTAL PROGRAM

4.1 Soil Materials

Two types of crushed gravel (i.e. coarse gravel and fine gravel), natural sand and clay were used as the major components for preparation of soil mixtures. The coarse- and fine-gravels were products of a limestone quarry. The sand component was a natural fine aggregate. The gravels and the sand components were obtained from the Building Materials Laboratory of Dokuz Eylül University. The clay was obtained from Salihli/Turkey. In the following sections, the clay is named as Salihli clay.

4.1.1 Sieve and Hydrometer Analysis

Sieve analysis tests of crushed coarse and fine gravels, natural sand and Salihli Clay were performed according to ASTM D 422-63. The stack of 1″, 3/4″, 1/2″, 3/8″, No.4, No.10, No.20, No.40, and No.200 sieves were used in the tests. During sieve analysis, a representative oven-dry soil material of adequate mass was used. The material on the No.200 sieve was washed until the wash water has became clear. The material retained on the No.200 sieve was kept and following the washing procedure dried in the oven. The following day, the retained soil material was subjected to sieve test. Grain size distribution curves of the soil materials are plotted in Figure 4.1. Hydrometer analysis was performed on 50g of oven-dry Salihli clay sample according to ASTM D 422-63 in order to obtain particle size distribution of the fine fraction (i.e. Salihli clay).

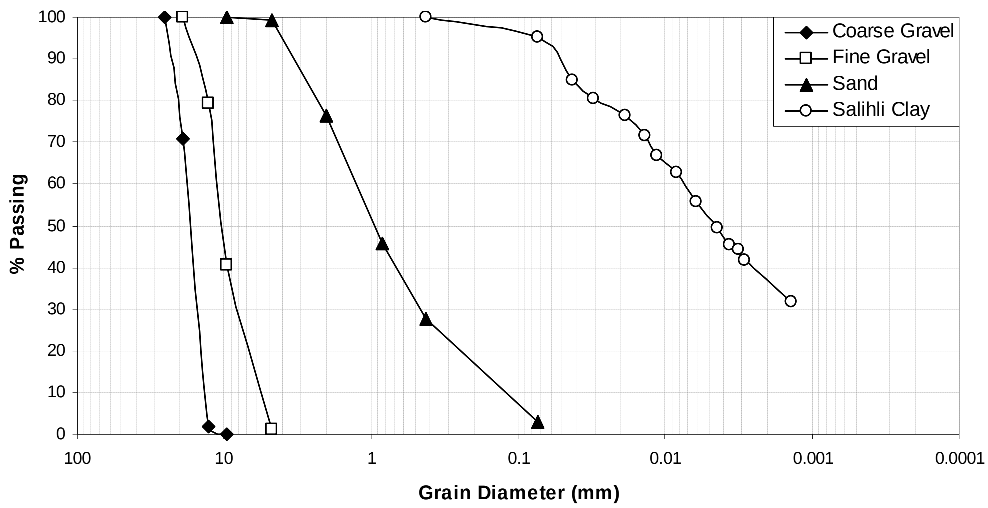

Figure 4.1 Grain size distribution curves of soil materials.

4.1.2 Specific Gravity Test

Specific gravity tests of crushed gravels, natural sand and Salihli clay were performed according to ASTM D 854-92. In the test, 500 ml volumetric pycnometer was used. Two different air removing processes were performed; (1) boiling and (2) deairing by means of vacuum application. Due to requirements of ASTM D 854-92, approximately, 100-150g of representative soil samples passing through No.4 sieve were used for gravel and sand samples whereas 50g sample was used for Salihli clay. Soil samples were carefully placed into pycnometer and filled with de-aired water. In order to remove air from the soil-water suspension, firstly the suspension was boiled and then vacuumed. During these processes, the soil sample was gently agitated by carefully shaking and turning the pycnometer. The vacuuming process continued until there was no air bubbles in the suspension.

4.1.3 Consistency Limit Tests

Liquid limit (ω_L) and plastic limit (ω_P) tests were performed on the fraction of Salihli clay that passes through No.40 sieve. The liquid limit test was performed using fall-cone test method as described in BS 1377. The plastic limit of Salihli clay was determined in accordance with ASTM D 4318-98. The liquid limit of Salihli clay was found as ω_L = 58%. Plastic limit test was repeated three times. Average plastic limit and plasticity index of Salihli clay were determined as ω_P = 27% and I_P = 31%, respectively. Consistency limits, sieve analysis, specific gravity test results and Unified Soil Classification System (USCS) group symbols of coarse gravel, fine gravel, sand and clay materials are presented in Table 4.1.

Table 4.1 Classification parameters of soil materials

Soil Material	Index Properties								USCS Group Symbols
	Specific Gravity	Atterberg Limits			Sieve Analysis		Granulemetric Coefficients		
	Gs	ω_L %	ω_P %	I_P %	-No.4 %	-No.200 %	C_u	C_c	
Coarse Gravel	2.715	-	NP	-	0.0	0.0	1.33	0.97	GP
Fine Gravel	2.714	-	NP	-	0.93	0.0	1.89	0.98	GP
Natural Sand	2.679	-	NP	-	99.3	2.9	10.67	1.44	SW
Salihli Clay	2.730	58	27	31	100.0	95.7	-	-	CH

4.2 Soil Mixtures

Soil mixtures were prepared by blending the major soil components (i.e. coarse gravel, fine gravel, sand and clay) in different proportions to form 200 soil mixtures. Predetermined percent of the soil components were mixed in dry state and then were subjected to experimental tests. The proportions of four soil components used in mixtures are tabulated in Table 4.2.

Table 4.2 Proportions of soil mixtures

Mixture #	Coarse Gravel (%)	Fine Gravel (%)	Sand (%)	Clay (%)	Mixture #	Coarse Gravel (%)	Fine Gravel (%)	Sand (%)	Clay (%)
Mix.#1	10	10	20	60	**Mix.#101**	0	0	55	45
Mix.#2	5	40	30	25	**Mix.#102**	0	0	65	35
Mix.#3	0	35	50	15	**Mix.#103**	0	0	75	25
Mix.#4	0	15	40	45	**Mix.#104**	0	0	85	15
Mix.#5	15	10	35	40	**Mix.#105**	0	15	20	65
Mix.#6	10	10	50	30	**Mix.#106**	0	15	25	60
Mix.#7	0	15	15	70	**Mix.#107**	0	15	35	50
Mix.#8	5	5	30	60	**Mix.#108**	0	15	70	15
Mix.#9	0	0	20	80	**Mix.#109**	0	10	40	50
Mix.#10	0	5	45	50	**Mix.#110**	0	10	45	45
Mix.#11	10	10	60	20	**Mix.#111**	0	10	55	35
Mix.#12	5	10	70	15	**Mix.#112**	0	10	75	15
Mix.#13	0	0	95	5	**Mix.#113**	0	5	30	65
Mix.#14	15	5	50	30	**Mix.#114**	0	5	35	60
Mix.#15	0	10	65	25	**Mix.#115**	0	5	50	45
Mix.#16	10	20	50	20	**Mix.#116**	0	5	60	35
Mix.#17	5	10	30	55	**Mix.#117**	0	5	70	25
Mix.#18	15	25	40	20	**Mix.#118**	0	5	80	15
Mix.#19	10	10	60	20	**Mix.#119**	0	46	50	4
Mix.#20	5	25	40	30	**Mix.#120**	0	59	40	1
Mix.#21	0	40	30	30	**Mix.#121**	0	55	40	5
Mix.#22	0	50	30	20	**Mix.#122**	0	54	36	10
Mix.#23	0	60	20	20	**Mix.#123**	0	50	35	15
Mix.#24	0	65	20	15	**Mix.#124**	0	70	23	7
Mix.#25	0	55	25	20	**Mix.#125**	0	20	10	70
Mix.#26	0	20	40	40	**Mix.#126**	0	20	15	65
Mix.#27	0	15	45	40	**Mix.#127**	0	20	20	60
Mix.#28	0	10	50	40	**Mix.#128**	0	20	25	55
Mix.#29	0	5	55	40	**Mix.#129**	0	20	75	5
Mix.#30	0	0	60	40	**Mix.#130**	0	25	10	65
Mix.#31	0	20	50	30	**Mix.#131**	0	25	15	60
Mix.#32	0	15	55	30	**Mix.#132**	0	25	20	55
Mix.#33	0	10	60	30	**Mix.#133**	0	25	25	50
Mix.#34	0	5	65	30	**Mix.#134**	0	25	35	40
Mix.#35	0	0	70	30	**Mix.#135**	0	25	45	30
Mix.#36	5	15	30	50	**Mix.#136**	0	25	65	10
Mix.#37	0	20	35	45	**Mix.#137**	0	30	65	5
Mix.#38	0	20	45	35	**Mix.#138**	0	30	60	10
Mix.#39	0	20	55	25	**Mix.#139**	0	30	55	15
Mix.#40	0	20	65	15	**Mix.#140**	0	30	50	20
Mix.#41	0	20	60	20	**Mix.#141**	0	30	45	25
Mix.#42	0	15	65	20	**Mix.#142**	0	30	40	30
Mix.#43	0	10	70	20	**Mix.#143**	0	30	35	35
Mix.#44	0	5	75	20	**Mix.#144**	0	30	30	40
Mix.#45	0	0	80	20	**Mix.#145**	0	30	25	45
Mix.#46	0	20	70	10	**Mix.#146**	0	30	20	50
Mix.#47	0	15	75	10	**Mix.#147**	0	30	15	55
Mix.#48	0	10	80	10	**Mix.#148**	0	30	10	60
Mix.#49	0	5	85	10	**Mix.#149**	0	40	55	5
Mix.#50	0	0	90	10	**Mix.#150**	0	40	50	10
Mix.#51	0	20	76	4	**Mix.#151**	0	15	80	5
Mix.#52	0	15	81	4	**Mix.#152**	0	10	85	5
Mix.#53	0	10	86	4	**Mix.#153**	0	5	90	5
Mix.#54	0	5	91	4	**Mix.#154**	0	15	50	35
Mix.#55	0	0	96	4	**Mix.#155**	0	25	55	20
Mix.#56	0	10	35	55	**Mix.#156**	0	15	60	25
Mix.#57	0	5	40	55	**Mix.#157**	0	25	71	4
Mix.#58	0	10	30	60	**Mix.#158**	0	30	66	4
Mix.#59	0	10	25	65	**Mix.#159**	0	35	58	7
Mix.#60	0	5	25	70	**Mix.#160**	0	0	93	7
Mix.#61	0	5	20	75	**Mix.#161**	0	5	88	7
Mix.#62	0	5	15	80	**Mix.#162**	0	10	83	7
Mix.#63	0	5	10	85	**Mix.#163**	0	15	78	7
Mix.#64	0	55	41	4	**Mix.#164**	0	20	73	7
Mix.#65	0	60	36	4	**Mix.#165**	0	25	68	7
Mix.#66	0	70	26	4	**Mix.#166**	0	30	63	7
Mix.#67	0	80	16	4	**Mix.#167**	0	0	88	12

Table 4.2 Proportions of soil mixtures (continued)

Mixture #	Coarse Gravel (%)	Fine Gravel (%)	Sand (%)	Clay (%)	Mixture #	Coarse Gravel (%)	Fine Gravel (%)	Sand (%)	Clay (%)
Mix.#68	0	75	21	4	**Mix.#168**	0	5	83	12
Mix.#69	0	25	30	45	**Mix.#169**	0	10	78	12
Mix.#70	0	25	40	35	**Mix.#170**	0	15	73	12
Mix.#71	0	25	50	25	**Mix.#171**	0	20	68	12
Mix.#72	0	25	60	15	**Mix.#172**	0	25	63	12
Mix.#73	0	25	70	5	**Mix.#173**	0	30	58	12
Mix.#74	0	50	40	10	**Mix.#174**	0	0	83	17
Mix.#75	0	55	35	10	**Mix.#175**	0	5	78	17
Mix.#76	0	60	30	10	**Mix.#176**	0	10	73	17
Mix.#77	0	65	25	10	**Mix.#177**	0	15	68	17
Mix.#78	0	70	20	10	**Mix.#178**	0	20	63	17
Mix.#79	0	35	40	25	**Mix.#179**	0	25	58	17
Mix.#80	0	35	45	20	**Mix.#180**	0	30	53	17
Mix.#81	0	35	55	10	**Mix.#181**	0	0	78	22
Mix.#82	0	35	60	5	**Mix.#182**	0	5	73	22
Mix.#83	0	45	30	25	**Mix.#183**	0	10	68	22
Mix.#84	0	45	35	20	**Mix.#184**	0	15	63	22
Mix.#85	0	45	40	15	**Mix.#185**	0	20	58	22
Mix.#86	0	45	45	10	**Mix.#186**	0	25	53	22
Mix.#87	0	45	50	5	**Mix.#187**	0	30	48	22
Mix.#88	0	20	30	50	**Mix.#188**	0	0	73	27
Mix.#89	0	15	30	55	**Mix.#189**	0	5	68	27
Mix.#90	0	60	35	5	**Mix.#190**	0	10	63	27
Mix.#91	0	60	35	5	**Mix.#191**	0	15	58	27
Mix.#92	0	55	35	10	**Mix.#192**	0	20	53	27
Mix.#93	0	55	35	10	**Mix.#193**	0	25	48	27
Mix.#94	0	55	30	15	**Mix.#194**	0	30	43	27
Mix.#95	0	55	38	7	**Mix.#195**	0	0	68	32
Mix.#96	0	55	33	12	**Mix.#196**	0	5	63	32
Mix.#97	0	55	28	17	**Mix.#197**	0	10	58	32
Mix.#98	0	55	20	25	**Mix.#198**	0	15	53	32
Mix.#99	0	55	15	30	**Mix.#199**	0	20	48	32
Mix.#100	0	0	50	50	**Mix.#200**	0	25	43	32

4.2.1 Grain Size Distributions of Soil Mixtures

The grain size distributions of 200 soil mixtures that were used in compaction tests were obtained by multiplying base curves (i.e. source materials' grain size distribution curves) with corresponding weight factors. Accordingly obtained grain size distribution curves of the soil mixtures fall in the variation range shown in Figure 4.2.

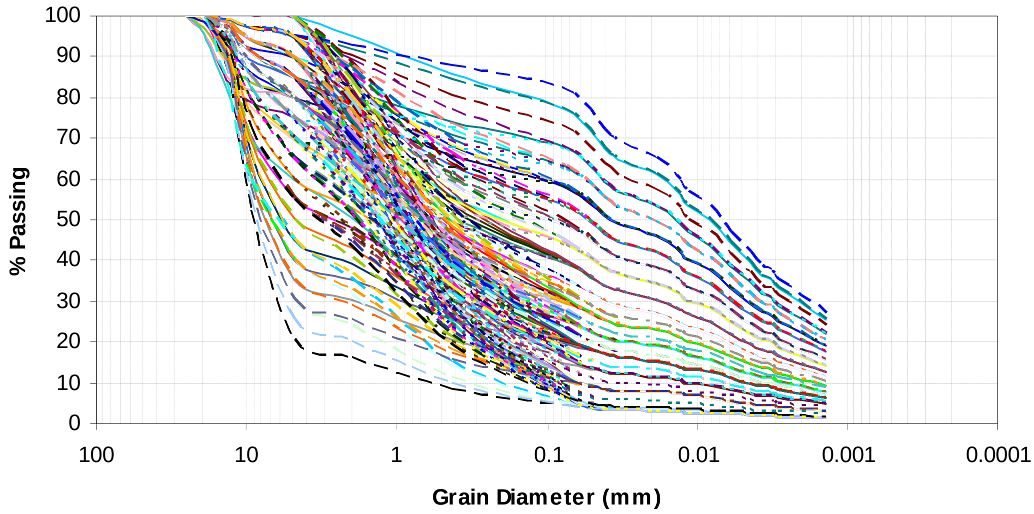

Figure 4.2 Grain size distribution curves range of 200 soil mixtures

4.2.2 Consistency Limits of Soil Mixtures

Liquid and plastic limit tests were performed on 45 different soil mixtures. The liquid limit values of the tested soil mixtures were determined using fall-cone test method as described in BS 1377. The plastic limit values of the tested soil mixtures were determined in accordance with ASTM D 4318-98. These representative soil mixtures include a wide variety of sand and clay proportion (Table 4.2). In order to determine liquid and plastic limit values of the remaining soil mixtures, multiple linear regression (MLR) analyses were conducted using MINITAB statistical commercial computer program. The sand and clay ratios were used as independent variables in MLR analysis. The following equations were obtained in statistical analyses and used to calculate ω_L and ω_P of the remaining soil mixtures.

$$w_L\,(\%) = 48.4 - 0.253 \cdot (Sand\ \ Ratio) + 0.146 \cdot (Clay\,Ratio) \qquad [R^2 = 0.91] \tag{4.1}$$

$$w_P\,(\%) = 14.3 + 0.002 \cdot (Sand\ \ Ratio) + 0.144 \cdot (Clay\,Ratio) \qquad [R^2 = 0.87] \tag{4.2}$$

where the sand ratio and clay ratio are expressed as percent. In Figure 4.3, the linear relationship between predicted and actual values of consistency limits are shown.

The solid lines indicate the 45° line whereas the dashed lines correspond to the regression equations.

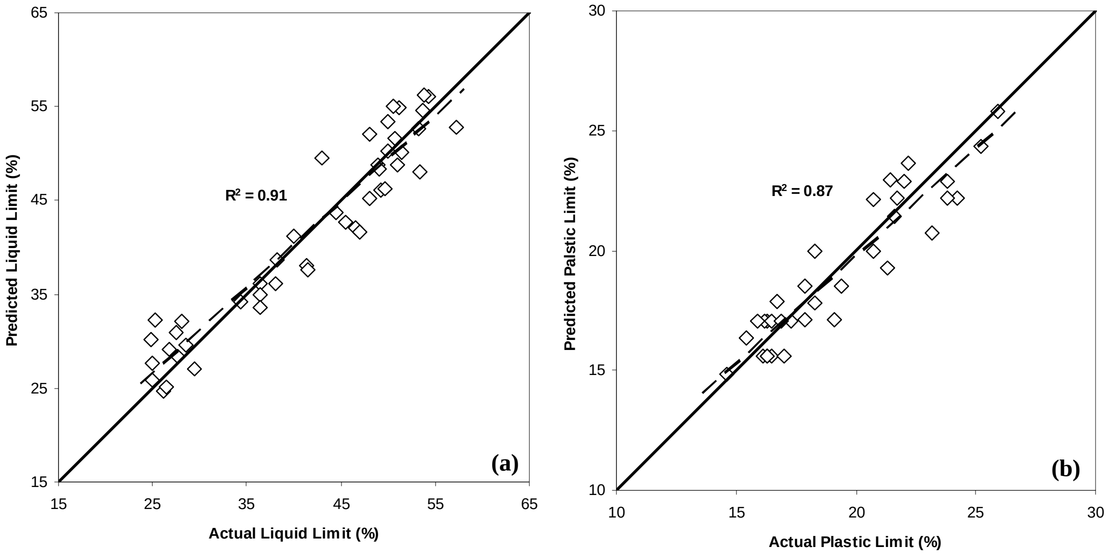

Figure 4.3 MLR analysis results for (a) ω_L and (b) ω_P.

Table 4.2 Soil mixtures used for predicting liquid and plastic limits

Soil Mixture	Sand (%)	Clay (%)	w_L (%)	w_P (%)
1	20	60	48.0	20.7
7	15	70	51.2	21.4
8	30	60	43.0	18.9
9	20	80	50.6	22.2
13	95	5	26.4	NP
16	50	20	38.2	15.4
17	30	55	51.0	20.7
18	40	20	40.0	17.9
19	60	20	36.5	19.1
20	40	30	45.5	16.7
21	30	30	48.0	18.3
22	30	20	44.5	17.3
28	50	40	47.0	19.4
33	60	30	41.5	21.5
36	30	50	53.4	18.3
37	35	45	49.2	21.3
38	45	35	46.5	22.5
39	55	25	41.4	16.5
40	65	15	34.3	22.4
41	60	20	38.0	20.9
42	65	20	36.5	16.3
43	70	20	36.4	16.2
46	70	10	28.1	16.1
47	75	10	27.5	16.3
48	80	10	28.6	16.5
49	85	10	27.7	17.0
50	90	10	29.4	16.3
55	96	4	26.2	NP

Table 4.2 Soil mixtures used for predicting liquid and plastic limits (continued)

Soil Mixture	Sand (%)	Clay (%)	w_L (%)	w_P (%)
57	40	55	49.6	17.9
59	25	65	50.7	19.4
62	15	80	53.8	18.9
89	30	55	49.0	23.2
105	20	65	57.2	19.8
113	30	65	50.0	22.0
114	35	60	49.1	21.7
125	10	70	54.3	19.6
128	25	55	51.5	21.6
129	75	5	24.8	NP
131	15	60	50.0	23.8
147	15	55	53.3	24.2
148	10	60	53.7	23.8
152	85	5	24.9	NP
158	66	4	25.2	NP
160	93	7	24.9	NP
168	83	12	26.8	NP

Index properties (liquid and plastic limits, and percent passing through No.4 and No.200 sieves) and Unified Soil Classification System (USCS) group symbols of the soil mixtures were presented in Table 4.3. It can be seen from Table 4.3 that the index properties and USCS of the soil mixtures exhibit a wide variation ranging from well-graded gravels to highly plastic inorganic clays.

Table 4.3 Soil mixture index properties

Soil Mixture	w_L (%)	w_P (%)	- No.4 (%)	- No.200 (%)	USCS Symbol
Mix.#1	48.0	20.7	80.0	58.0	CH
Mix.#2	44.5	18.0	55.2	24.8	SC
Mix.#3	37.9	16.6	55.1	15.5	SC
Mix.#4	44.9	20.9	84.9	44.2	SC
Mix.#5	45.4	20.1	74.9	39.3	SC
Mix.#6	40.1	18.7	79.9	31.5	SC
Mix.#7	51.2	21.4	85.1	70.2	CH
Mix.#8	43.0	18.9	89.4	60.3	CH
Mix.#9	50.6	22.2	99.8	79.8	CH
Mix.#10	44.3	21.6	94.7	50.1	CH
Mix.#11	36.1	17.3	79.6	19.7	SC
Mix.#12	32.9	16.6	84.4	14.7	SC
Mix.#13	26.4	NP	99.3	7.5	SW-SM
Mix.#14	40.1	18.7	79.5	29.9	SC
Mix.#15	35.6	18.0	89.5	24.8	SC
Mix.#16	38.2	15.4	69.8	20.6	SC
Mix.#17	51.0	20.7	84.9	53.5	CH
Mix.#18	40.0	17.9	69.9	20.6	SC
Mix.#19	36.5	19.1	79.7	20.9	SC
Mix.#20	45.5	16.7	70.0	29.9	SC
Mix.#21	48.0	18.3	60.2	29.6	SC
Mix.#22	44.5	17.3	50.3	20.0	SC
Mix.#23	46.3	17.2	40.4	19.7	GC
Mix.#24	45.5	16.5	35.5	14.9	GC
Mix.#25	45.0	17.2	45.3	19.9	GC
Mix.#26	44.1	20.1	79.9	39.4	SC
Mix.#27	42.9	20.2	84.8	39.6	SC
Mix.#28	47.0	19.4	89.7	39.7	SC
Mix.#29	40.3	20.2	94.7	39.9	SC
Mix.#30	39.1	20.2	99.6	40.0	SC

Table 4.3 Soil mixture index properties (continued)

Soil Mixture	w_L (%)	w_P (%)	- No.4 (%)	- No.200 (%)	USCS Symbol
Mix.#31	40.1	18.7	79.8	30.2	SC
Mix.#32	38.9	18.7	84.8	30.3	SC
Mix.#33	41.5	21.5	89.7	30.5	SC
Mix.#34	36.3	18.8	94.6	30.6	SC
Mix.#35	35.1	18.8	99.5	30.7	SC
Mix.#36	53.4	18.3	80.0	48.7	SC
Mix.#37	49.2	21.3	79.9	44.1	SC
Mix.#38	46.5	22.5	79.9	34.8	SC
Mix.#39	41.4	16.5	79.8	25.5	SC
Mix.#40	34.3	22.4	79.7	16.2	SC
Mix.#41	38.0	20.9	79.8	20.9	SC
Mix.#42	36.5	16.3	84.7	21.0	SC
Mix.#43	36.4	16.2	89.6	21.2	SC
Mix.#44	32.3	17.3	94.5	21.3	SC
Mix.#45	31.1	17.3	99.4	21.5	SC
Mix.#46	28.1	16.1	79.7	11.6	SW-SC
Mix.#47	27.5	16.3	84.6	11.7	SW-SC
Mix.#48	28.6	16.5	89.5	11.9	SW-SC
Mix.#49	27.7	17.0	94.5	12.0	SW-SC
Mix.#50	29.4	16.3	99.4	12.2	SW-SC
Mix.#51	29.8	NP	79.7	6.0	SW-SM
Mix.#52	28.5	NP	84.6	6.2	SW-SM
Mix.#53	27.2	NP	89.5	6.3	SW-SM
Mix.#54	26.0	NP	94.4	6.5	SW-SM
Mix.#55	26.2	NP	99.3	6.6	SW-SM
Mix.#56	47.6	22.3	89.9	53.7	CH
Mix.#57	49.6	17.9	94.8	53.8	CH
Mix.#58	49.6	23.0	89.9	58.3	CH
Mix.#59	50.7	19.4	89.9	62.9	CH
Mix.#60	52.3	24.4	94.9	67.7	CH
Mix.#61	54.3	25.1	94.9	72.4	CH
Mix.#62	53.8	18.9	94.9	77.0	CH
Mix.#63	58.3	26.6	95.0	81.6	CH
Mix.#64	38.6	NP	45.2	5.0	GW
Mix.#65	39.9	NP	40.3	4.9	GW
Mix.#66	42.4	NP	30.5	4.6	GP
Mix.#67	44.9	NP	20.6	4.3	GP
Mix.#68	43.7	NP	10.8	4.0	GP
Mix.#69	47.4	20.8	75.0	43.9	SC
Mix.#70	43.4	19.4	75.0	34.7	SC
Mix.#71	39.4	18.0	74.9	25.4	SC
Mix.#72	35.4	16.6	74.8	16.1	SC
Mix.#73	31.4	NP	74.8	6.8	SW-SM
Mix.#74	39.7	15.8	50.2	10.7	GW-GC
Mix.#75	41.0	15.8	45.3	10.6	GW-GC
Mix.#76	42.3	15.8	40.4	10.4	GP-GC
Mix.#77	43.5	15.8	35.4	10.3	GP-GC
Mix.#78	44.8	15.8	30.5	10.2	GP-GC
Mix.#79	41.9	18.0	65.1	25.1	SC
Mix.#80	39.9	17.3	65.0	20.4	SC
Mix.#81	35.9	15.9	64.9	11.2	SC
Mix.#82	34.0	NP	64.9	6.5	SW-SC
Mix.#83	44.5	18.0	55.2	24.8	GP-GC
Mix.#84	42.5	17.3	55.2	20.2	GP-GC
Mix.#85	40.5	16.5	55.1	15.5	GP-GC
Mix.#86	38.5	15.8	55.1	10.9	GP-GC
Mix.#87	36.5	NP	55.1	6.2	SW-SM
Mix.#88	48.1	21.6	80.0	48.7	SC
Mix.#89	49.0	23.2	84.9	53.5	CH
Mix.#90	40.3	NP	40.3	5.8	GW-GM
Mix.#91	40.3	NP	40.3	5.8	GP-GM
Mix.#92	41.0	15.8	45.3	10.6	GW-GC
Mix.#93	41.0	15.8	45.3	10.6	GP-GC
Mix.#94	43.0	16.5	45.3	15.2	GC
Mix.#95	39.8	NP	45.25	7.8	GW-GM
Mix.#96	41.8	16.1	45.29	12.4	GP-GM

Table 4.3 Soil mixture index properties (continued)

Soil Mixture	w_L (%)	w_P (%)	- No.4 (%)	- No.200 (%)	USCS Symbol
Mix.#97	43.8	16.8	45.32	17.1	GW-GC
Mix.#98	47.0	17.9	45.38	24.5	GP-GC
Mix.#99	49.0	18.7	45.41	29.2	GC
Mix.#100	43.1	21.6	99.7	49.3	SC
Mix.#101	41.1	20.9	99.6	44.7	SC
Mix.#102	37.1	19.5	99.6	35.4	SC
Mix.#103	33.1	18.1	99.5	26.1	SC
Mix.#104	29.1	16.6	99.4	16.8	SC
Mix.#105	57.2	19.8	85.0	62.8	CH
Mix.#106	50.8	23.0	85.0	58.1	CH
Mix.#107	46.8	21.6	84.9	48.9	SC
Mix.#108	32.9	16.6	84.7	16.4	SC
Mix.#109	45.6	21.6	89.8	49.0	CH
Mix.#110	43.6	20.9	89.8	44.4	SC
Mix.#111	39.6	19.5	89.7	35.1	SC
Mix.#112	31.6	16.6	89.6	16.5	SC
Mix.#113	50.0	22.0	94.8	63.1	CH
Mix.#114	49.1	21.7	94.8	58.4	CH
Mix.#115	42.3	20.9	94.7	44.5	SC
Mix.#116	38.3	19.5	94.6	35.2	SC
Mix.#117	34.3	18.0	94.6	26.0	SC
Mix.#118	30.4	16.6	94.5	16.7	SC
Mix.#119	36.3	NP	55.7	5.2	SW-SM
Mix.#120	38.4	NP	40.7	1.6	GW
Mix.#121	39.0	NP	45.2	5.9	SW-SM
Mix.#122	40.8	15.8	46.9	10.9	GW-GM
Mix.#123	41.7	16.5	49.3	14.7	GC
Mix.#124	43.6	15.4	32.0	6.9	GC
Mix.#125	54.3	19.6	80.1	67.3	CH
Mix.#126	54.1	23.7	80.1	62.6	CH
Mix.#127	52.1	23.0	80.0	58.0	CH
Mix.#128	51.5	21.6	80.0	53.4	CH
Mix.#129	24.8	NP	79.7	7.0	SW-SM
Mix.#130	55.4	23.7	75.2	62.5	CH
Mix.#131	50.0	23.8	75.1	57.9	CH
Mix.#132	51.4	22.3	75.1	53.2	CH
Mix.#133	49.4	21.6	75.1	48.6	SC
Mix.#134	45.4	20.1	75.0	39.3	SC
Mix.#135	41.4	18.7	74.9	30.0	SC
Mix.#136	33.4	15.9	74.8	11.5	SC
Mix.#137	32.7	NP	69.8	6.7	SW-SM
Mix.#138	34.7	15.9	69.9	11.3	SW-SC
Mix.#139	36.7	16.6	69.9	16.0	SC
Mix.#140	38.7	17.3	69.9	20.6	SC
Mix.#141	40.7	18.0	70.0	25.2	SC
Mix.#142	42.7	18.7	70.0	29.9	SC
Mix.#143	44.7	19.4	70.0	34.5	SC
Mix.#144	46.7	20.1	70.1	39.2	SC
Mix.#145	48.6	20.8	70.1	43.8	GC
Mix.#146	50.6	21.5	70.1	48.4	GC
Mix.#147	52.6	22.3	70.2	53.1	CH
Mix.#148	54.6	23.0	70.2	57.7	CH
Mix.#149	35.2	NP	60.0	6.4	SW-SM
Mix.#150	37.2	15.8	60.0	11.0	SW-SC
Mix.#151	28.9	NP	84.6	7.1	SW-SM
Mix.#152	24.9	NP	89.5	7.3	SW-SM
Mix.#153	26.4	NP	94.4	7.4	SW-SM
Mix.#154	40.9	19.4	84.8	34.9	SC
Mix.#155	37.4	17.3	74.9	20.7	SC
Mix.#156	36.9	18.0	84.7	25.7	SC
Mix.#157	31.0	NP	74.7	5.9	SW-SM
Mix.#158	25.2	NP	69.8	5.7	SW-SM
Mix.#159	34.7	15.4	69.9	11.3	SW-SC
Mix.#160	24.9	NP	99.4	9.4	SW-SM
Mix.#161	27.2	NP	94.4	9.3	SW-SM
Mix.#162	28.4	NP	89.5	9.1	SW-SM

Table 4.3 Soil mixture index properties (continued)

Soil Mixture	w_L (%)	w_P (%)	- No.4 (%)	- No.200 (%)	USCS Symbol
Mix.#163	29.7	NP	84.6	9.0	SW-SM
Mix.#164	31.0	NP	79.7	8.8	SW-SM
Mix.#165	32.2	NP	74.8	8.7	SW-SM
Mix.#166	33.5	NP	69.8	8.5	SW-SM
Mix.#167	27.9	NP	99.4	14.0	SC
Mix.#168	26.8	NP	94.5	13.9	SC
Mix.#169	30.4	16.2	89.6	13.8	SC
Mix.#170	31.7	16.2	84.6	13.6	SC
Mix.#171	32.9	16.2	79.7	13.5	SC
Mix.#172	34.2	16.2	74.8	13.3	SC
Mix.#173	35.5	16.1	69.9	13.2	SC
Mix.#174	29.9	16.9	99.4	18.7	SC
Mix.#175	31.1	16.9	94.5	18.5	SC
Mix.#176	32.4	16.9	89.6	18.4	SC
Mix.#177	33.7	16.9	84.7	18.2	SC
Mix.#178	34.9	16.9	79.8	18.1	SC
Mix.#179	36.2	16.9	74.8	18.0	SC
Mix.#180	37.5	16.9	69.9	17.8	SC
Mix.#181	31.9	17.6	99.5	23.3	SC
Mix.#182	33.1	17.6	94.5	23.2	SC
Mix.#183	34.4	17.6	89.6	23.0	SC
Mix.#184	35.7	17.6	84.7	22.9	SC
Mix.#185	36.9	17.6	79.8	22.7	SC
Mix.#186	38.2	17.6	74.9	22.6	SC
Mix.#187	39.5	17.6	69.9	22.4	SC
Mix.#188	33.9	18.3	99.5	28.0	SC
Mix.#189	35.1	18.3	94.6	27.8	SC
Mix.#190	36.4	18.3	89.7	27.7	SC
Mix.#191	37.7	18.3	84.7	27.5	SC
Mix.#192	38.9	18.3	79.8	27.4	SC
Mix.#193	40.2	18.3	74.9	27.2	SC
Mix.#194	41.5	18.3	70.0	27.1	SC
Mix.#195	35.9	19.0	99.5	32.6	SC
Mix.#196	37.1	19.0	94.6	32.5	SC
Mix.#197	38.4	19.0	89.7	32.3	SC
Mix.#198	39.7	19.0	84.8	32.2	SC
Mix.#199	40.9	19.0	79.9	32.0	SC
Mix.#200	42.2	19.0	74.9	31.9	SC

4.2.3 Compaction Tests Results of Soil Mixtures

In this thesis, both Standard Proctor (ASTM D 698) and Modified Proctor (ASTM D 1557) compaction tests were performed on 200 soil mixtures. The compaction characteristics of dry unit weight (γ_{dmax}) and optimum water content (ω_{opt}) were determined. Based on the study of Howell et al. (1997), the predetermined proportions of soil materials were blended in their dry state using a hand spoon. Afterwards, predetermined portion of water was added with a spray bottle into soil mixtures and then they were cured in a covered plastic bag for a day. After curing period, the soil mixtures were compacted by means of an automatic soil compactor machine capable of compacting the soil mixtures under both standard and modified

Proctor compaction energy levels (Figure 4.4). This machine can also compact the soil mixture either in 4″ mold or 6″ mold.

Figure 4.4 Automatic
soil compactor machine

Howell et al. (1997) mentioned that γ_{dmax} and ω_{opt} of the tested soil could be determined by drawing a third-order polynomial curve on the measured compaction data. In this thesis, however, cubic splines were constructed of piecewise between each measured compaction data point. A typical third-order polynomial curve fitting method involves forming one equation through all data points. In contrast, cubic spline curve fitting method allows provides a unique equation between each data point. The second derivative of each equation is commonly set to zero at the end points in cubic spline method. In order to fit cubic splines between the measured compaction data points, an iteration algorithm was developed in Matlab. The gradient of fitted cubic splines was calculated at each iteration step. The optimum point of compaction curve was determined when the gradient was equal to zero. The compaction characteristics obtained from Standard and Modified Proctor tests are presented in Table 4.4. Standard and Modified compaction curves of soil mixtures are plotted in Figure 4.5 and Figure 4.6, respectively.

Table 4.4 Compaction characteristics of soil mixtures

Soil Mixture	Standard Proctor Test		Modified Proctor Test	
	g_{dmax} (kN/m^3)	w_{opt} (%)	g_{dmax} (kN/m^3)	w_{opt} (%)
Mix.#1	18.431	13.83	20.708	9.37
Mix.#2	20.571	8.88	21.920	6.62
Mix.#3	21.162	8.37	22.175	5.32
Mix.#4	18.993	12.22	20.911	9.20
Mix.#5	18.354	13.00	20.734	8.49
Mix.#6	21.346	7.28	21.852	6.35
Mix.#7	17.522	18.08	19.731	10.88
Mix.#8	17.866	15.60	19.988	10.41
Mix.#9	16.407	19.65	19.719	10.30
Mix.#10	18.384	13.87	20.428	9.39
Mix.#11	20.523	10.03	21.937	6.65
Mix.#12	20.183	9.17	21.554	6.32
Mix.#13	19.114	10.52	21.004	7.46
Mix.#14	19.726	9.98	21.564	7.35
Mix.#15	19.726	10.04	21.475	7.03
Mix.#16	19.710	10.74	21.825	6.58
Mix.#17	18.592	13.49	20.411	9.61
Mix.#18	19.873	9.66	22.040	6.45
Mix.#19	20.139	9.15	21.817	7.14
Mix.#20	19.454	10.50	21.619	7.52
Mix.#21	20.309	9.06	21.839	6.97
Mix.#22	21.283	7.67	22.052	5.66
Mix.#23	20.612	7.68	22.169	5.95
Mix.#24	21.062	6.18	22.593	5.69
Mix.#25	20.767	7.03	22.349	5.72
Mix.#26	19.460	12.14	21.109	8.72
Mix.#27	19.149	11.69	21.146	8.55
Mix.#28	19.263	11.39	21.569	7.32
Mix.#29	18.846	13.69	21.032	7.45
Mix.#30	18.696	13.04	20.917	8.00
Mix.#31	19.930	10.17	21.603	7.16
Mix.#32	19.854	10.96	21.535	7.63
Mix.#33	19.414	11.57	21.304	7.27
Mix.#34	19.466	11.56	21.283	6.87
Mix.#35	19.288	10.74	21.195	7.52
Mix.#36	18.931	13.07	20.977	9.85
Mix.#37	19.085	12.64	21.195	8.27
Mix.#38	19.818	10.44	21.441	7.44
Mix.#39	20.091	9.32	21.763	6.88
Mix.#40	20.687	8.59	21.873	6.75
Mix.#41	20.357	8.60	21.783	6.56
Mix.#42	20.092	8.97	21.948	6.52
Mix.#43	20.026	9.38	21.805	6.54
Mix.#44	19.775	9.82	21.568	7.07
Mix.#45	19.727	9.61	21.434	6.74
Mix.#46	20.768	8.50	21.873	6.43
Mix.#47	20.434	9.41	21.747	5.75
Mix.#48	20.183	9.61	21.561	6.15
Mix.#49	19.984	10.09	21.466	6.49
Mix.#50	19.615	11.37	21.334	7.31
Mix.#51	20.154	10.04	21.730	6.42
Mix.#52	19.666	10.82	21.691	7.66
Mix.#53	19.624	11.17	21.504	6.93
Mix.#54	19.151	12.20	21.340	7.45
Mix.#55	19.097	12.14	21.014	7.66
Mix.#56	18.051	15.58	20.788	9.61
Mix.#57	18.057	15.18	20.448	9.48
Mix.#58	17.839	15.51	20.308	11.46
Mix.#59	17.379	16.40	20.118	10.89
Mix.#60	17.139	17.67	19.797	11.66
Mix.#61	16.935	17.10	19.811	11.62
Mix.#62	16.670	19.21	19.280	12.40
Mix.#63	16.436	19.15	19.158	11.94
Mix.#64	21.469	7.40	22.827	5.08
Mix.#65	21.210	7.75	23.235	5.38
Mix.#66	21.231	8.26	22.516	5.03
Mix.#67	20.768	8.83	23.275	5.72

Table 4.4 Compaction characteristics of soil mixtures (continued)

Soil Mixture	**Standard Proctor Test**		**Modified Proctor Test**	
	g_{dmax} **(kN/m^3)**	w_{opt} **(%)**	g_{dmax} **(kN/m^3)**	w_{opt} **(%)**
Mix.#68	21.104	7.79	22.571	5.95
Mix.#69	19.485	11.41	21.149	9.00
Mix.#70	20.131	9.18	21.763	7.50
Mix.#71	20.646	8.74	22.221	6.10
Mix.#72	20.680	8.19	22.336	5.68
Mix.#73	20.513	10.40	21.729	5.78
Mix.#74	21.126	7.48	22.307	5.61
Mix.#75	21.361	8.40	22.980	5.43
Mix.#76	21.118	7.76	22.903	5.23
Mix.#77	20.958	9.06	22.843	5.20
Mix.#78	20.841	10.09	22.677	5.49
Mix.#79	19.940	10.26	22.087	6.36
Mix.#80	20.265	9.42	22.244	5.83
Mix.#81	20.736	8.65	22.271	6.25
Mix.#82	20.347	9.90	22.213	6.37
Mix.#83	20.682	8.39	22.166	6.67
Mix.#84	20.647	8.44	22.287	6.07
Mix.#85	20.989	8.30	22.550	5.48
Mix.#86	21.085	9.70	22.462	5.69
Mix.#87	21.274	7.54	22.123	5.91
Mix.#88	18.618	12.45	21.238	8.62
Mix.#89	18.196	13.50	20.698	9.56
Mix.#90	21.654	7.49	22.330	5.42
Mix.#91	21.805	6.94	22.461	5.47
Mix.#92	21.669	7.55	22.205	4.83
Mix.#93	21.849	8.16	22.418	5.17
Mix.#94	21.185	8.47	22.370	5.69
Mix.#95	21.251	7.29	21.917	5.84
Mix.#96	20.867	8.94	21.796	6.43
Mix.#97	20.372	9.73	21.785	6.76
Mix.#98	20.414	8.40	21.553	6.97
Mix.#99	19.485	11.29	21.496	8.31
Mix.#100	18.312	13.10	20.668	8.63
Mix.#101	18.423	12.88	20.783	8.01
Mix.#102	18.849	11.63	20.824	7.77
Mix.#103	19.427	11.26	21.480	6.27
Mix.#104	19.379	11.45	21.340	6.53
Mix.#105	17.624	15.71	20.582	8.99
Mix.#106	18.069	15.30	20.541	10.84
Mix.#107	18.373	14.05	20.872	8.12
Mix.#108	20.531	10.39	22.137	6.06
Mix.#109	18.482	14.15	21.039	8.74
Mix.#110	19.200	12.79	21.266	7.43
Mix.#111	19.218	10.75	21.314	7.21
Mix.#112	19.929	9.63	21.546	6.11
Mix.#113	17.721	16.58	19.959	9.77
Mix.#114	17.938	16.01	20.476	8.97
Mix.#115	18.541	13.02	20.648	8.62
Mix.#116	18.901	10.31	21.326	7.58
Mix.#117	19.372	10.85	21.511	6.71
Mix.#118	19.820	10.42	21.821	6.29
Mix.#119	21.974	10.30	23.152	7.40
Mix.#120	20.405	9.00	20.993	7.60
Mix.#121	21.112	8.77	21.966	5.91
Mix.#122	22.083	7.00	22.703	4.81
Mix.#123	20.225	9.40	21.784	6.52
Mix.#124	20.708	7.32	22.002	6.06
Mix.#125	18.590	15.36	19.724	14.03
Mix.#126	17.793	15.66	20.342	9.73
Mix.#127	18.062	14.44	20.458	10.61
Mix.#128	18.506	13.35	20.677	9.29
Mix.#129	20.051	9.11	21.811	6.54
Mix.#130	17.611	16.80	19.955	11.51
Mix.#131	17.988	16.29	20.669	9.01
Mix.#132	18.193	14.63	20.825	8.79
Mix.#133	18.604	13.29	21.352	8.05
Mix.#134	19.079	12.48	21.429	7.80

Table 4.4Compaction characteristics of soil mixtures (continued)

Soil Mixture	Standard Proctor Test		Modified Proctor Test	
	g_{dmax} (kN/m^3)	w_{opt} (%)	g_{dmax} (kN/m^3)	w_{opt} (%)
Mix.#135	19.952	10.08	21.950	5.44
Mix.#136	20.583	8.71	22.027	6.85
Mix.#137	20.129	9.45	21.847	5.67
Mix.#138	20.385	8.78	22.033	5.29
Mix.#139	20.078	10.10	21.852	6.35
Mix.#140	19.236	9.61	21.677	6.56
Mix.#141	19.545	11.24	21.601	6.27
Mix.#142	19.421	11.17	21.573	6.77
Mix.#143	19.118	12.15	21.030	7.67
Mix.#144	18.391	10.82	20.991	8.09
Mix.#145	18.345	13.99	20.922	9.59
Mix.#146	17.986	15.06	20.670	11.17
Mix.#147	17.838	16.16	20.624	10.04
Mix.#148	17.051	18.13	20.095	11.30
Mix.#149	21.104	8.01	21.809	5.57
Mix.#150	20.840	8.28	22.263	4.79
Mix.#151	19.396	10.89	21.362	6.34
Mix.#152	19.499	10.14	21.207	8.27
Mix.#153	19.181	10.02	21.111	6.73
Mix.#154	19.260	11.13	21.223	8.47
Mix.#155	20.241	9.68	22.271	6.39
Mix.#156	19.509	9.88	21.848	6.36
Mix.#157	20.348	9.61	21.901	6.67
Mix.#158	19.670	9.74	21.271	6.83
Mix.#159	20.399	9.20	21.914	6.24
Mix.#160	19.135	10.61	20.966	7.78
Mix.#161	19.485	11.69	20.944	7.11
Mix.#162	19.734	9.99	21.449	6.85
Mix.#163	19.816	9.93	21.572	7.05
Mix.#164	20.274	9.17	21.677	6.30
Mix.#165	20.651	8.58	21.932	5.54
Mix.#166	20.196	9.50	21.829	6.14
Mix.#167	19.516	11.20	21.023	6.56
Mix.#168	19.947	9.46	21.455	6.41
Mix.#169	20.341	9.23	21.517	6.62
Mix.#170	20.122	9.50	21.867	5.99
Mix.#171	20.507	9.75	22.021	5.43
Mix.#172	20.665	8.80	22.113	5.95
Mix.#173	20.388	9.26	21.599	6.05
Mix.#174	19.706	9.76	21.355	7.01
Mix.#175	19.613	9.84	21.447	6.84
Mix.#176	19.993	9.21	21.456	6.61
Mix.#177	20.028	9.12	21.939	6.81
Mix.#178	20.250	10.00	21.890	5.66
Mix.#179	20.447	9.41	22.187	6.46
Mix.#180	20.134	9.53	21.801	6.25
Mix.#181	19.273	10.59	21.229	7.24
Mix.#182	19.513	9.54	21.402	6.77
Mix.#183	19.848	9.85	21.265	7.44
Mix.#184	19.828	9.59	21.795	6.58
Mix.#185	20.165	9.17	21.806	6.16
Mix.#186	20.511	9.02	22.194	6.41
Mix.#187	19.851	10.37	21.722	6.35
Mix.#188	19.163	10.67	21.203	7.29
Mix.#189	19.217	10.84	21.280	7.42
Mix.#190	19.933	9.79	21.333	7.24
Mix.#191	19.608	9.95	21.555	6.88
Mix.#192	19.899	9.87	21.685	6.50
Mix.#193	20.154	8.51	21.874	6.58
Mix.#194	19.666	10.40	21.529	7.15
Mix.#195	19.006	11.43	21.097	7.30
Mix.#196	19.361	10.19	20.917	7.70
Mix.#197	19.685	11.34	21.255	6.86
Mix.#198	19.617	10.70	21.451	7.34
Mix.#199	19.509	10.63	21.269	7.78
Mix.#200	19.745	10.86	21.530	6.68

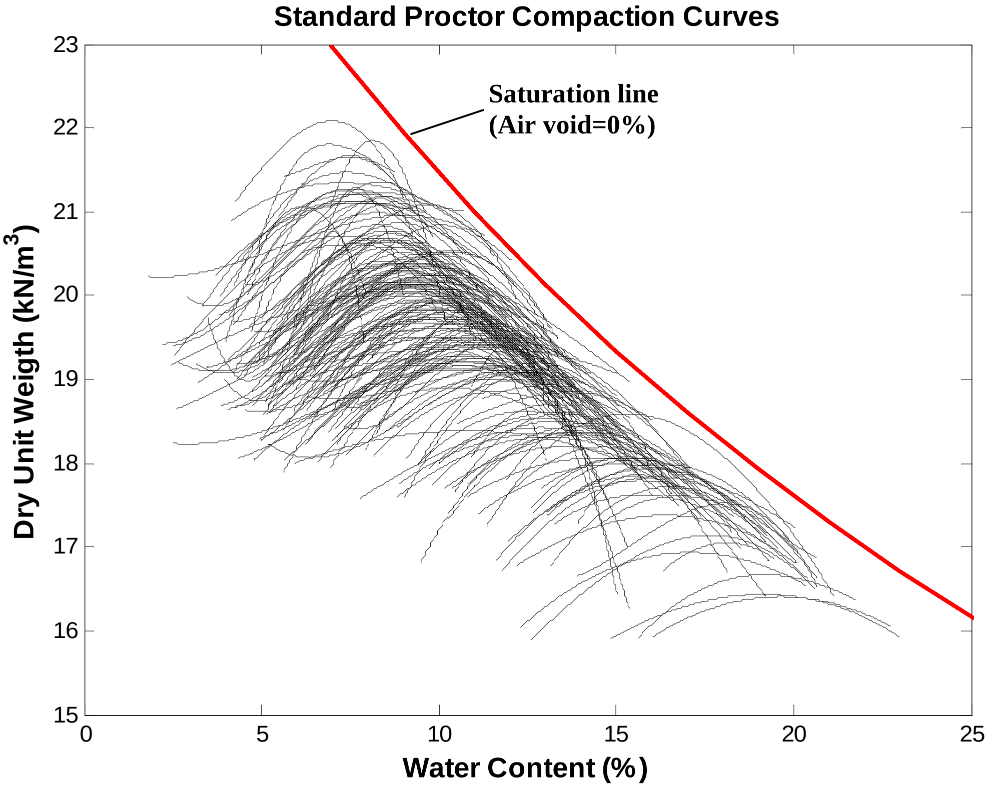

Figure 4.5 Standard Proctor compaction curves of soil mixtures

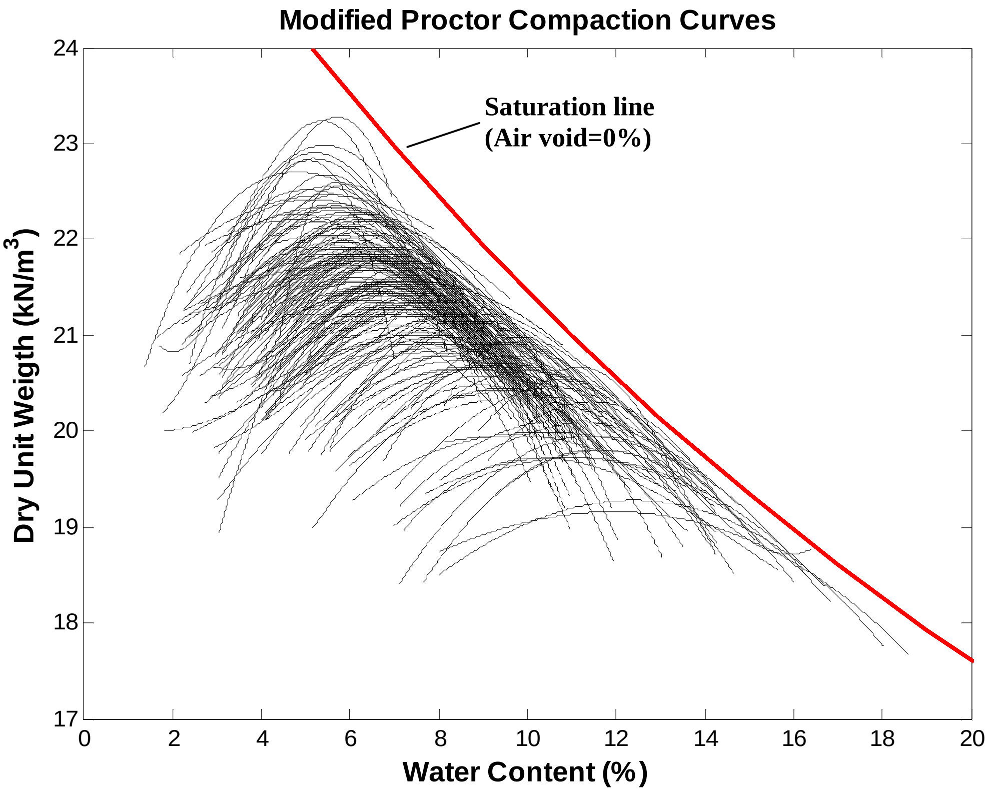

Figure 4.6 Modified Proctor compaction curves of soil mixtures

4.3 Discussion of Compaction Test Results

In this section compaction characteristics of soil mixtures are evaluated in terms of fine content. Additionally, the effect of compaction energy and the effect of automatic soil compactor are also investigated.

4.3.1 Effect of Fine Content on Compaction Behavior

Research publications available in the literature on the influence of fine content (FC) on engineering behavior of soils showed that transition from fine to coarse soil behavior can be effectively expressed by means of the intergranular void ratio concept (Thevanayagam, 1998; Thevanayagam, 2007(a), 2007(b); Monkul and Ozden, 2007). They mentioned that there is a transition zone between 20% and 30% FC for non-plastic fines and it is less than 20% for clayey fines. Below the transition zone, soils behave like a sand or gravel and beyond the transition zone fine matrix governs the behavior of soils. It is decided that, similarly, a transition zone may exist affecting the compaction behavior of gravelly and sandy soils. Some researchers focused on the influence of FC on compaction (Howell et al., 1997; Arvelo, 2004). In these studies, generally, they dealt with fine-grained soils. Ören (2007) observed similar transitional behavior on compacted bentonite-granular zeolite mixtures. He mentioned that γ_{dmax} increases up to 20% bentonite content and then starts to decrease by increasing bentonite content and vice versa for ω_{opt} (Figure 4.7).

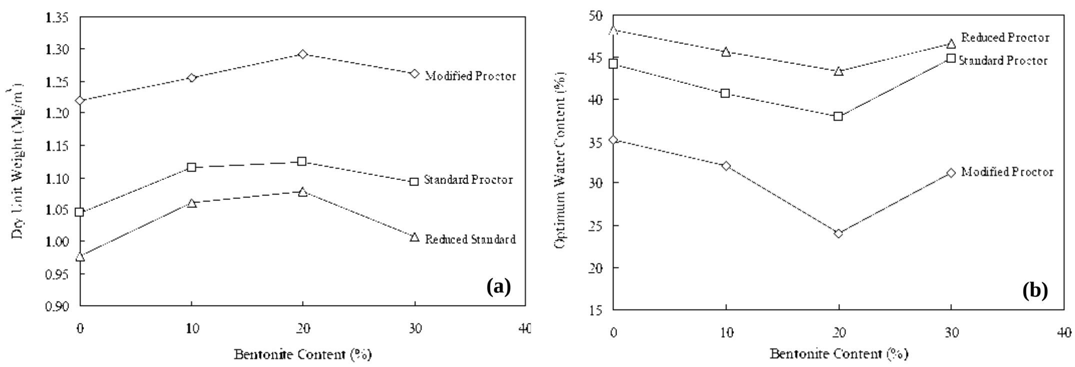

Figure 4.7 Transitional behavior of compacted bentonite-granular zeolite mixtures for (a) γ_{dmax} and (b) ω_{opt} (after Ören, 2007)

According to the present knowledge, an increase in FC of soils usually results in a decrease in γ_{dmax} causing a corresponding increase of ω_{opt}. However, a closer look at the soil mixtures revealed that γ_{dmax} increases until FC becomes 12%. Beyond this transition value γ_{dmax} decreases steadily as FC increases. A similar but reverse trend is also noticed for the relationship between ω_{opt} and FC, as depicted in Figure 4.8.

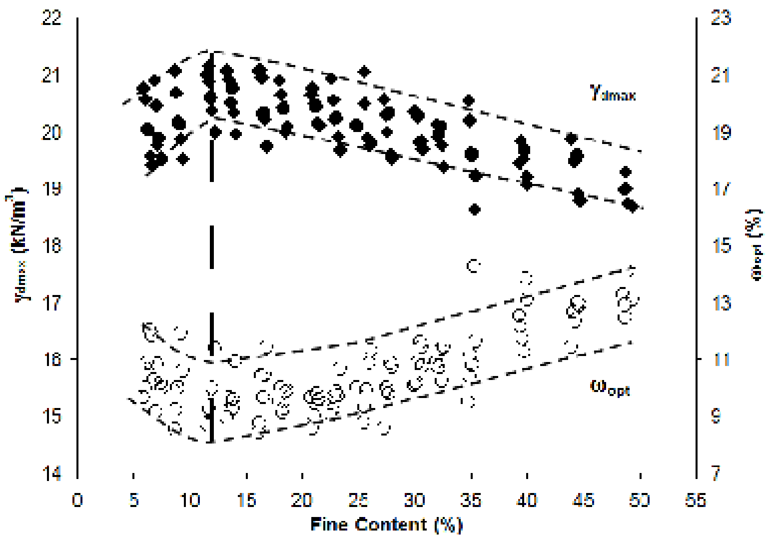

Figure 4.8 Relationship between FC-γ_{dmax} and ω_{opt}

It was considered that the discontinuity point where a transition takes place has a significant effect on compaction behavior. A dimensionless parameter was defined as "Transition Fine Content Ratio" (TFR).

$$\text{Transition Fine Content Ratio}\,\{TFR\} = \frac{\text{Fine Content of Mixture}\,\{FC\}\,(\%)}{\text{Transition Fine Content}\,\{TFC = 12\}\,(\%)} \tag{4.3}$$

The transition fine content was set to be a constant value (i.e. 12%). This value is in parallel with the observed test data and the commonly known soil classification threshold above which the soil is classified as a soil with considerable fines such as SM, SC, etc. The TFR parameter varies between 0.13 and 6.80. If TFR is less than 1, it means that coarser particles govern the compaction behavior. Conversely, the soil matrix starts to behave as fine soil after TFR is equal and higher than 1. Variations for the Standard and Modified Proctor tests γ_{dmax} and ω_{opt} with TFR are given in Figure 4.9a and Figure 4.9b, respectively.

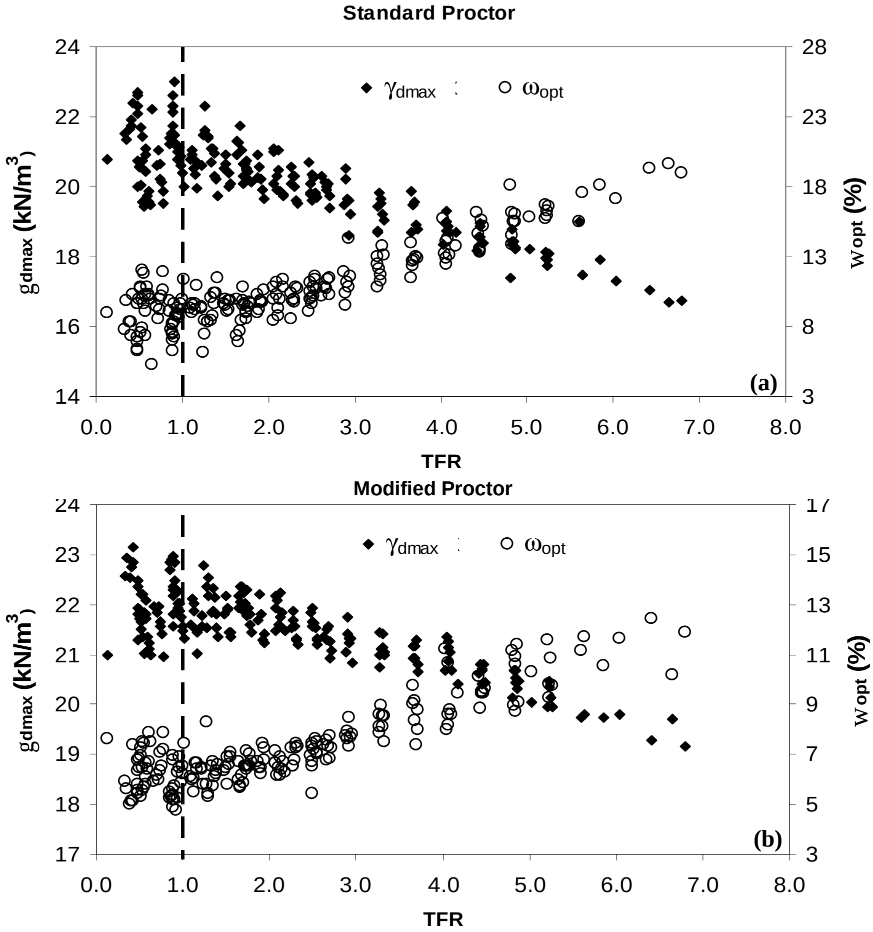

Figure 4.9 Variation of γ_{dmax} and ω_{opt} with TFR (a) Standard Proctor, (b) Modified Proctor

Thevanayagam (2007a,b) made a conceptual study on intergrain contact density of liquefiable soils. He mentioned that attempts on sands with a considerable amount of fines showed that cyclic strength of silty sand decreased until a specific transition range with an increase in FC. Beyond this transition FC, the strength increased with a further increase in FC. He sketched up microstructure phases of a granular mix containing two distinct sizes of spherical particles (Figure 4.10).

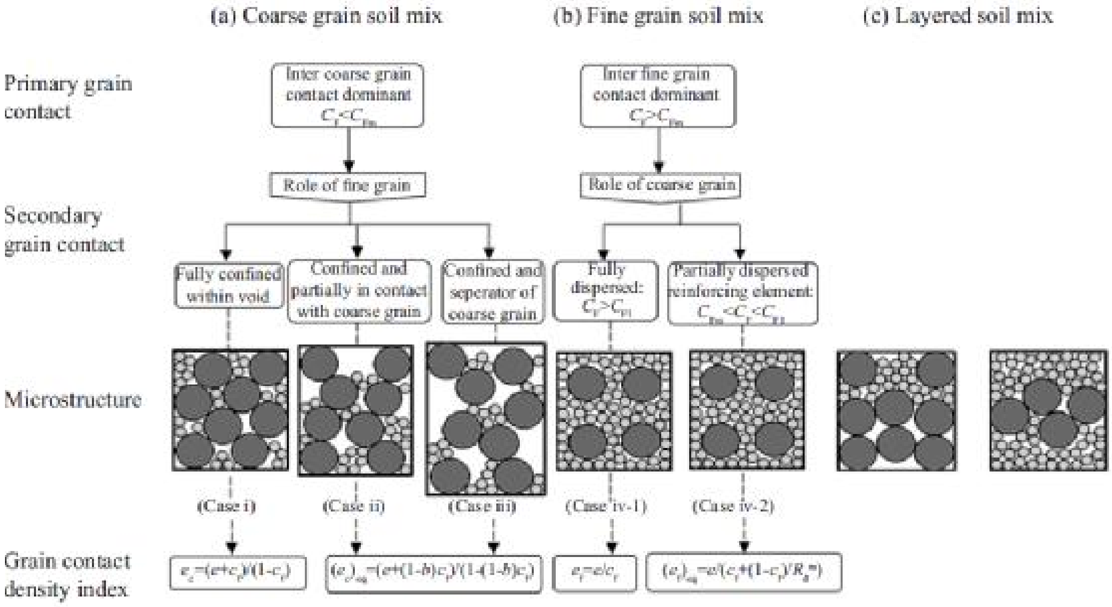

Figure 4.10 Intergranular phases of a soil mix (after Thevanayagam, 2007a)

In the first case (Figure 4.10a), the fine grains are fully enclosed within the voids of coarse grains. At this phase, the fine grains do not have a role in supporting the coarse grain skeleton. In other words, there is no contribution in the internal contact force chain by the finer grains. By altering the position of some of the fine grains without adding more fines, the microstructure appears as Case-ii and Case-iii in Figure 4.10a. In these two cases, some of the fine grains become active participants in the internal contact force chain. Thevanayagam (2007a) described the threshold fine content (C_{Fth}) as; it is the fine content that fine-grain to fine-grain contacts directly begin to have an active role in the internal force chain. In Figure 4.10a, FC values of three cases are all lower than C_{Fth}. If FC quite exceeds C_{Fth}, the Case-iv is observed (Figure 4.10b). Thevanayagam (2007a) mentioned that “the fine grains make active contacts among themselves while the coarse grains become gradually dispersed and act as embedded reinforcement elements within the fine grain matrix until they are separated sufficiently apart. This occurs until limiting fines content, beyond which the effects of coarse grains is negligible and the behavior of the soil mix is entirely governed by the fine-grain to fine-grain contact.” by his own words. In the last case (Figure 4.10c), the coarse and fine grains are in fully layered system.

In order to investigate the role of fine grains on compaction behavior, seven different soil mixtures that were believed to exhibited transitional behavior, were compacted at their own Standard Proctor optimum water contents. The compacted specimens were scanned by means of computed tomography (CT) technique. CT is a non-destructive technique mainly used in medical services. The density distribution of different materials can be monitored using CT images. A schematic illustration of CT technique is shown in Figure 4.11. As can be seen from Figure 4.11 that a CT system consists of an X-ray source from which an X-ray beam is transmitted through a specimen and a multi-detector collector is used to detect X-ray radiation. During the scanning process, the entire X-ray beam is not only transmitted through the soil specimen but also some part of the radiation is absorbed by the specimen and some part is scattered. Using the scattered and transmitted radiation, the density information is deduced about the composition of the scanned specimen. From these density measurements, reconstructions of 2D and 3D images of the specimen are created.

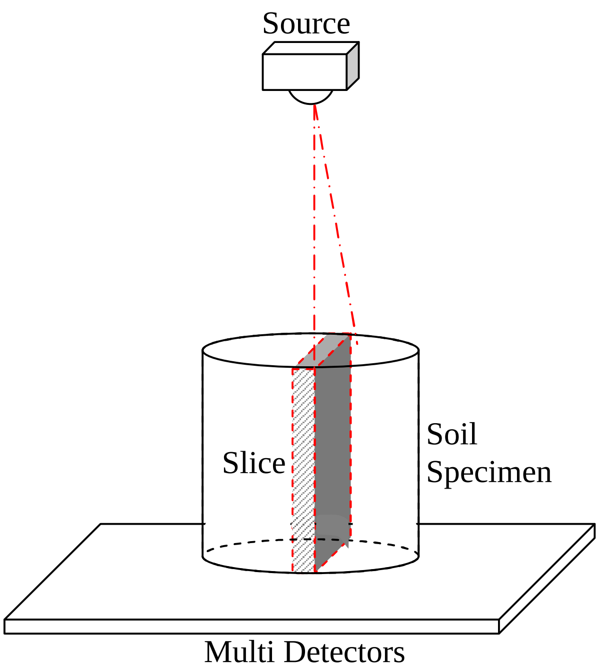

Figure 4.11 Schematic illustration of CT scanning system

CT scanning technique was used to visualize the soil particle distribution along with the pore characteristics of the compacted specimens without destroying them. The CT scans were performed in a commercial institution where the CT system was able to scan materials at 1 mm thick intervals using a multi-detector technology. In general, each 1 mm thick scan is named as a “Slice”. All the seven soil specimens were scanned and 2D/3D images were reconstructed by means of a DICOM Viewer computer program. Figure 4.12 shows slice, plan and 3D views of compacted soil specimens.

The gravel particles in the soil specimen appear as “white” volumes whereas “black” volumes are the air voids as depicted in Figure 4.12a. The “gray” volumes represent the sand-clay matrix of the soil specimen. The comparison of CT images showed that there were no considerable differences between all seven CT images. In other words, small differences were observed when the seven CT images were compared. Findings revealed that the sand component in soil mixture plays an important role in supporting the soil skeleton. Sand particles fill voids between gravels and contribute to the internal contact force chain. In this respect, a new set of soil mixtures were prepared that were composed of gravel and clay components. The Set-1 contains soil mixture #1 to #6 and the remaining mixtures are Set-2. Table 4.5 summarizes percents of gravel-sand-clay components and tabulates the results of Standard Proctor compaction tests.

Table 4.5 Soil fractions in the mixtures and Proctor test results used for CT analyses

Soil Mixture	**Gravel (%)**	**Sand (%)**	**Clay (%)**	**Standard Proctor**	
				g_{dmax} **(kN/m^3)**	w_{opt} **(%)**
#1	55	40	5	21.11	8.82
#2	55	38	7	21.25	7.33
#3	55	33	12	21.43	7.80
#4	55	28	17	20.53	10.04
#5	55	20	25	20.41	8.40
#6	55	15	30	19.52	10.96
#7	95	0	5	17.34	7.23
#8	93	0	7	17.33	7.30
#9	88	0	12	18.12	6.45
#10	83	0	17	19.35	12.58
#11	75	0	25	19.28	12.29
#12	70	0	30	19.10	11.91
#13	55	0	45	19.24	12.30

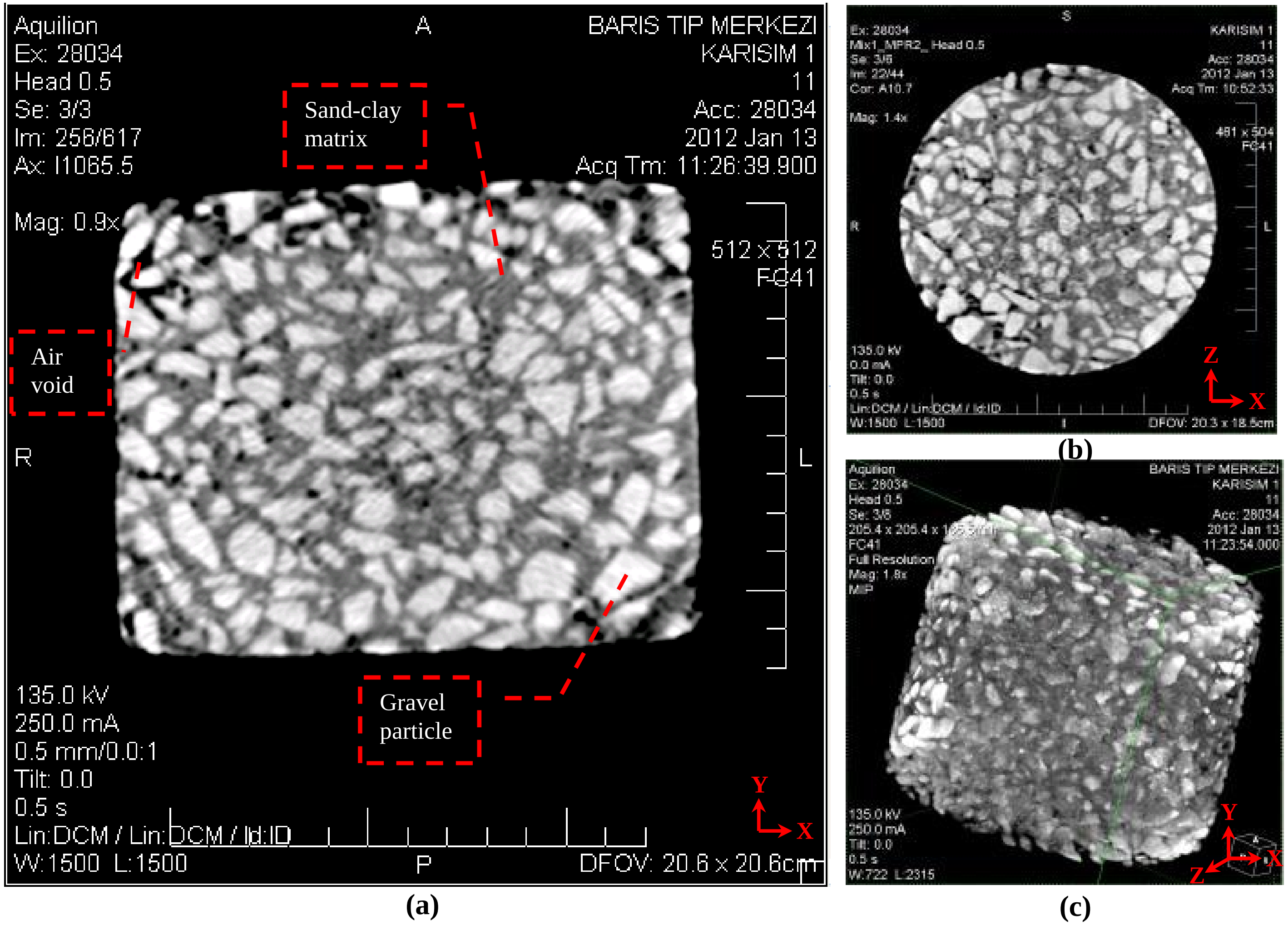

Figure 4.12 Representation of CT (a) slice view, (b) plan view and (c) 3D view of compacted soil specimen

Comparative CT images are displayed in Figure 4.13 through Figure 4.19. Comparisons are visually made using these figures. CT-Mix#1 versus CT-Mix#7 is compared in Figure 4.13. The clay content of these soil mixtures is 5%. In addition to the clay content, CT-Mix#1 contains 55% and 40% of gravel and sand particles respectively, whereas CT-Mix#7 contains 95% gravel. It is obviously seen that CT-Mix#7 contains more voids than CT-Mix#1 (Figure 4.13). It is inferred that the sand-clay matrix fills voids and separates the gravel particles each other. The sand particles play an active role in force chain (Figure 4.13a). On the other hand, the clay particles are fully surrounded within voids of the gravel particles in Figure 4.13b. The edge to edge contact between gravel particles is more pronounced in CT-Mix#7 (Figure 4.13b) as compared to CT-Mix#1 (Figure 4.13a).

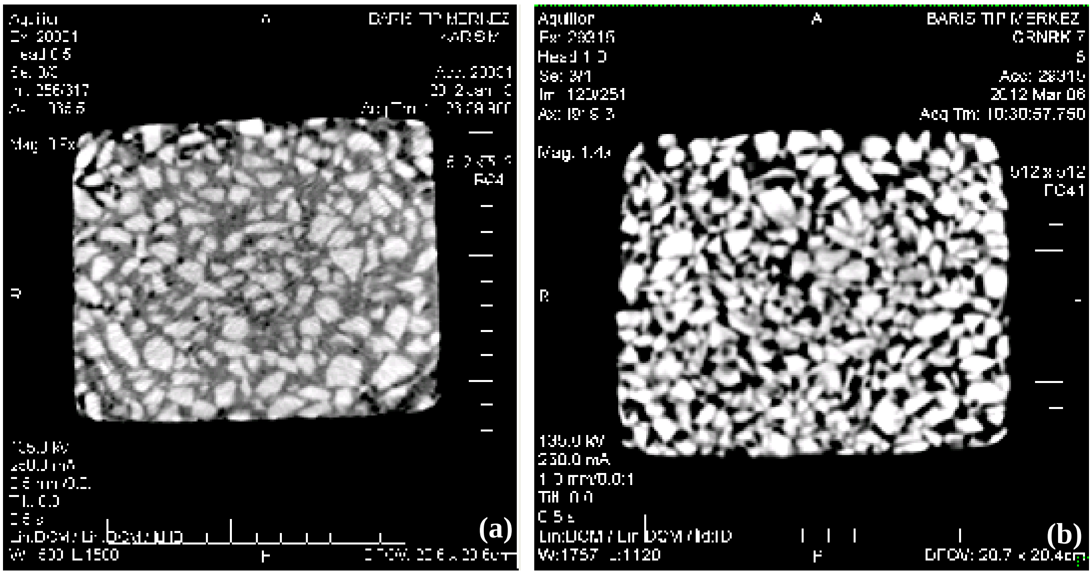

Figure 4.13 Reconstructed CT images of (a) CT-Mix#1 and (b) CT-Mix#7 from center slice of the specimens

The comparative images of CT-Mix#2 and CT-Mix#8 are given in Figure 4.14. The sand-clay matrix fill approximately all air void within the gravel particles in CT-Mix#2, however, some voids appear as air voids in the soil specimen (Figure 4.14a). On the other hand, there is no considerable change when clay content increases from 5% to 7% at CT-Mix#8 (Figure 4.14b). The air voids are still continuous and there is no contribution to the internal contact force chain by the clay particles at CT-Mix#8, yet.

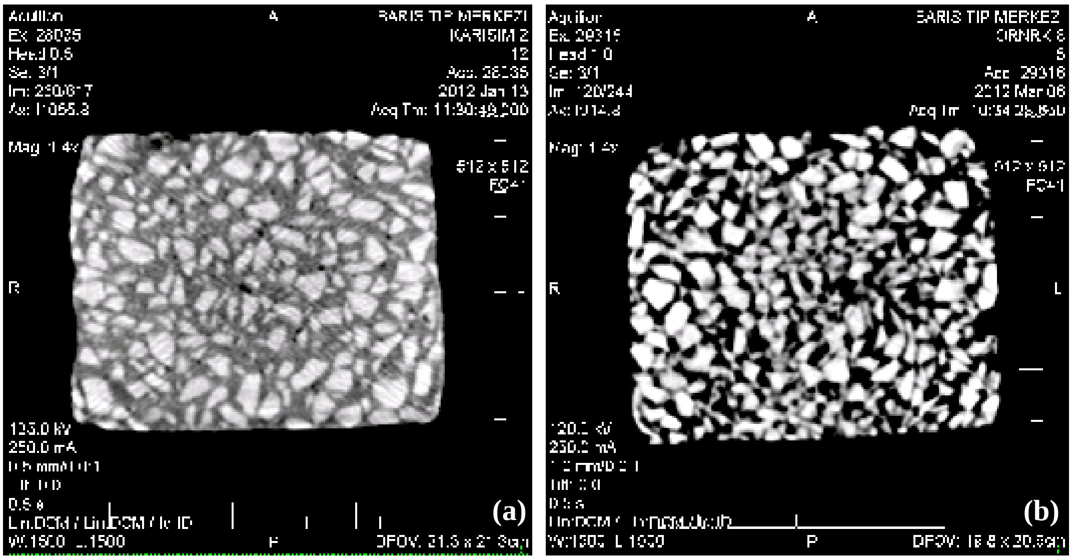

Figure 4.14 Reconstructed CT images of (a) CT-Mix#2 and (b) CT-Mix#8 from center slice of the specimens

Figure 4.15 shows the CT images of CT-Mix#3 and CT-Mix#9. The clay content of these mixtures is 12% where the transitional behavior takes place. The air voids decrease by increasing clay content at CT-Mix#3, however, air voids are still visible (Figure 4.15a). Furthermore, the gravel particles become gradually dispersed, as depicted in Figure 4.15a. The clay particles fill voids within the gravel particles progressively and start to play an active role in the internal contact force chain in CT-Mix#9. However, there are still large air voids (Figure 4.15b).

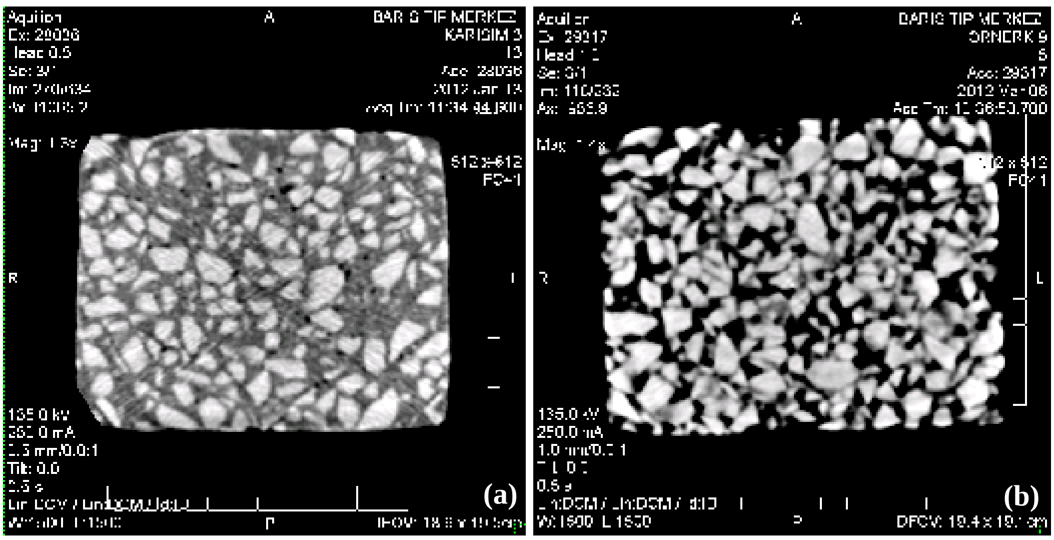

Figure 4.15 Reconstructed CT images of (a) CT-Mix#3 and (b) CT-Mix#9 from center slice of the specimens

The comparison of CT-Mix#4 versus CT-Mix#10 is made by means of Figure 4.16. As clay content increases to 17% causes visually no change is observed in CT-Mix#4. As seen in Figure 4.16a, the air voids are still present and the sand-clay matrix dominates the internal force chain mechanism. A closer look at Figure 4.16b shows that the clay particles fill voids and contribute to the internal contact force chain. Also, an increase in clay content causes a decrease in voids at CT-Mix#10 (Figure 4.16b).

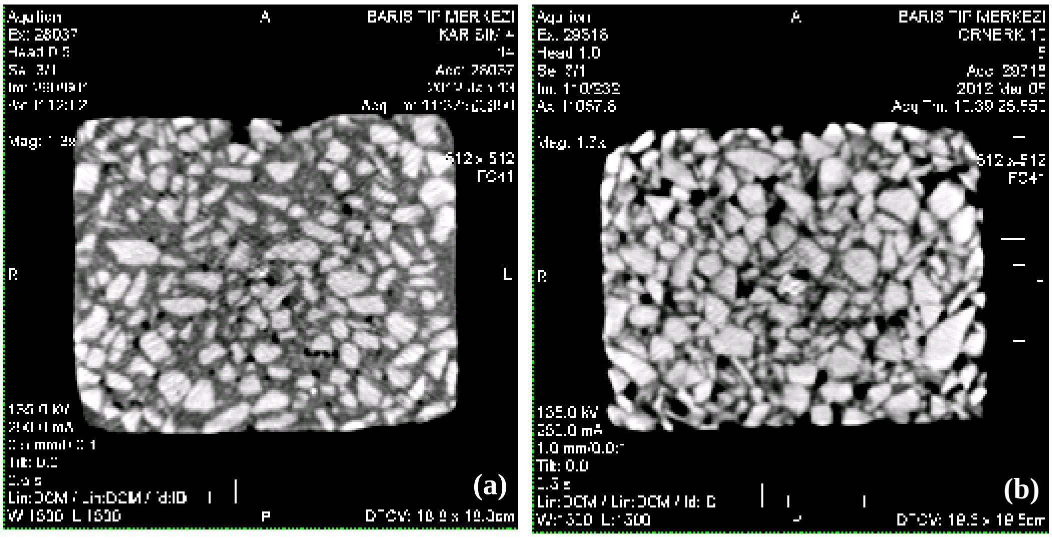

Figure 4.16 Reconstructed CT images of (a) CT-Mix#4 and (b) CT-Mix#10 from center slice of the specimens

Figure 4.17 depicts the CT images of CT-Mix#5 and CT-Mix#11. As tabulated in Table 4.5, the clay content of these mixtures is 25%. It is apparent that the gravel particles in CT-Mix#5 are almost completely separated from each other (Figure 4.17a). A similar effect also exists in CT-Mix#11 where grains are slightly less separated as compared with CT-Mix#5. As expected, an increase in clay content causes a decrease in voids and clay particles play an important role in the internal contact force chain (Figure 4.17b).

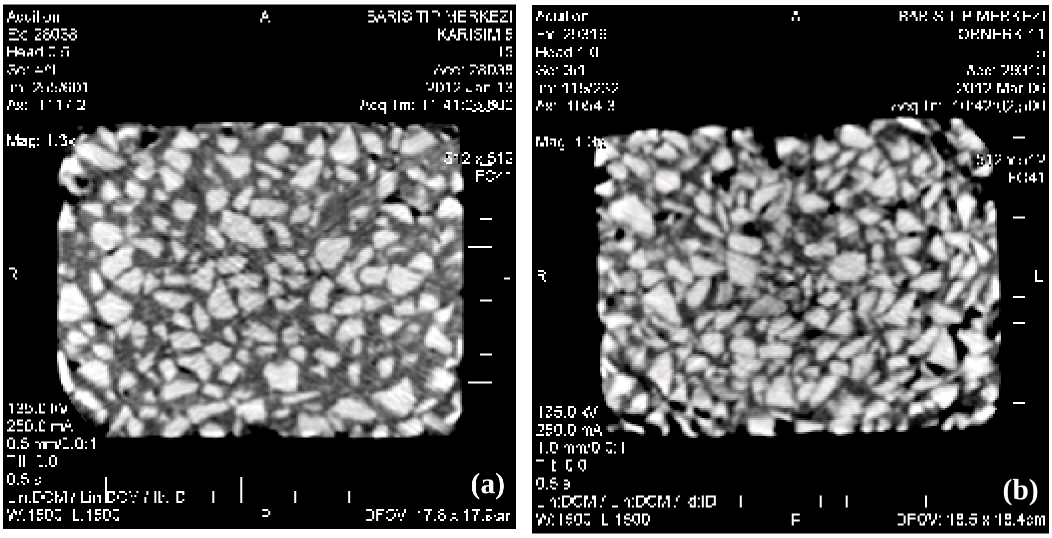

Figure 4.17 Reconstructed CT images of (a) CT-Mix#5 and (b) CT-Mix#11 from center slice of the specimens

The comparative images of CT-Mix#6 and CT-Mix#12 are given in Figure 4.18. It is evident that the sand-clay matrix in CT-Mix#6 and the clay particles in CT-Mix#12 dominate the soil behavior since the gravel particles become almost entirely dispersed as shown in Figure 4.18a and 4.18b.

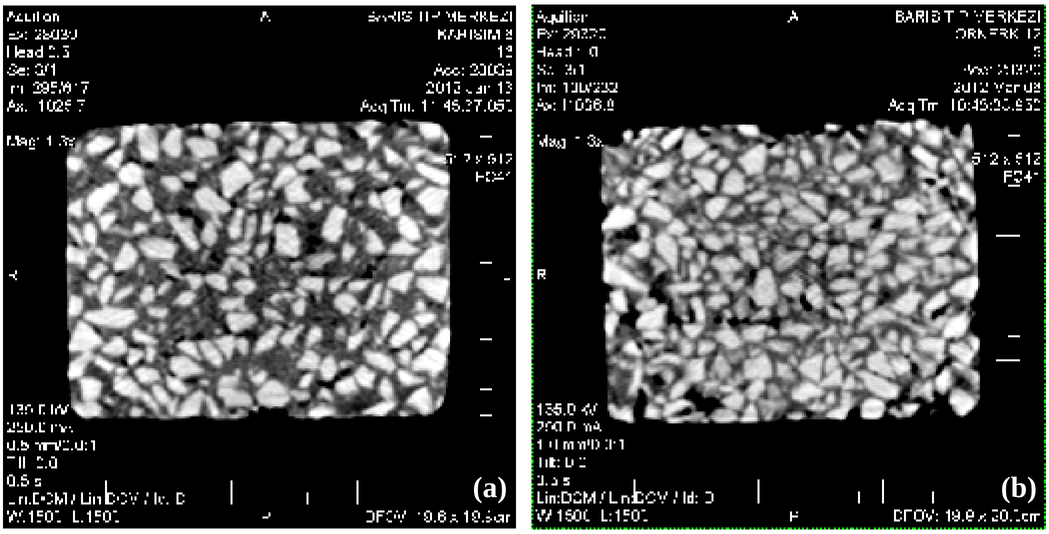

Figure 4.18 Reconstructed CT images of (a) CT-Mix#6 and (b) CT-Mix#12 from center slice of the specimens

CT image of CT-Mix#13 composed of 55% gravel and 45% clay particles is given in Figure 4.19. It is obviously seen that the clay particles dominate behavior of the soil specimen. Gravel particles are separated from each other and there are no edge to edge gravel contacts.

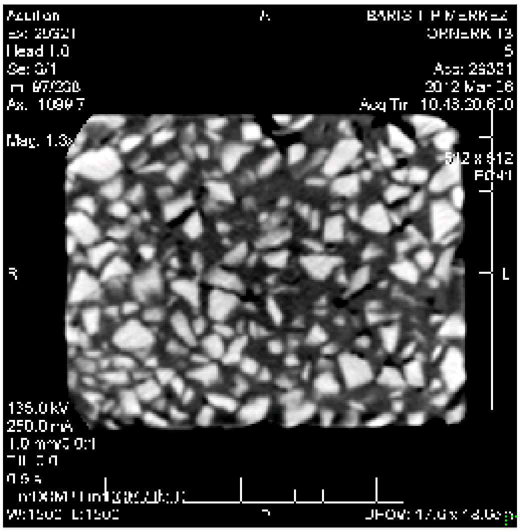

Figure 4.19 Reconstructed CT images of CT-Mix#13

The CT imaging technique creates an intensity value for each pixel in a CT image. This feature was used to quantize the transitional behavior of soil mixtures. For this reason, the center slices of each CT images were analyzed by means of MATLAB Image Processing Toolbox. The quantization was made calculating the total gravel area of each slices. Before the determination of total gravel area, a raw CT image should be converted to a binary image whose pixels are displayed as black and white. In order to convert the raw image to binary image, the threshold intensity value of each slice has to be determined. Therefore, a procedure was followed; (1) the center slice was opened with Image Processing Toolbox, (2) then a region on image was selected, (3) the selected region was magnified step by step and (4) at last the threshold intensity values of this image was determined, as depicted in Figure 4.20. All lower intensity values than the threshold value were pictured as black representing the air void and the sand-clay matrix. Conversely, high intensity values were pictured as white representing the gravel particles. Figure 4.21 presents a CT slice before and after thresholding process.

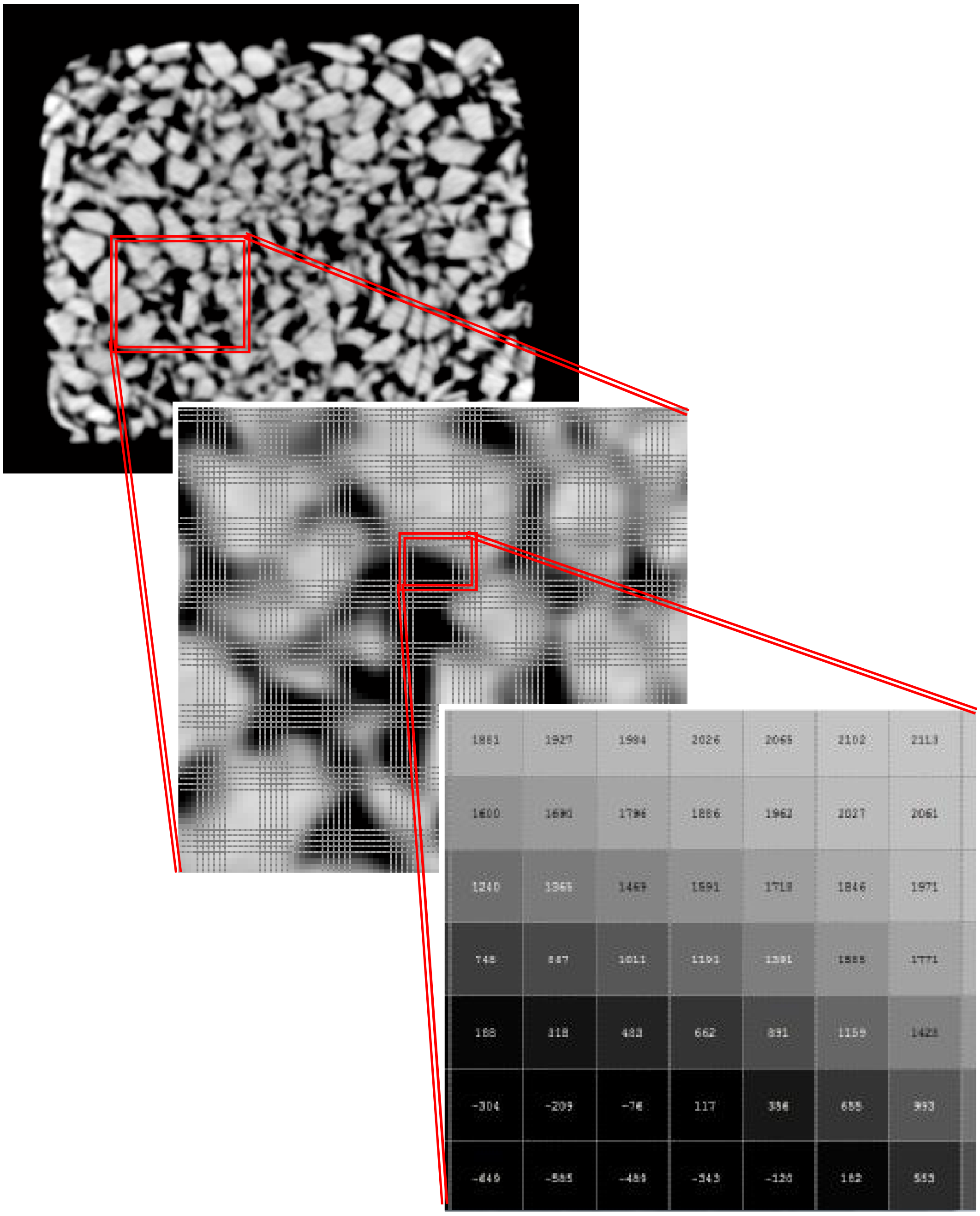

Figure 4.20 Determination of the threshold intensity value of a CT slice

After thresholding process, total slice area (i.e. total black area) and total gravel area (i.e. total white area) were determined for each binary image. Percent area of these images was calculated as follow:

$$Percent\ Area = \frac{Total\ \ Gravel\ Area}{Total\ \ Slice\ Area} \times 100 \tag{5.4}$$

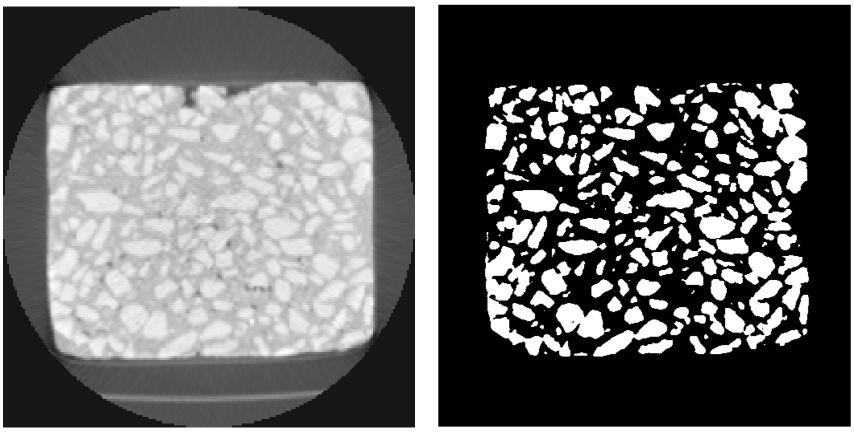

(a) (b)

Figure 4.21 CT images (a) before and (b) after thresholding process

The image processing analysis results are summarized in Table 4.6. As seen in Table 4.6, each CT slice has its own threshold intensity value. All the total slice areas are approximately equal to each other. As it is mentioned before, two different set of soil mixtures were used in CT imaging process; Mixture #1 to #6 were grouped in Set-1 and the remaining mixtures were grouped in Set-2. It is inferred from the calculated total gravel area, there is a compatible trend with aforementioned transitional behavior of soil mixtures. The total gravel area, also percent area, of each slice increases to a threshold value and then it starts to decrease both for Set-1 and Set-2 (Table 4.6). The relationship between percent area and fine content is sketch up in Figure 4.22.

Table 4.6 Image processing analysis results of mixtures

Soil Mixture	**Slice Threshold Intensity Value**	**Total Slice Area (Pixel)**	**Total Gravel Area (Pixel)**	**Percent Area (%)**
#1 (Set-1)	1750	262139	44459	17.0
#2 (Set-1)	1700	262139	45531	17.4
#3 (Set-1)	1650	262140	52906	20.2
#4 (Set-1)	1675	262140	53742	20.5
#5 (Set-1)	1700	262141	54594	20.8
#6 (Set-1)	1600	262140	49074	18.7
#7 (Set-2)	1400	262136	56000	21.4
#8 (Set-2)	1450	262140	57372	21.9
#9 (Set-2)	1450	262134	68327	26.1
#10 (Set-2)	1600	262140	65864	25.1
#11 (Set-2)	1600	262140	63265	24.1
#12 (Set-2)	1600	262140	52930	20.2
#13 (Set-2)	1500	262141	50266	19.2

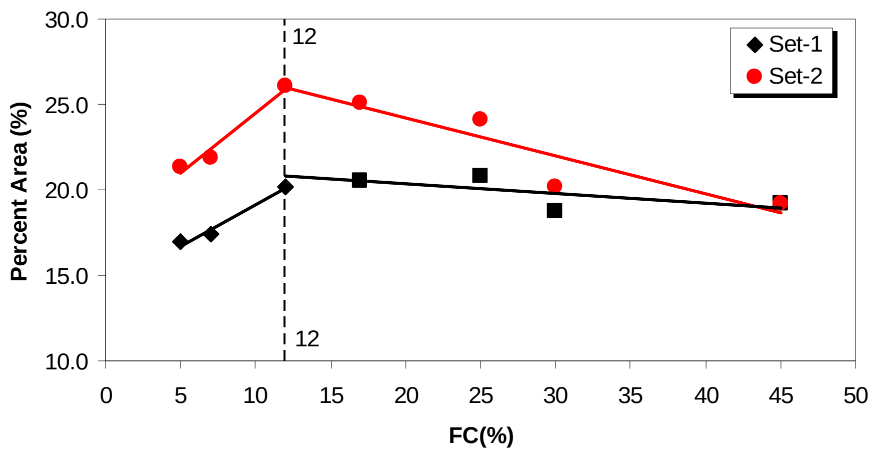

Figure 4.22 Relationship between percent area and fine content of mixtures

4.3.2 Effect of Compaction Energy

The influence of compaction energy was also investigated. The soil mixtures were compacted both under Standard and Modified Proctor compaction energy levels. It is well known that an increase in compaction energy causes an increase in γ_{dmax} and a decrease in ω_{opt}. A similar trend was also observed in this study. The modified compaction curve of each soil mixture shifts towards left upper side of the standard compaction curve. Three different arbitrary selected soil mixtures representing soil types compaction curves are shown in Figure 4.23. The USCS group symbols of these mixtures are CH, SC and GP-GC, respectively.

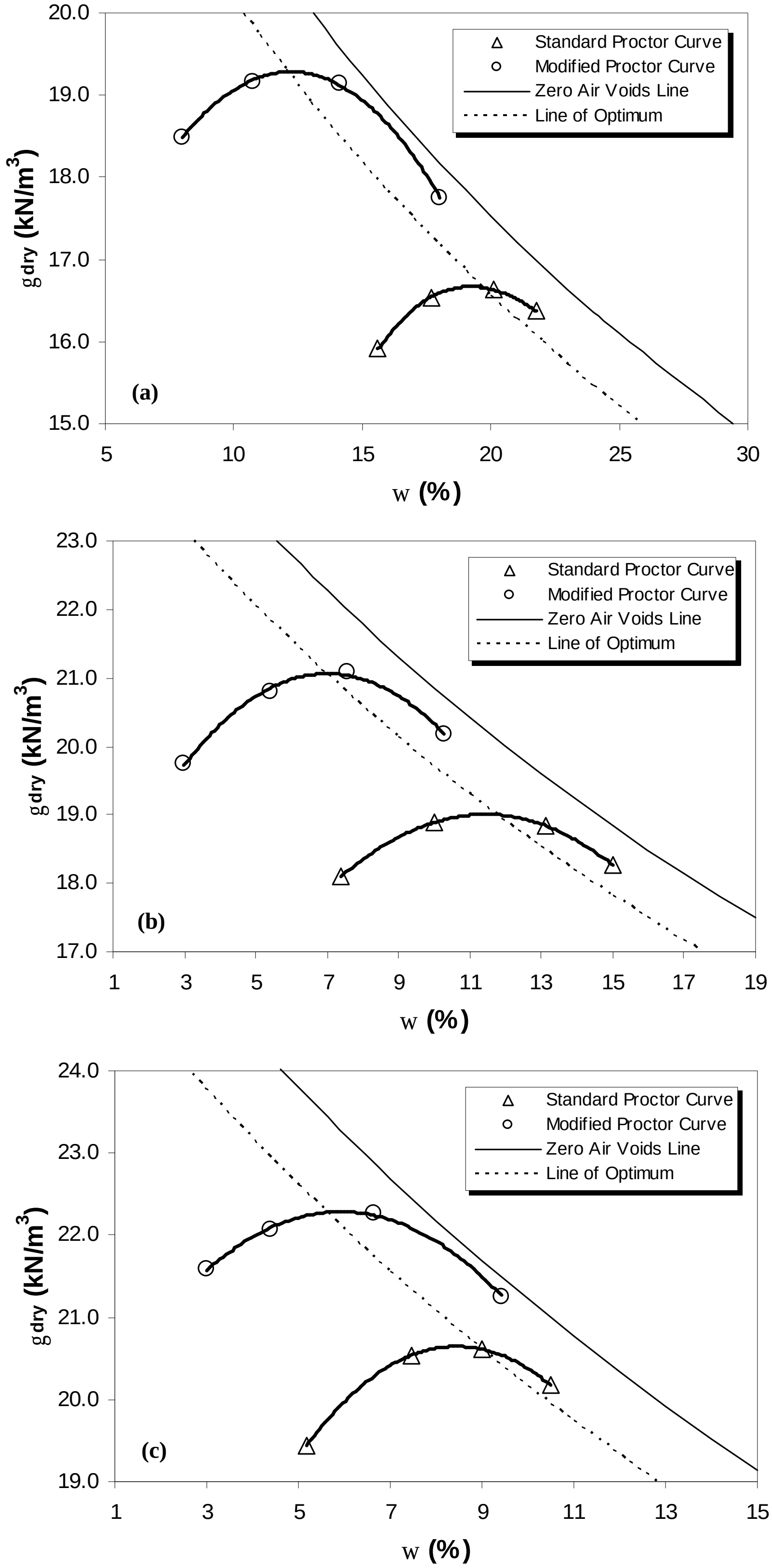

Figure 4.23 Standard and modified Proctor compaction curves of (a) CH, (b) SC and (c) GP-GC soil mixtures

4.3.3 Effect of Automatic Soil Compactor

In order to determine whether the usage of automatic soil compactor has an effect on soil compaction, two different soil mixtures (i.e. Mix#62 and Mix#195) were manually compacted both at Standard and Modified Proctor energy levels. The soil mixtures used for comparison were highly plastic clay and clayey sand grouped as CH and SC according to USCS, respectively. The effect of automatic soil compactor is illustrated in Figure 4.24.

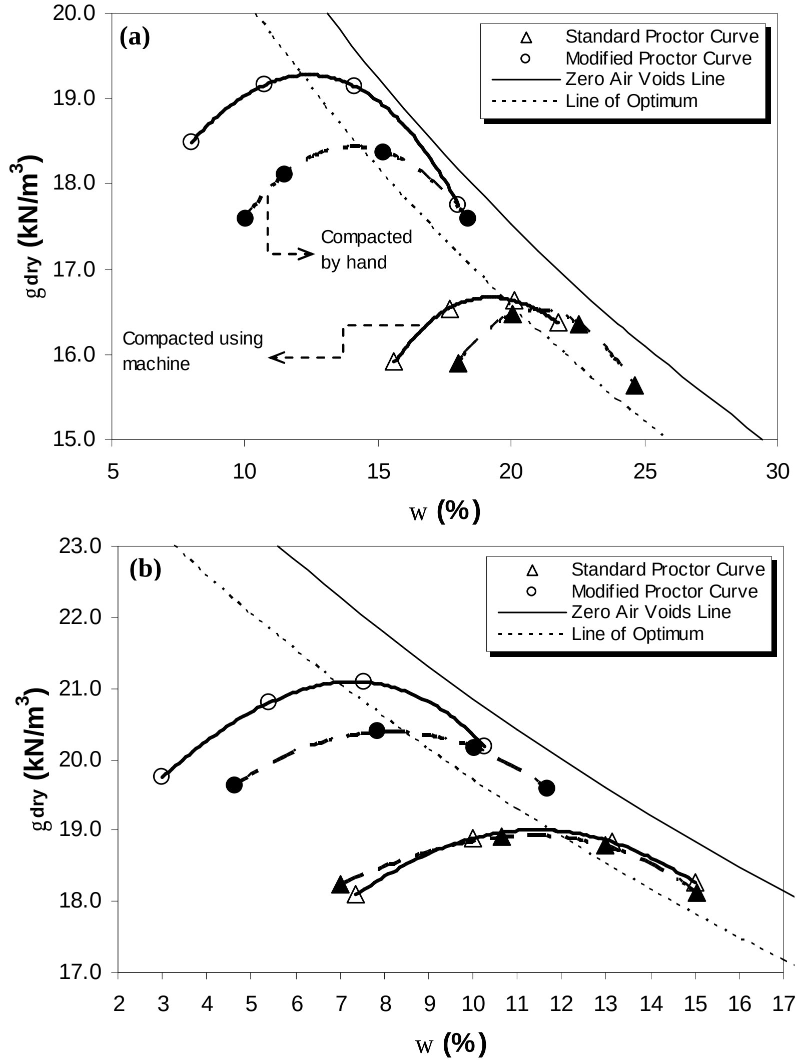

Figure 4.24 Comparison of compaction curves of (a) Mix#62 and (b) Mix#195 compacted by means of the automatic compactor versus by hand

One may notice that the difference between compaction curves obtained by hand and automatic compaction is negligible for Standard Proctor energy level. It is believed that larger and more significant differences for Modified Proctor energy level may be attributed to operator effect since the hammer may not be lifted to the standard height during labor intensive hand compaction process.

CHAPTER FIVE
MODELLING OF COMPACTION CHARACTERISTICS

5.1 Comparison of Literature Equations using Author's Experimental Results

Many researchers tried to relate soil index parameters with compaction characteristics. Some of them are tabulated in Table 5.1. These equations were employed to predict the compaction characteristics of 200 soil mixtures. The prediction accuracy of them was evaluated by plotting scatter graphs of the predicted compaction characteristics with respect to the corresponding actual values, as shown in Figure 5.1 through 5.5.

Table 5.1 Correlation equations gathered from literature

Literature Source	**Regression Equation**	**Proctor Test Type**	**Valid for**
Sivrikaya (2008)	$\omega_{opt} = 0.92\cdot\ \omega_P$ $\gamma_{dmax} = 21.84 - 0.27\cdot\omega_{opt}$	Standard	Fine grained soils
Ölmez (2007)	$\omega_{opt} = 0.618\cdot\ \omega_P - 0.453\cdot\ I_P$ $\gamma_{dmax} = 0.223\cdot G + 0.411\cdot FC$ -- $\omega_{opt} = 0.284\cdot\omega_L$ $\gamma_{dmax} = 0.234\cdot G + 0.233\cdot S + 0.055\cdot FC$	Standard ----------- Modified	Coarse grained soils
Sridharan and Nagaraj (2005)	$\omega_{opt} = 0.92\cdot\ \omega_P$ $\gamma_{dmax} = 0.23\cdot\ (93.3 - \omega_P)$	Standard	Fine grained soils
Engin (2003)	$\omega_{opt} = 0.2108 + 0.0227\cdot(\text{-No.4}) - 0.1470\cdot(\text{+No.200})$ $\gamma_{dmax} = 1.6148 - 0.1329\cdot(\text{-No.4}) + 0.5576\cdot(\text{+No.200})$ -- $\omega_{opt} = 0.1589 + 0.0212\cdot(\text{-No.4}) - 0.1118\cdot(\text{+No.200})$ $\gamma_{dmax} = 1.9300 - 0.1940\cdot(\text{-No.4}) + 0.4166\cdot(\text{+No.200})$	Standard ----------- Modified	All soil types
Blotz et al. (1998)	$\omega_{opt.} = (12.39 - 12.21 \log \omega_L) \log E + 0.67\ \omega_L + 9.21$ $\gamma_{dmax} = (2.27 \log \omega_L - 0.94) \log E - 0.16\ \omega_L + 17.02$	All compaction energy	Fine grained soils

[Note: ω_{opt}, ω_L, ω_P, I_p, G (i.e. gravel), S (i.e. sand), FC (i.e. fine content) are expressed in percentage, E (i.e. compaction energy) is in kJ/m^3 unit, and γ_{dmax} is in kN/m^3 unit. However, Engin (2003) used γ_{dmax} is in ton/m^3 unit and –No.4 and +No.200 in decimal.]

Sivrikaya (2008) related ω_{opt} with ω_P and γ_{dmax} with ω_{opt} for estimating compaction characteristics of fine grained soils compacted under Standard Proctor energy level. The prediction results of 29 soil mixtures, which are classified as fine grained soils, are plotted in Figure 5.1a and 5.1b. As can be seen from Figure 5.1a, the predicted ω_{opt} values are larger than the actual values. In other words, this equation over estimates the ω_{opt} values of the soil mixtures. The actual γ_{dmax} versus the predicted γ_{dmax} relationship is shown in Figure 5.1b. Sivrikaya (2008) mentioned that γ_{dmax} can be well predicted using ω_{opt}. However, the inclusion of ω_{opt} in estimating γ_{dmax} is decided irrational because of two reasons. The first one; ω_{opt} of soils can not be known without performing an experimental compaction test. If ω_{opt} is determined from an experimental compaction test, there is no need to estimate γ_{dmax} by means of an equation. The second one; if a correlation equation is used to estimate ω_{opt}, the predicted γ_{dmax} includes the error involved in estimating ω_{opt}. On the other hand and the most importantly, there is a logical fault due to usage of ω_{opt} for predicting γ_{dmax}. It is well known that the input parameters have to be independent variables from the target parameter. However, γ_{dmax} and ω_{opt} are interrelated parameters.

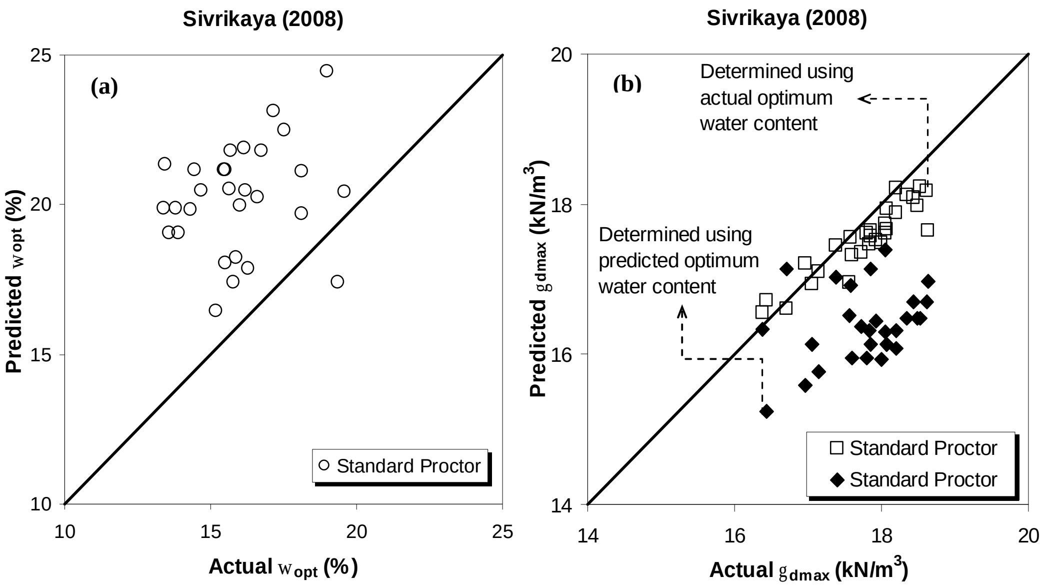

Figure 5.1 Scatter plots of (a) ω_{opt} and (b) γ_{dmax} using Sivrikaya (2008) equations

In order to visualize the prediction results of Sivrikaya's equation with respect to the actual ω_{opt} and the predicted ω_{opt}, Figure 5.1b is sketched up. The solid symbols in Figure 5.1b show the prediction results of Sivrikaya's equation using the predicted ω_{opt}. It is clear that Sivrikaya's equation underestimates γ_{dmax}. There is significant scatter in the predicted γ_{dmax} values due to inclusion of the prediction error of ω_{opt}. On the other hand, the predicted γ_{dmax} values are perfectly fit with the actual γ_{dmax} values if experimental ω_{opt} values are used in regression equation as depicted by blank symbols in Figure 5.1b.

Ölmez (2007) conducted a laboratory work on coarse grained soils and developed regression equations to estimate Standard and Modified Proctor compaction characteristics. For Standard Proctor compaction, he related ω_{opt} with only consistency limits whereas he used grain size parameters to predict γ_{dmax}. Ölmez (2007) used only the liquid limit to estimate Modified Proctor ω_{opt}. Likewise; he related modified γ_{dmax} with gravel-sand-fine content ratios. There is a considerable scatter for ω_{opt} and γ_{dmax} under Standard and Modified Proctor energy levels, as shown in Figure 5.2. Particularly, the predicted γ_{dmax} is distributed in a narrow band both for Standard and Modified Proctor energy levels indicating no relevance of the correlations with the data acquired in this thesis.

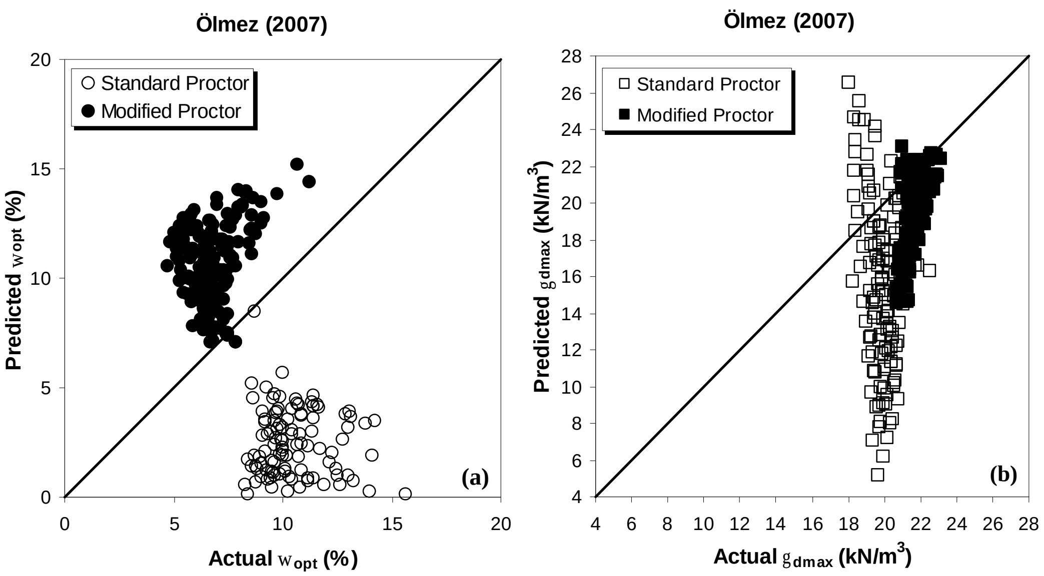

Figure 5.2 Scatter plots of (a) ω_{opt} and (b) γ_{dmax} using Ölmez (2007) equations

Sridharan and Nagaraj (2005) related Standard Proctor compaction characteristics with only plastic limit (ω_P). They mentioned that ω_{opt} of fine grained soils could be predicted with a high accuracy using ω_P. However, Figure 5.3a and 5.3b presents that there is no good agreement between the predicted and the corresponding experimental values of ω_{opt} and γ_{dmax}. The Sridharan and Nagaraj's equations overestimate ω_{opt} (Figure 5.3a) and underestimate γ_{dmax} (Figure 5.3b). This noticeable error might be due to the fact that Sridharan and Nagaraj's equations were developed using fine-grained soils which had no gravel and less than 35% sand grains in the samples. However, the tested soil mixtures in this thesis have remarkable amount of gravel and sand grains.

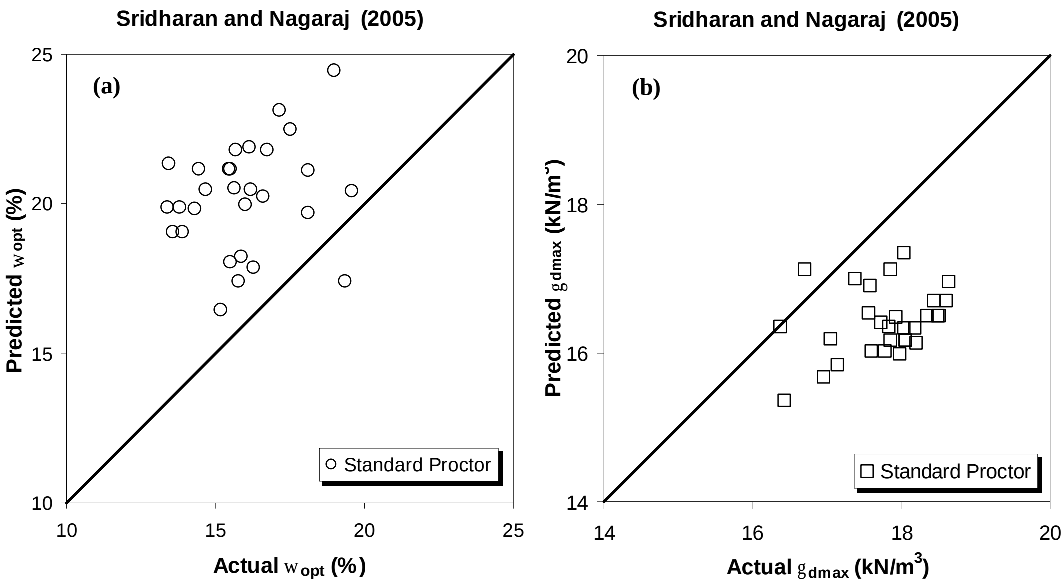

Figure 5.3 Scatter plots of (a) ω_{opt} and (b) γ_{dmax} using Sridharan and Nagaraj (2005) equations

Engin (2003) correlated Standard and Modified Proctor compaction characteristics with different combinations of consistency limits, grain size distribution parameters, specific gravity and loose dry unit weight. The developed equations which include only granulometric parameters were preferred because of simplicity. The prediction results of Engin's equations are displayed in Figure 5.4a and 5.4b. It is evident that the equations are able to predict both standard and modified compaction characteristics with a high accuracy. However, the predicted ω_{opt} values are somewhat larger than the experimental ω_{opt} values, and the predicted γ_{dmax} values are a little bit underestimated by regression equations.

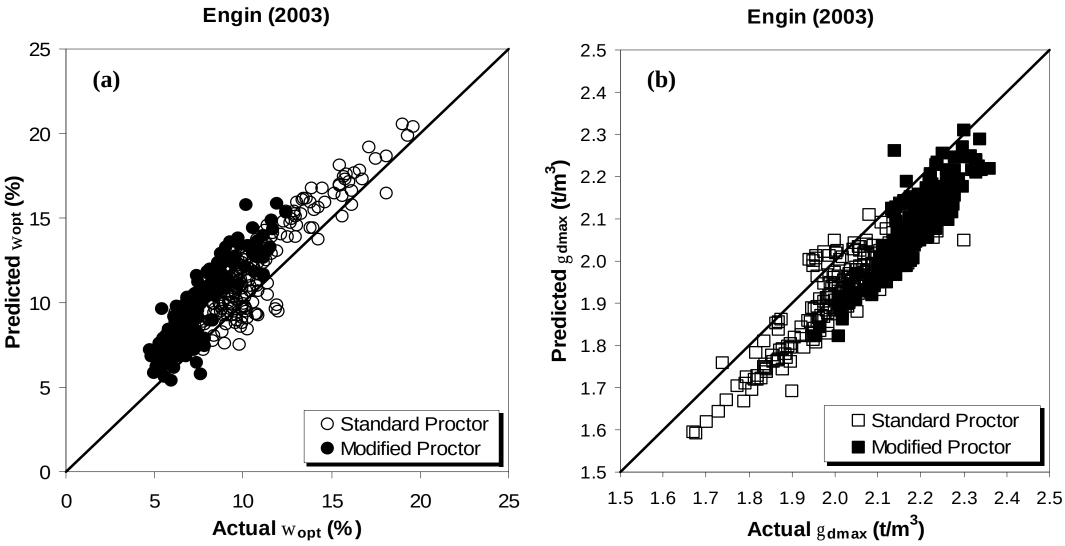

Figure 5.4 Scatter plots of (a) ω_{opt} and (b) γ_{dmax} using Engin (2003) equations

It is known that the soil samples were compacted by hand in Engin (2003) study. However, an automatic soil compactor was used in this thesis, and the differences between the compaction characteristics that were obtained by hand and by automatic soil compactor is given in Section 4.3.3. It may be helpful to apply a correction factor to Engin's (2003) correlations. Correction process is made by multiplying the predicted values with a correction factor. The correction factors are determined as 0.04 and -0.10 for Standard Proctor γ_{dmax} and ω_{opt}, respectively. Similarly, the correction factors for Modified Proctor γ_{dmax} and ω_{opt} are determined as 0.05 and -0.20, respectively. Finally, the corrected prediction value is calculated as follows;

$$Corrected\,Value = \Pr edicted\,Value + \left(Correction\,Factor \times \Pr edicted\,Value\right) \qquad (5.1)$$

The scatter plots of corrected predictions are shown in Figure 5.5.

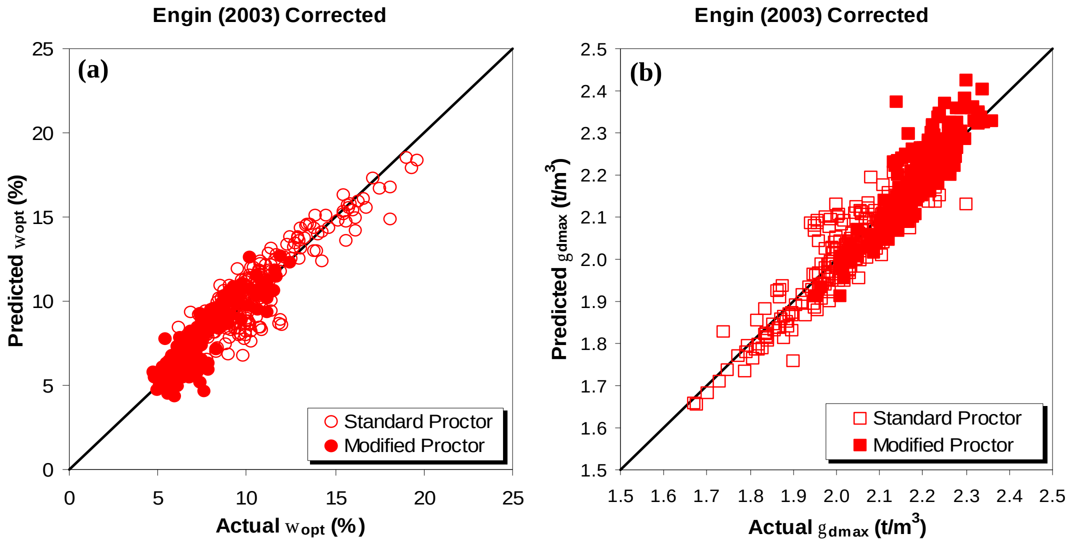

Figure 5.5 Corrected scatter plots of (a) ω_{opt} and (b) γ_{dmax} using Engin (2003) equations

Blotz et al. (1998) developed regression equations for estimating compaction characteristics of fine grained soils at all compaction energy levels. They used liquid limit (ω_L) and compaction energy (E) as input variables in their equations. The prediction results of ω_{opt} are shown in Figure 5.6a. It is evident that the developed equations for estimating ω_{opt} over estimate ω_{opt} at Standard and Modified Proctor energy levels. On the other hand, the predicted γ_{dmax} values are somewhat smaller than the actual γ_{dmax} values, as depicted in Figure 5.6b.

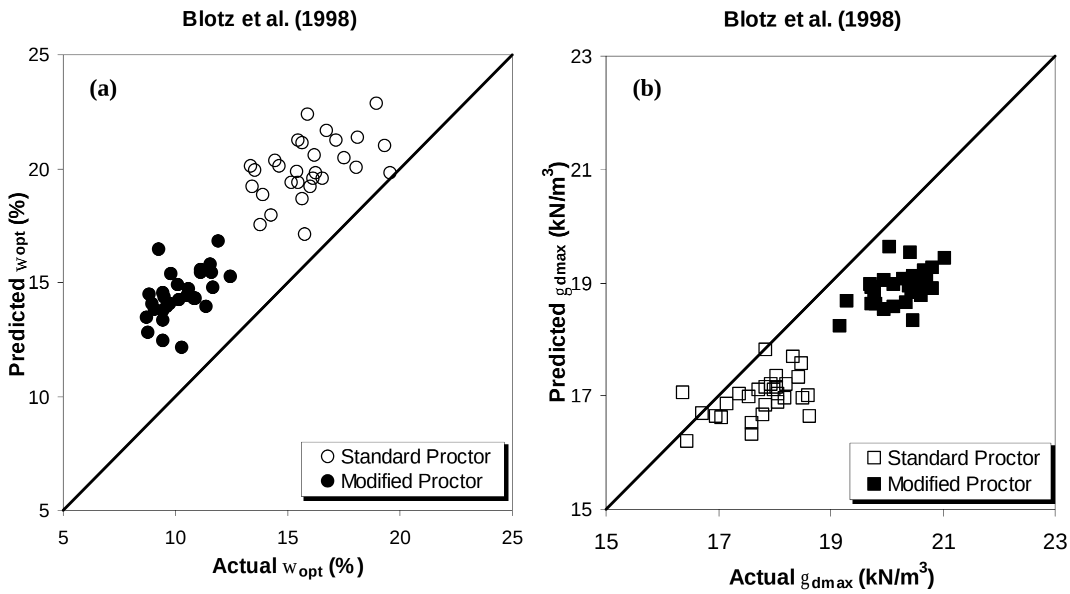

Figure 5.6 Scatter plots of (a) ω_{opt} and (b) γ_{dmax} using Blotz et al. (1998) equations

5.2 Multiple Linear Regression Analysis

Even though there are numerous available regression equations in the literature for estimating compaction characteristics, they were mainly developed for fine grained soils compacted under standard Proctor energy level and rarely for coarse grained soils. Some of the developed regression equations are applied to the author's experimental data in Section 5.1. The comparisons show that the compaction characteristics can not be predicted well with an exception of Engin (2003) study. Therefore, the new empirical equations were developed using multiple linear regression (MLR) method. It is well known that compaction characteristics of coarse-grained soils are influenced by grain size distribution whereas consistency limits play an important role on the compaction parameters of fine-grained soils. Therefore, in this study the MLR models include liquid limit (ω_L), plastic limit (ω_P), passing No.4 sieve (-No.4) and passing No.200 sieve (-No.200) fractions as input variables. It should be mentioned that an assumption was made; the ω_P value was taken equal to the value of ω_L for the non-plastic soil mixtures.

The stepwise regression method was used to find out which variable would affect the compaction characteristics and used to determine the best predictive equation. Montgomery and Runger (2007) mentioned that this procedure iteratively constructs a sequence of regression models by adding or removing variables at each step. The criterion for adding and removing a variable at any step is usually expressed in terms of a partial F-test. Let f_{in} be the value of the F-random variable for adding a variable to the model, and let f_{out} be the value of the F-random variable for removing a variable from the model. Instead of f_{in} and f_{out} parameters, the significance level (α) can be used for adding or removing a variable from the model (i.e. α_{in} or α_{out}). The details of this procedure can be found in Montgomery and Runger (2007). Minitab computer program was used in stepwise regression modeling. In the analysis, forward selection method was utilized using the α_{in} and α_{out} values of 0.05. In order to evaluate the final regression model, C_p and PRESS statistics as well as coefficient of determination (R^2) were used as statistical verification tools. C_p statistic is a measure of the total mean square error for the regression model. It is expected that the C_p value would be small and close to the number of the input variables used in the model. Models with considerable lack of fit and bias have values of C_p larger than the input variables. PRESS (i.e. acronym of Prediction Error Sum of Squares) is used to assess the predictive ability of the developed model. It is defined as the sum of the squares of the differences between each observation y_i and the corresponding predicted value based on a model fit to the remaining observations. Generally, the smaller the PRESS value, the better the performance accuracy of the model. R^2 is the percentage of total variation in the response that is explained by predictors in the model. It is well known that the higher the R^2, the better the model fits to the data. The final model selection is made where the model being investigated yields the minimum value of both C_p and PRESS statistics and the maximum value of R^2.

5.2.1 MLR Models for Standard Proctor Compaction

The stepwise regression results of the optimum water content at Standard Proctor energy level ($\omega_{opt\text{-}st}$) are given in Table 5.2. The first step includes only the input variable of –No.200. The ω_L and ω_P variables are added to the regression analysis one by one at each step. Step-3 model including input variables of -No.200, ω_L and ω_P is observed to give the best results (maximum R^2, and minimum C_p and PRESS). In terms of R^2, it increases regularly from 76.88 to 83.62. Similar but inverse trend is observed in PRESS statistics, it decreases from 332.572 to 240.902. There is a significant decrease in C_p statistic. The value of C_p decreases from 79.4 to 44.1 at Step-2 and finally decreases to 3.0 at Step-3.

Table 5.2 Stepwise regression results for $\omega_{opt\text{-}st}$

Step	Regression Equation	Statistical Features		
		R^2	C_p	PRESS
1	$\omega_{opt\text{-}st} = 7.420 + 0.1270\cdot(\text{-No.200})$	76.88	79.4	332.572
2	$\omega_{opt\text{-}st} = 10.491 + 0.1585\cdot(\text{-No.200}) - 0.099\cdot(\omega_L)$	80.01	44.1	291.288
3	$\omega_{opt\text{-}st} = 9.108 + 0.1696\cdot(\text{-No.200}) - 0.116\cdot(\omega_L) + 0.083\cdot(\omega_P)$	83.62	3.0	240.902

It is revealed that the regression equation developed in Step-3 is the final model that can be used to predict the $\omega_{opt\text{-}st}$. In this equation, $\omega_{opt\text{-}st}$, –No.200, ω_L and ω_P are expressed in percentages.

$$\omega_{opt\text{-}st} = 9.108 + 0.1696\cdot(\text{-No.200}) - 0.116\cdot(\omega_L) + 0.083\cdot(\omega_P) \quad (5.2)$$

The scatter plot of the predicted $\omega_{opt\text{-}st}$ values are shown in Figure 5.7. It is clear that the predicted and the actual values of $\omega_{opt\text{-}st}$ are in good agreement, with errors acceptable for engineering purpose. However, there is a considerable scatter, particularly between 7% and 13% values of $\omega_{opt\text{-}st}$ (Figure 5.7).

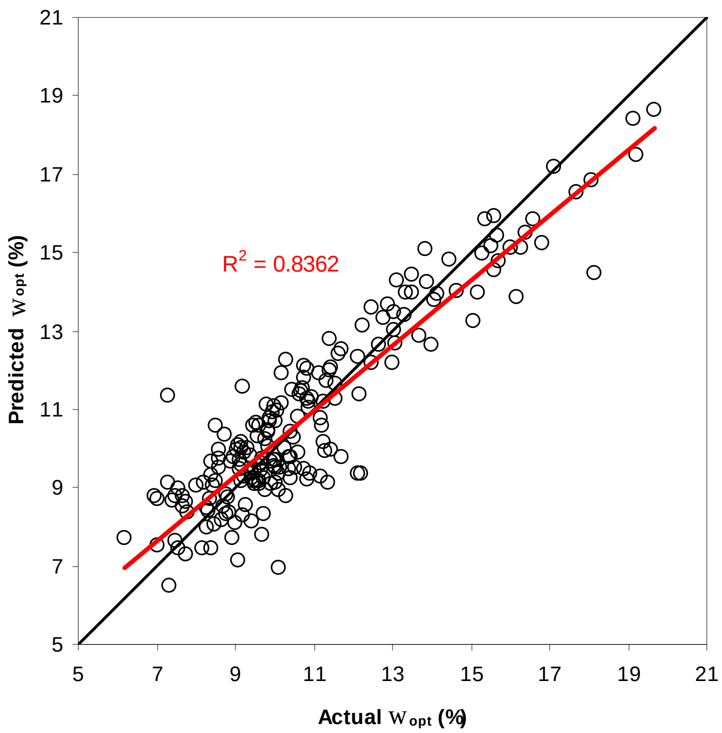

Figure 5.7 Scatter plot of ω_{opt} at standard Proctor energy level using Equation 5.2

The stepwise regression results of the maximum dry unit weight at Standard Proctor energy ($\gamma_{dmax\text{-}st}$) are summarized in Table 5.3. Similar to $\omega_{opt\text{-}st}$ stepwise regression modeling, –No.200 variable was used in the first step of $\gamma_{dmax\text{-}st}$. The ω_L, ω_P and –No.4 input variables were added to the regression analysis one by one up to

Step-4. It is evident that the prediction accuracy of the developed models increases by addition of new input variables. There is a slight increase observed when –No.4 is used as input variable in Step-4. In terms of R^2, it increases from 84.64 to 84.95, C_p and PRESS statistics decrease from 6.9 to 5.0 and from 40.118 to 39.690, respectively.

Table 5.3 Stepwise regression results for $\gamma_{dmax\text{-}st}$

Step	**Regression Equation**	**Statistical Features**		
		$\mathbf{R^2}$	$\mathbf{C_p}$	**PRESS**
1	$\gamma_{dmax\text{-}st}$ = 21.08 – 0.0523·(-No.200)	73.68	145.0	66.926
2	$\gamma_{dmax\text{-}st}$ = 18.87 – 0.0751·(-No.200) + 0.0713·(ω_L)	82.89	27.7	44.153
3	$\gamma_{dmax\text{-}st}$ = 19.27 – 0.0783·(-No.200) + 0.0762·(ω_L) –0.0243·(ω_P)	84.64	6.9	40.118
4	$\gamma_{dmax\text{-}st}$ = 21.21 – 0.0618·(-No.200) + 0.0387·(ω_L) –0.0259·(ω_P) – 0.0113·(-No.4)	84.95	5.0	39.690

The results in Table 5.3 show that the improvement in prediction accuracy is negligible when the regression equation developed at Step-4 is used instead of the equation developed at Step-3. Therefore, the model including input variables of –No.200, ω_L and ω_P is considered as the final prediction model;

$$\gamma_{dmax\text{-}st} = 19.27 - 0.0783\cdot(\text{-No.200}) + 0.0762\cdot(\omega_L) - 0.0243\cdot(\omega_P) \qquad (5.3)$$

where -No.200, ω_L and ω_P are expressed in percentages and $\gamma_{dmax\text{-}st}$ in kN/m^3. The scatter diagram of Equation 5.3 is given in Figure 5.8.

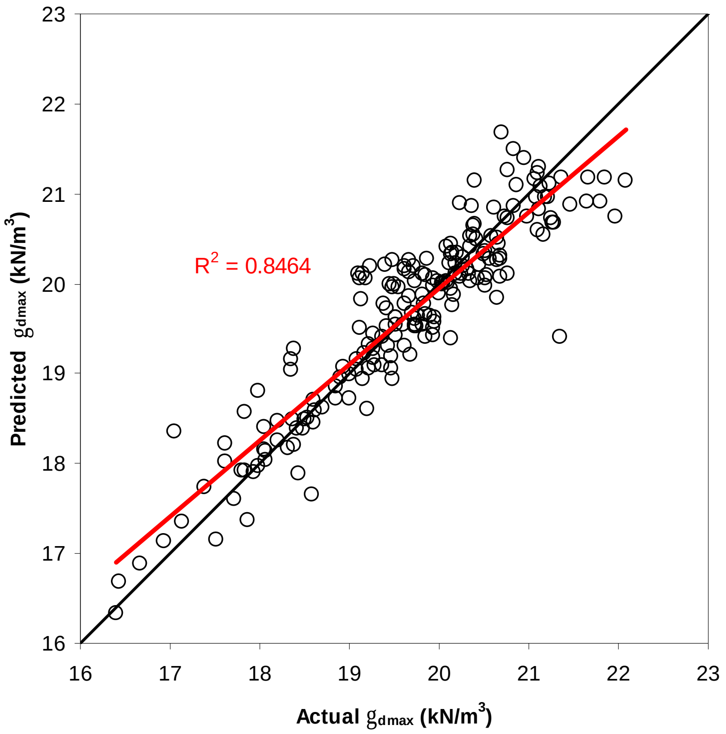

Figure 5.8 Scatter plot of γ_{dmax} at Standard Proctor energy level using Equation 5.3

It is clear from Figure 5.8 that there is somewhat good agreement between the predicted and the corresponding actual $\gamma_{dmax\text{-}st}$ values with considerable scatter at higher values.

5.2.2 MLR Models for Modified Proctor Compaction

Table 5.4 summarizes the results of stepwise regression of the optimum water content at Modified Proctor energy level ($\omega_{opt\text{-}md}$). The analysis was conducted for the significance level of 0.5. The model includes only -No.200 in Step-1 whereas ω_P variable is added to the model in Step-2. At last, -No.200, ω_L and ω_P are used as input variables in Step-3.

Table 5.4 Stepwise regression results for $\omega_{opt\text{-}md}$

Step	Regression Equation	Statistical Features		
		R^2	C_p	PRESS
1	$\omega_{opt\text{-}md} = 5.164 + 0.0787\cdot(\text{-No.200})$	75.95	47.3	135.046
2	$\omega_{opt\text{-}md} = 4.108 + 0.0818\cdot(\text{-No.200}) + 0.0458\cdot(\omega_P)$	78.87	19.7	120.197
3	$\omega_{opt\text{-}md} = 5.464 + 0.0975\cdot(\text{-No.200}) - 0.048\cdot(\omega_L) + 0.0516\cdot(\omega_P)$	80.72	3.0	110.804

As seen in Table 5.4, the regression equation developed in Step-3 is the best predictive model. In terms of C_p statistic, it decreases from 47.3 to 19.7 in Step-2. However, there may be bias because of larger C_p value than the number of input variables. In Step-3, C_p value is equal to the number of input variables which shows the best of fit of the predicted values of $\omega_{opt\text{-}md}$. Therefore, the regression equation developed in Step-3 is determined as the final regression model;

$$\omega_{opt\text{-}md} = 5.464 + 0.0975\cdot(\text{-No.200}) - 0.048\cdot(\omega_L) + 0.0516\cdot(\omega_P) \tag{5.4}$$

where $\omega_{opt\text{-}md}$, -No.200, ω_L and ω_P are expressed in percentages. The scatter plot of Equation 5.4 is shown in Figure 5.9. There is a good fit observed between the predicted and the corresponding actual values of $\omega_{opt\text{-}md}$. However, some scatter values are observed, especially at the higher values.

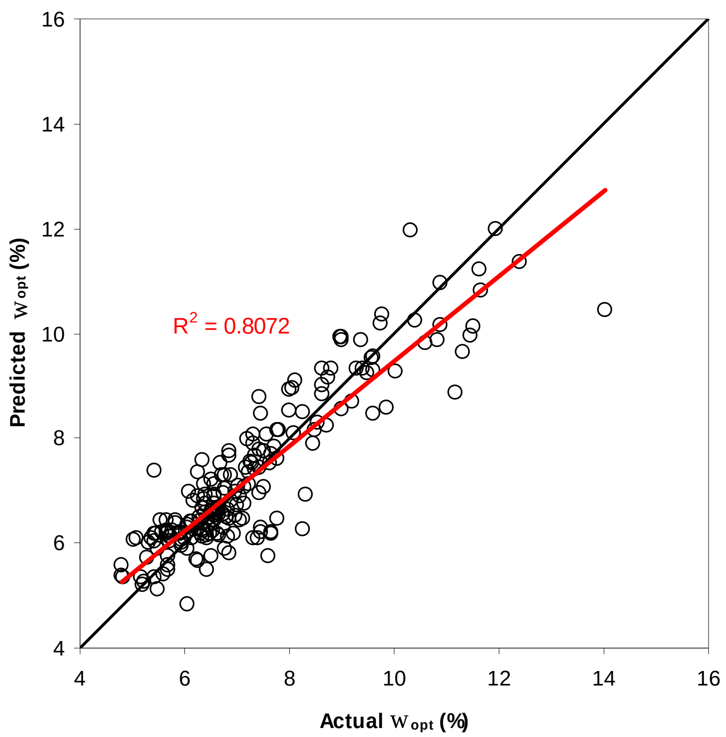

Figure 5.9 Scatter plot of ω_{opt} at Modified Proctor energy level using Equation 5.4

The stepwise regression results of the maximum dry unit weight at Modified Proctor energy level ($\gamma_{dmax\text{-}md}$) are given in Table 5.5. As seen in Table 5.5, R^2 value increases from 66.46 to 81.88 and C_p value decreases from 165.9 to 3.5. This means that the regression model developed in Step-3 is the best fit equation.

Table 5.5 Stepwise regression results for $\gamma_{dmax\text{-}md}$

Step	Regression Equation	Statistical Features		
		R^2	C_p	PRESS
1	$\gamma_{dmax\text{-}md} = 22.36 - 0.0325\cdot(\text{-No.200})$	66.46	165.9	36.419
2	$\gamma_{dmax\text{-}md} = 20.66 - 0.0499\cdot(\text{-No.200}) + 0.0547\cdot(\omega_L)$	79.18	30.6	22.975
3	$\gamma_{dmax\text{-}md} = 20.99 - 0.0525\cdot(\text{-No.200}) + 0.0587\cdot(\omega_L) - 0.0197\cdot(\omega_P)$	81.88	3.5	20.492

In this thesis, the regression equation developed in Step-3 is preferred to predict the maximum dry unit weight at Modified Proctor energy level ($\gamma_{dmax\text{-}md}$);

$$\gamma_{dmax\text{-}md} = 20.99 - 0.0525\cdot(\text{-No.200}) + 0.0587\cdot(\omega_L) - 0.0197\cdot(\omega_P) \tag{5.5}$$

where -No.200, ω_L and ω_P are expressed in percentages and $\gamma_{dmax-md}$ in kN/m^3. The scatter plot of Equation 5.5 is shown in Figure 5.10.

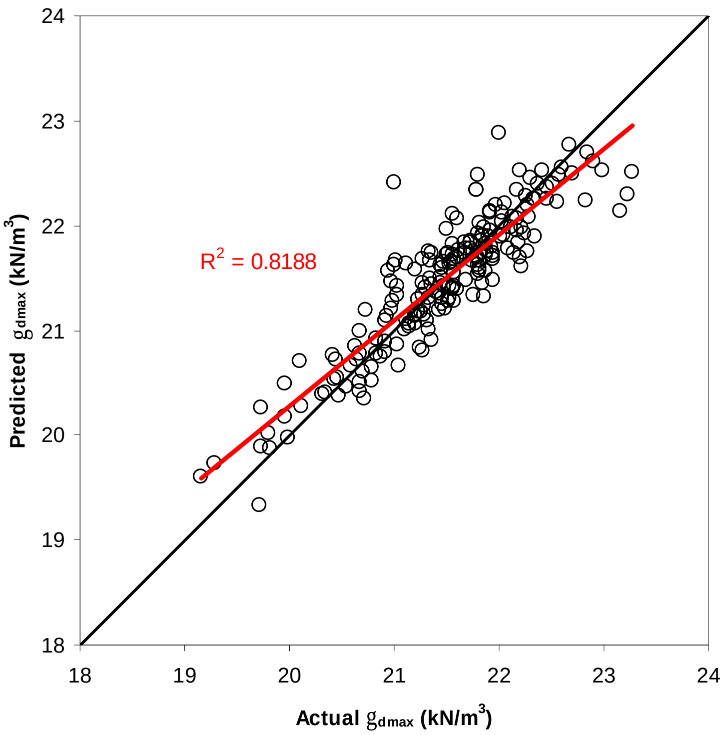

Figure 5.10 Scatter plot of γ_{dmax} at Modified Proctor energy level using Equation 5.5

It is evident that the predicted $\gamma_{dmax-md}$ values are in agreement with the actual $\gamma_{dmax-md}$ with errors acceptable for engineering purposes (Figure 5.10). Eventually, it is evaluated that MLR models could be able to predict the compaction characteristics. However, some scatter data points were observed. This might be occurred due to nonlinear nature of the data and existence of both fine and coarse materials in the data set. Therefore, a nonlinear modeling technique was preferred to use to predict the compaction characteristics.

5.3 Artificial Neural Networks Analysis

ANNs have already been applied successfully to several geotechnical engineering problems as discussed in Chapter 3. ANNs were also used to predict the compaction characteristics of soils (Najjar et al., 1996; Abdel-Rahman, 2008; Sinha & Wang, 2008; Günaydın, 2009; and Sivrikaya & Soycan 2010) or sketch a whole compaction curve (Basheer 2001). However, the developed ANN models were mainly used to predict either fine-grained or coarse-grained compaction characteristics of soils. In this thesis, the compaction characteristics of both fine and coarse-grained soils are predicted. On the other hand and most importantly, the structural information (i.e. the connection weight and bias values, the used transfer functions and etc) of the developed ANN models were not provided by most researchers. Without knowing this information, another person can not use that ANNs model to predict the compaction characteristics of a soil sample. Because of the discussed reasons, new ANN models were developed.

In this thesis, two different ANN models were developed to predict the compaction characteristics; one for maximum dry unit weight (γ_{dmax}) and second for optimum water content (ω_{opt}) of both coarse and fine-grained soils. Additionally, three different ANN models were developed in order to estimate the compaction characteristics under Standard Proctor and Modified Proctor energy levels. The three-layer feed-forward back-propagation (FFBP) algorithm in MATLAB R2009b was used for training the models. In order to determine the best ANN model topology and the model inputs, a trial-and-error approach was performed. MLR analysis showed that the most important variables were liquid limit (ω_L), plastic limit (ω_P), No.4 sieve passing (–No.4) and No.200 sieve passing (–No.200). Therefore, these four soil parameters were used as input variables in ANN models. The effect of transition fine content ratio (TFR) was also investigated. It should be mentioned that TFR was used instead of –No.200 in the models. The coefficient of correlation (R), mean squared error (MSE) and root mean squared error (RMSE) were used as statistical verification parameters while evaluating the performance of the developed ANN models. A total number of 200 individual data cases were used in the models.

All these data were the experimental test results evaluated in this study. Each case included ω_L, ω_P, –No.4 and –No.200 or TFR instead of –No.200 as input, γ_{dmax} and ω_{opt} were the targets for all cases. The statistical features of the input variables are summarized in Table 5.6

Table 5.6 Statistical features of the input variables

Variables	**Mean**	**Standard Deviation**	**Minimum**	**Maximum**
w_L **(%)**	39.6	7.6	24.8	58.3
w_P **(%)**	18.7	2.4	15.4	26.6
-No.4 (%)	76.1	18.5	10.8	99.8
-No.200 (%)	26.8	18.4	1.6	81.6
TFR	2.22	1.54	0.13	6.80
$g_{dmax-ST}$* **(kN/m^3)**	19.68	1.12	16.41	22.08
w_{opt-ST} **(%)**	10.8	2.7	6.2	19.7
$g_{dmax-MD}$* **(kN/m^3)**	21.49	0.73	19.16	23.28
w_{opt-MD} **(%)**	7.3	1.7	4.8	14.0

*ST: Standard Proctor, MD: Modified Proctor

Effects of data transformation and data division methods on ANN models were explored by comparing the performances of ANN models developed to estimate compaction characteristics of soil mixtures at Standard Proctor compaction energy level.

In order to investigate the effect of transformation techniques discussed in Chapter 3.5.1, only the raw input data were normalized from their original units. Before the training process, the transformed data were portioned into training, testing and validation subsets on a random basis of 70%, 15% and 15%, respectively. ANN models' performances were evaluated using a trial-and-error approach where ANN models were trained using one hidden layer with varying number of neurons between 3 and 21. The relation between the hidden layer neuron number and the coefficient of correlation (R) of the testing set of ANN models is shown in Figure 5.11 with respect to the aforementioned four transformation methods. As can be seen from Figure 5.10, there is no direct relation between the hidden layer neuron number and R values of the models.

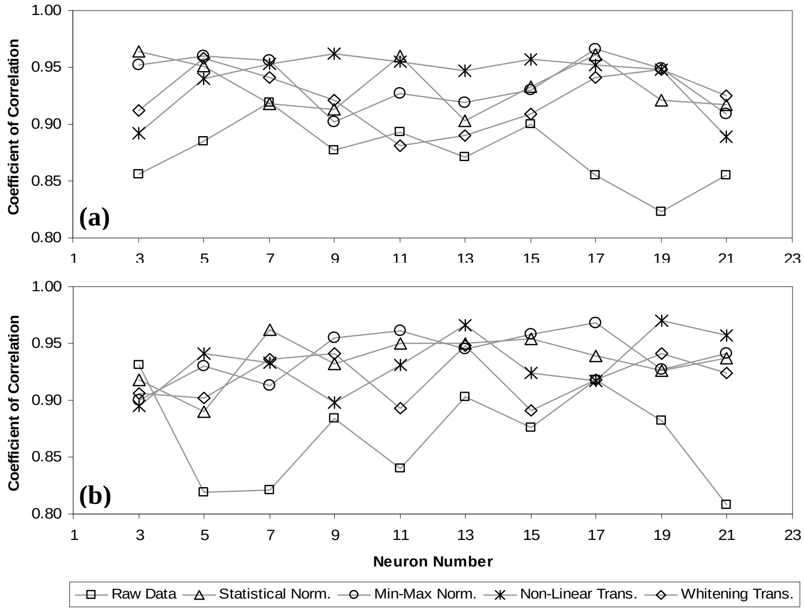

Figure 5.11 Coefficient of correlation values of ANN prediction models of (a) γ_{dmax} and (b) ω_{opt} versus hidden neuron number using the four transformation methods and raw data.

When comparing R values with respect to the raw data and the transformed data, it is clear that performance of the raw data is worse than the four transformation methods. The findings from transformation methods reveal that none of the four transformation methods have superiority to each other. However, if one prefers to transform the output variable(s), there will be some limitations due to the de-transformation of the output variable(s) to its/their original scale. Especially, there will be wrong reverse scaling when non-linear transformation method used. Therefore, in this study all the input and target variables of the data were transformed using generally accepted min-max normalization method for ANN models. The outputs of the ANN models were then de-normalized to their original units.

The data division effect on ANN models was also examined. For this reason, the random data division method was compared with the fuzzy c-means clustering method. The main data set was divided into training, testing and validation subsets using two division methods. It is proper to mention that the training subset was used to adjust the connection weights. The validation subset was used to check the performance of the network in each step in order to stop training process if it started to overfit the training data. After convergence of the training process, generalization ability of the trained network is evaluated with the testing subset as mentioned before. In random division method, a total number of 200 data cases were randomly divided into training, testing and validation subsets. In total, 70% of the data (140 individual cases) were used for training. The rest was equally shared by the testing and validation subsets (for each subset 30 individual cases).

In fuzzy c-means clustering (FCM) method, the main data set was clustered using the procedure outlined in Chapter 3.5.2.2 by means of MATLAB R2009b computer program. Prior to the clustering process, one should choose the optimum number of clusters (NC). In this study, NC was determined utilizing a trial and error approach by means of the Cluster Validity Analysis Platform (CVAP) (Wang et al. 2009). Each trial was then compared by the Silhouette, Calinski-Harabasz, Dunn and Davies-Bouldin validity indices (Wang et al. 2009). The NC yielding the lowest index number is said to be the optimum cluster number in Davies-Bouldin Index whereas the reverse is true for the others. It was seen that the main data set used in this study should be divided into three clusters (Figure 5.12).

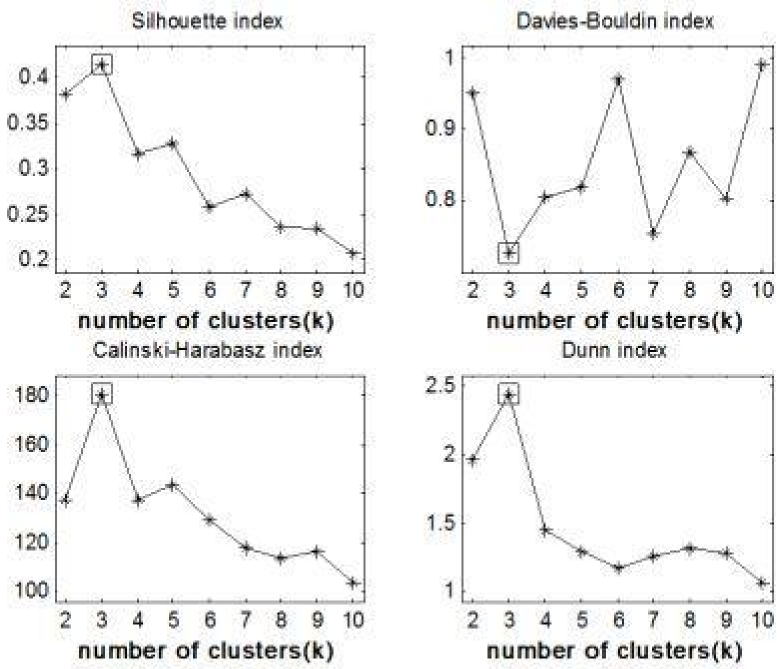

Figure 5.12 Cluster validity analysis results

Determination of the optimum NC was followed by clustering of the data set using FCM method. The Cluster #1 consists of 44 individual cases. In a similar manner, Cluster #2 and Cluster #3 contain 50 and 106 cases, respectively. When the data have been clustered successfully, the modeler should collect the data cases from each cluster to form training, testing and validation subsets. In this respect, different approaches were suggested (Kocjancic & Zupan, 2000; and Bowden et al. 2002). In general, from each cluster one case is selected for validation and one case for testing and the remaining cases are devoted to the training subset. If an exception occurs in a case where a cluster includes two data cases, one case is sent to training and the remaining one is sent to testing subset. If only one data case exists, it is used in the training subset. In this study, however, this approach could not be applied to these three clusters. If it was applied, only three data cases would contain both testing and validation subsets. Hence, the clustered data were randomly divided into training (70%), testing (15%) and validation (15%) subsets. Such a method of data division is called as the "Cluster Method" in the rest of the text as depicted in Figure 5.13.

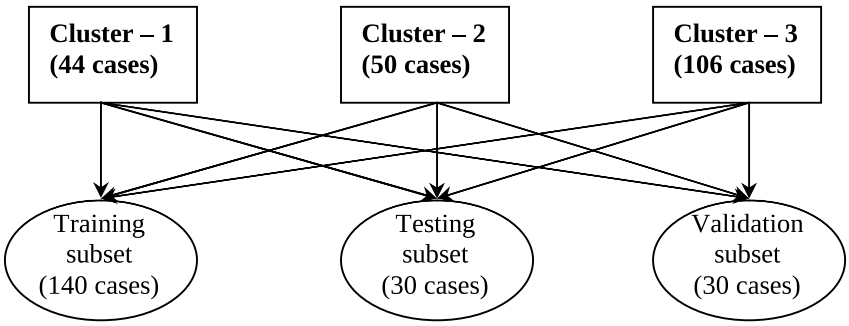

Cluster Method

Figure 5.13 Schematic representation of "Cluster Method"

The data were also partitioned into sub-clusters in order to check possibility of performance increase with sub-clustered data. Therefore, the above given clusters were further subject to clustering analysis. The above mentioned analysis showed that Cluster #1, #2 and #3 could be divided into 9, 5 and 10 sub-clusters, respectively. The data were then assigned to each sub-cluster using FCM clustering method. The sub-clustered data were divided into training, testing and validation subsets following two different approaches. The first one was the selection of the training, testing and validation subsets using aforementioned approach by deciding the exceptional conditions (The Sub-clustering Method #1). In total, 154 individual cases were used for training, 24 for testing and 22 for validation (Figure 5.14).

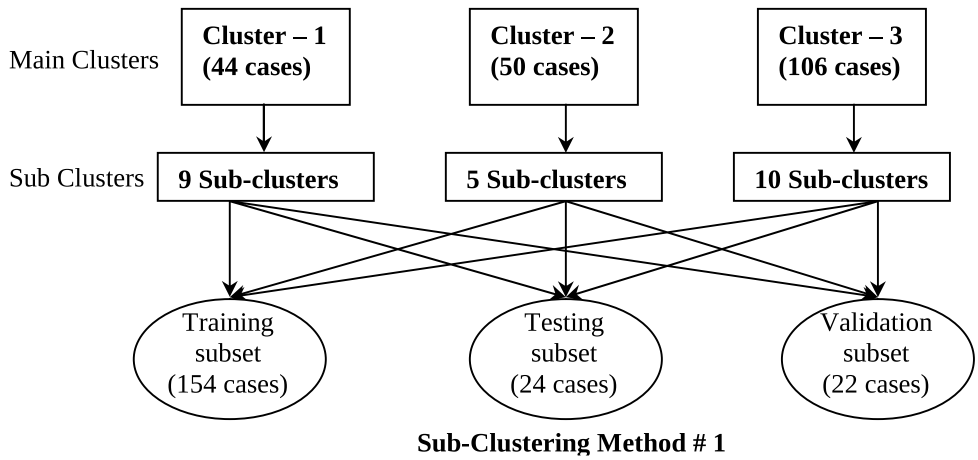

Figure 5.14 Schematic representation of "Sub-Clustering Method #1"

In the second approach, a systematic methodology was followed as suggested by Shahin et al. (2004). They recommended that the data cases are arranged with an order of increasing membership value. Then each case is separated in to ten membership intervals (i.e. 0.0-0.1, 0.1-0.2 … 0.9-1.0). From each interval, one data case is sent to testing and validation subsets, respectively. The remaining ones are sent to the training subset (Shahin et al. 2004). In this manner, a total of 123 cases were separated for training whereas 55 and 22 cases were sent to testing and validation subsets, respectively (The Sub-clustering Method #2). Figure 5.15 depicts schematic representation of Sub-clustering Method #2.

In order to determine how data division methods affect the performance of ANN models, 100 runs starting from different initial conditions for each method were made and statistical features were recorded. The optimum characteristics of ANN models varied depending on the division method. Table 5.7 summarizes the mean, the standard deviation, the minimum, the maximum, and the range values of the testing subset for each data division method.

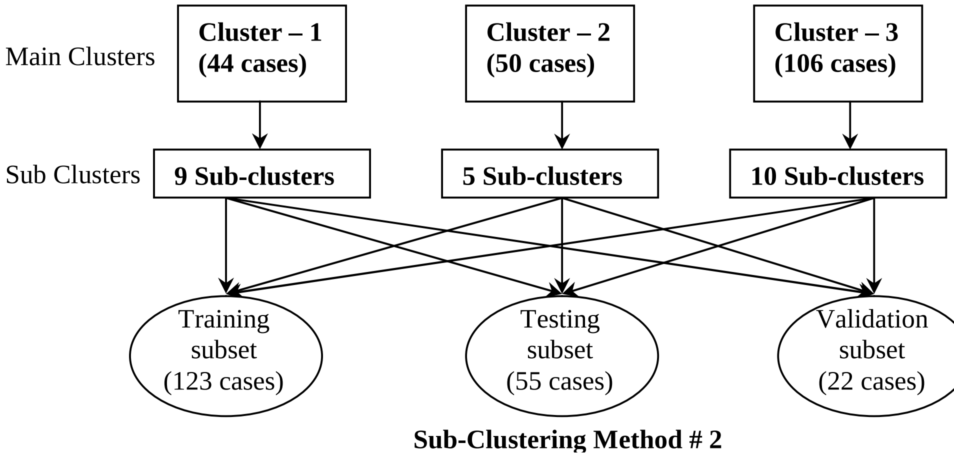

Figure 5.15 Schematic representation of "Sub-Clustering Method #2"

One can notice that the random division method is the most unstable with the highest standard deviation. This may be attributed to the fact that the data were not in the same range for the training, testing and validation subsets. As seen in Table 5.7, while the maximum values of MSE and RMSE decrease, the minimum values of R increase both in γ_{dmax} and ω_{opt} ANN models in "Cluster Method". Conversely, there is a little decrease in the maximum R values in "Cluster Method". It was observed that there was a steady increase in model performance when the main data set was separated into three clusters compared to randomly division. There was also an increase in performance when the sub-clustering methods were used. This is especially true at γ_{dmax} prediction models when the main data were divided using "Sub-clustering Method#1". However, there was no similar performance increase observed at ω_{opt} prediction models in the same division method. As noted from Table 5.7, although there was some performance decrease, the "Sub-clustering Method#2" was the most stable method.

The effect of the four division methods on the testing subset performance of γ_{dmax} prediction models was evaluated by comparing the best and the worst performances, as depicted in Figure 5.16. As it was mentioned previously, the testing subset consisted of 30 individual data cases when the main data set was divided randomly. Also, the testing subset included 30, 24 and 55 data cases when it was divided by the "Cluster Method", "Sub-clustering Method#1" and "Sub-clustering Method#2", respectively. An output of ANN model and the corresponding target is shown by a dot in Figure 5.16. It is well known that the closer the dots to each other around the equality line, the better the performance of the testing subset. It is clear from Figure 5.16 that the testing subset of the best performance of each division method is acceptable due to R values. In contrast, at the worst performance of the “Random Division” method, there is a dramatic performance decrease. This reduction occurs due to the existence of outlier data. This means that the training subset does not cover all pattern ranges in the data base. Consequently, at the testing stage the ANN model is forced to extrapolate the outlier data. Similarly, the performance of the ANN model decreases due to existing outlier data when data are divided using the “Cluster Method”. There is no major performance reduction when the main data are divided by both sub-clustering methods.

Table 5.7 Performance statistics of testing subset with respect to the data division methods

Division Method	Statistical Features	g_{dmax}			w_{opt}		
		MSE	**RMSE**	**R**	**MSE**	**RMSE**	**R**
Random Division Method	Mean	0.306	0.482	0.922	1.211	1.030	0.921
	St.Dev.	0.775	0.273	0.060	1.773	0.390	0.068
	Minimum	0.079	0.282	0.550	0.438	0.662	0.408
	Maximum	7.448	2.729	0.979	17.006	4.124	0.979
	Range	7.363	2.447	0.429	16.569	3.462	0.571
Cluster Method	Mean	0.129	0.463	0.922	1.151	1.049	0.925
	St.Dev.	0.063	0.065	0.020	0.552	0.226	0.030
	Minimum	0.082	0.287	0.854	0.566	0.753	0.795
	Maximum	0.434	0.659	0.973	3.549	1.884	0.962
	Range	0.352	0.372	0.119	2.983	1.131	0.167
Sub-clustering Method #1	Mean	0.083	0.288	0.977	0.875	0.921	0.935
	St.Dev.	0.013	0.022	0.005	0.168	0.090	0.017
	Minimum	0.053	0.230	0.962	0.547	0.740	0.874
	Maximum	0.132	0.364	0.985	1.396	1.182	0.963
	Range	0.080	0.134	0.024	0.849	0.442	0.089
Sub-clustering Method #2	Mean	0.150	0.387	0.950	0.932	0.963	0.943
	St.Dev.	0.022	0.027	0.007	0.140	0.071	0.008
	Minimum	0.096	0.310	0.929	0.619	0.787	0.922
	Maximum	0.214	0.463	0.968	1.602	1.266	0.962
	Range	0.119	0.154	0.038	0.982	0.478	0.040

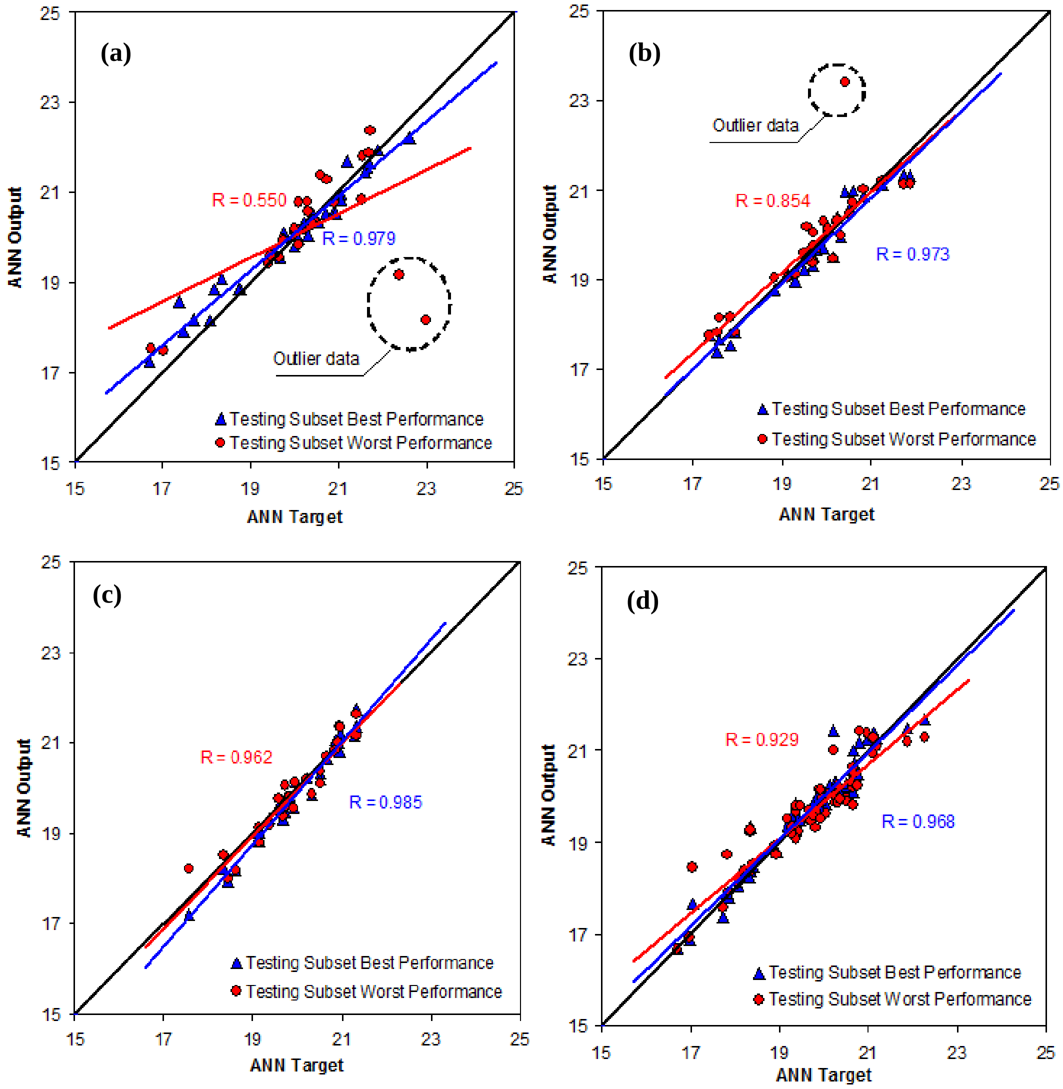

Figure 5.16 The best and worst performance comparison of γ_{dmax} prediction models: (a) Randomly division method, (b) Cluster method, (c) Sub-clustering method#1, (d) Sub-clustering method#2

In a similar manner, the best and worst testing subset performances of ω_{opt} prediction models are compared with respect to the four division methods in Figure 5.17. Performance trends of ω_{opt} prediction models were found to be similar with those of γ_{dmax} models. In general, predictions of the best performances are in good agreement with the corresponding targets. Conversely, some outlier data exist on the worst performance except for the “Sub-clustering Method#2”. These outlier data cause reductions in the performance of ω_{opt} prediction models like those in γ_{dmax}. It is understood that the random division method is the most unstable method with the highest standard deviation. The sub-clustering method according to the 2nd Approach is the most stable method with the lowest standard deviation.

Consequently, before the training process, the data set was normalized using min-max normalization method, and it was clustered by means of fuzzy c-means clustering approach. This methodology was named as Sub-clustering Method#2. In the analysis, only the author's experimental data were used. A total of 200 Proctor compaction test data were used in model development. In order to train the network, a total number of 123 data were used. Also, ANN model was cross-validated during training not to cause overfitting, 22 data were used for this purpose. When the model converged, its generalization ability was controlled by a testing subset which consisted of a total number of 55 data. In order to determine the best ANN model topology, a trial and error approach was performed on one hidden layer where number of neurons varied between 3 and 21 at equal increments of two. It should be pointed out that the robustness of developed ANN models was examined by running each trial of model ten times starting from different initial conditions (i.e. random initial weights and biases). The best ANN topology was determined by checking the average statistical features (i.e. coefficient of correlation {R}, mean squared error {MSE} and root mean squared error {RMSE}) values of the testing subset.

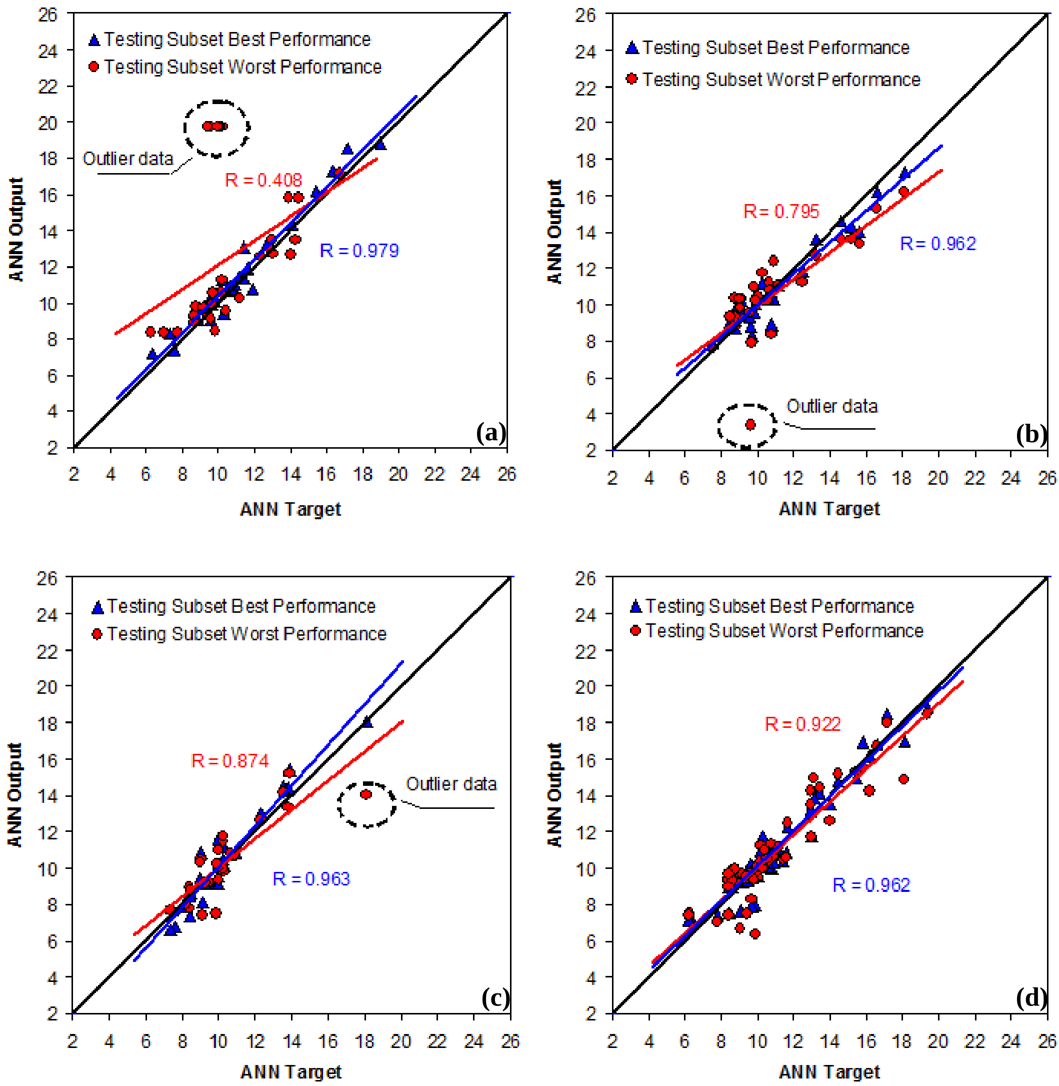

Figure 5.17 The best and worst performance comparison of ω_{opt} prediction models: (a) Randomly division method, (b) Cluster method, (c) Sub-clustering method#1, (d) Sub-clustering method#2

5.3.1 Standard Proctor Compaction ANN Models

The best model topology for γ_{dmax} was determined using a trial-and-error approach where ANN models were trained using one hidden layer where number of neurons varied between 3 and 21 at equal increments of two.

The ANN prediction models of γ_{dmax} are given in Table 5.8. M-1G-S and M-2G-S models yielded close results. The M-2G-S model may be preferred over the former since it was found that inclusion of the TFR parameter to the ANN model provided a slight yet noticeable improvement in the prediction of the optimum water content. Figure 5.18 shows the agreement plot of M-2G-S model.

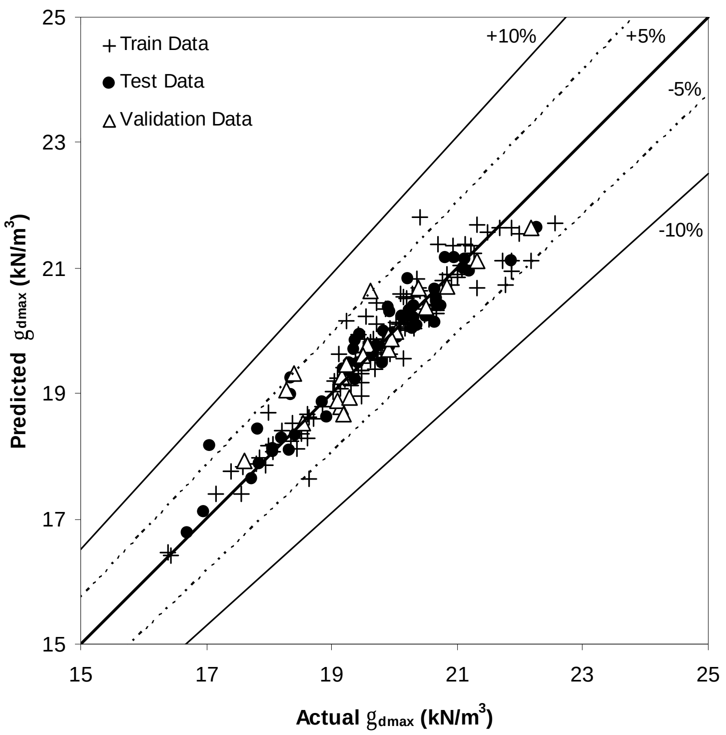

Figure 5.18 Agreement plots of M-2G-S ANN model

The best model topology for ω_{opt} was determined in the same manner that was made for γ_{dmax}. The performance statistics of ANN models are summarized in Table 5.9. The M-2W-S (4-17-1) is the best predictive model. Figure 5.19 presents the agreement plot of M-2W-S model. Comparison of the performance of ANN models reveals that the TFR parameter causes an increase in the prediction capability of M2-W-S as shown in Table 5.9 and Figure 5.19. The connection weights and biases of M-2G-S and M-2W-S are summarized in Table 5.10.

Table 5.8 Prediction results of Standard Proctor ANN models for γ_{dmax}

Model No.	Model Inputs	Best Topology	Statistical Features		
			Training Data	Testing Data	Validation Data
M-1G-S	ω_L,ω_P,-No.4, -No.200	4-7-1[d]	0.974[a] 0.078[b] 0.279[c]	0.950 0.148 0.383	0.926 0.157 0.394
M-2G-S	ω_L,ω_P, -No.4, TFR	4-5-1	0.966 0.079 0.281	0.951 0.144 0.379	0.924 0.160 0.399
M-3G-S	ω_L,ω_P, -No.4	3-5-1	0.956 0.047 0.216	0.947 0.156 0.393	0.919 0.168 0.409
M-4G-S	ω_L,ω_P, -No.200	3-5-1	0.945 0.094 0.306	0.935 0.193 0.438	0.919 0.167 0.408
M-5G-S	ω_L,ω_P, TFR	3-7-1	0.951 0.119 0.344	0.936 0.190 0.436	0.927 0.149 0.386
M-6G-S	ω_L, -No.4, -No.200	3-3-1	0.947 0.079 0.281	0.945 0.163 0.402	0.906 0.189 0.434
M-7G-S	ω_L,ω_P	2-5-1	0.936 0.228 0.477	0.936 0.190 0.436	0.923 0.156 0.392
M-8G-S	-No.4, -No.200	2-11-1	0.966 0.052 0.228	0.947 0.155 0.393	0.921 0.171 0.412

[a] *Coefficient of correlation (R)*
[b] *Mean squared error (MSE)*
[c] *Root mean squared error (RMSE)*
[d] *x-x-x refers the number of neurons in the input, hidden and output layers, respectively.*

Table 5.9 Prediction results of Standard Proctor ANN models for ω_{opt}

Model No.	**Model Inputs**	**Best Topology**	**Statistical Features**		
			Training Data	**Testing Data**	**Validation Data**
M-1W-S	ω_L,ω_P, -No.4, -No.200	4-17-1[d]	0.971[a] 0.649[b] 0.805[c]	0.944 0.908 0.952	0.944 0.572 0.756
M-2W-S	ω_L,ω_P, -No.4, TFR	4-17-1	0.973 0.327 0.571	0.952 0.766 0.875	0.948 0.544 0.875
M-3W-S	ω_L,ω_P, -No.4	3-19-1	0.972 0.389 0.623	0.948 0.839 0.915	0.941 0.606 0.778
M-4W-S	ω_L,ω_P, -No.200	3-3-1	0.937 0.709 0.842	0.938 0.981 0.989	0.923 0.802 0.894
M-5W-S	ω_L,ω_P, TFR	3-5-1	0.943 0.564 0.751	0.936 1.015 1.007	0.930 0.722 0.849
M-6W-S	ω_L, -No.4, -No.200	3-21-1	0.969 0.347 0.589	0.942 0.975 0.986	0.933 0.694 0.831
M-7W-S	ω_L,ω_P	2-7-1	0.945 0.637 0.798	0.938 0.974 0.986	0.930 0.737 0.854
M-8W-S	-No.4, -No.200	2-7-1	0.948 0.392 0.626	0.938 0.978 0.988	0.936 0.696 0.834

[a] *Coefficient of correlation (R)*
[b] *Mean squared error (MSE)*
[c] *Root mean squared error (RMSE)*
[d] *x-x-x refers the number of neurons in the input, hidden and output layers, respectively.*

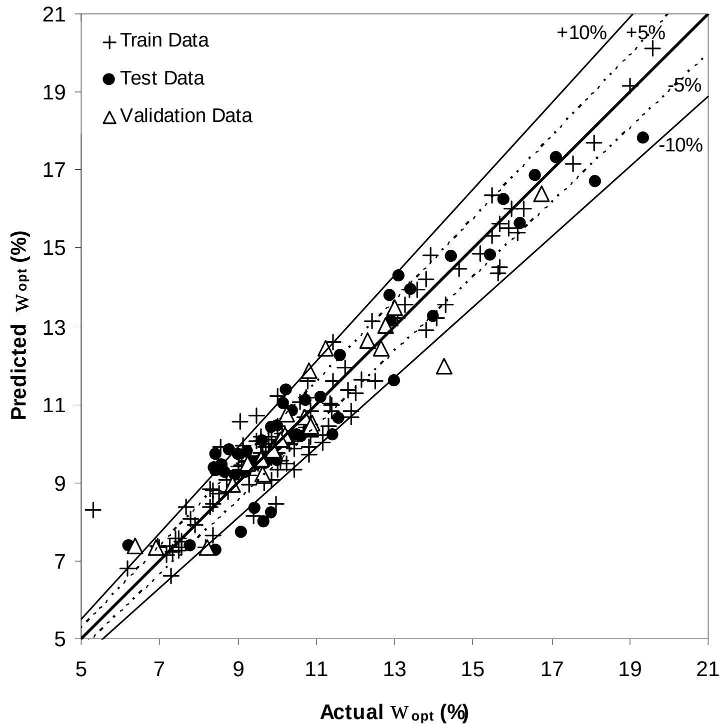

Figure 5.19 Agreement plots of M-2W-S ANN model

Table 5.10 Weight and bias values of Standard Proctor ANN models of M-2G-S and M-2W-S

Model No.	Hidden Neuron Number	Weight: Input neurons w_L	w_P	-No.4	TFR	Output neuron g_{dmax} / w_{opt} [a]	Bias: Hidden layer	Output layer
M-2G-S	1	2.9196	-0.9046	5.8786	-5.8664	-0.3174	-3.9300	0.3739
	2	1.7062	2.9127	0.9245	6.9295	-0.2316	-12.0320	
	3	0.3281	2.6715	1.1903	-6.4897	0.5599	1.6125	
	4	6.0121	-0.9815	0.5904	3.4605	-0.3235	-4.1519	
	5	-1.5558	5.2925	7.0268	-3.0360	-0.2713	-8.5444	
M-2W-S	1	5.7625	9.1063	-2.5363	-0.3118	0.8361	-12.8809	0.372
	2	10.2769	-5.7650	1.7426	1.7388	-1.7890	-7.2913	
	3	-7.9793	4.2851	6.2837	5.6012	2.1894	2.9395	
	4	5.0092	2.0755	1.8058	8.8577	-0.7459	-10.8061	
	5	-8.3762	1.8147	4.7882	6.5149	-1.2386	-1.5598	
	6	-4.4433	8.6604	-0.0978	-6.9600	-1.3826	4.3215	
	7	-7.9736	-3.9796	-6.4877	0.6891	0.4662	7.7564	
	8	9.6589	-4.5240	-1.1491	6.0885	1.9296	-6.3874	
	9	1.0589	-0.6334	7.0738	-9.1246	-1.2439	2.2074	
	10	-6.5381	-5.6584	4.3297	-6.8842	0.2267	2.2065	
	11	12.3637	-3.7119	-3.8345	3.4477	0.9056	-0.9883	
	12	8.6190	1.2928	-5.1053	-4.2122	-0.8849	0.0657	
	13	0.7709	-6.0275	-9.0712	0.2426	-1.4684	4.7755	
	14	-2.7730	5.9350	7.1598	-3.5769	1.0359	-5.8581	
	15	5.2816	3.4542	6.7350	0.7442	-1.0309	-3.7486	
	16	-6.2550	8.3590	3.6148	2.6229	0.9283	-11.3654	
	17	3.3958	0.3452	8.1388	-7.6364	1.4265	2.954	

[a] The output neuron of M-2G-S is γ_{dmax} and M-2W-S is ω_{opt}.

5.3.2 Modified Proctor Compaction ANN Models

The best average values of ten runs of each γ_{dmax} model are summarized in Table 5.11. There is no considerable performance increase when TFR is used instead of –No.200 (M-1G-M versus M-2G-M ANN models). The results in Table 5.11 show that the input of –No.4 is an important parameter for prediction of modified γ_{dmax}. For instance, R value of the testing subset decreases from 0.963 to 0.946, M-3G-M and M-4G-M models are compared. The R, MSE, and RMSE values of M-9G-M model are 0.946, 0.069, and 0.262, respectively where only the Atterberg limits are used as input features. It is inferred that use of only the Atterberg limits is not sufficient to predict modified γ_{dmax}. However, as seen in Table 5.11, the performance of M-11G-M model is adequate. Consequently, M-11G-M model was decided as the best ANN topology since use of –No.4 and –No.200 parameters may be preferred due to fewer numbers of input data. Following the determination of the best ANN topology, the model was run once more and the outputs of the ANN model were recorded. The outputs and the corresponding targets are displayed in Figure 5.20.

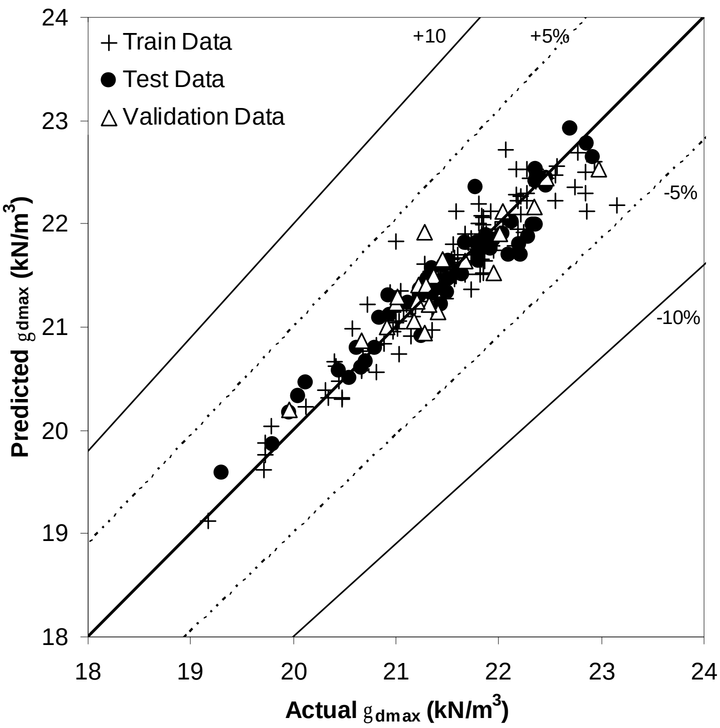

Figure 5.20 Agreement plot of M-11G-M prediction model

Table 5.11 Prediction results of Modified Proctor ANN models for γ_{dmax}

Model No.	Model Inputs	Best Topology	Statistical Features		
			Training Data	Testing Data	Validation Data
M-1G-M	ω_L,ω_P,-No.4, -No.200	4-9-1[d]	0.950[a] 0.057[b] 0.185[c]	0.967 0.049 0.221	0.904 0.077 0.277
M-2G-M	ω_L,ω_P, -No.4, TFR	4-19-1	0.970 0.012 0.079	0.964 0.051 0.224	0.908 0.074 0.271
M-3G-M	ω_L,ω_P, -No.4	3-5-1	0.943 0.063 0.194	0.963 0.052 0.228	0.898 0.083 0.287
M-4G-M	ω_L,ω_P, -No.200	3-19-1	0.959 0.071 0.231	0.946 0.068 0.261	0.897 0.083 0.289
M-5G-M	ω_L,ω_P, TFR	3-15-1	0.961 0.034 0.130	0.949 0.064 0.252	0.896 0.083 0.287
M-6G-M	ω_L, -No.4, -No.200	3-3-1	0.942 0.054 0.194	0.968 0.049 0.220	0.905 0.077 0.278
M-7G-M	ω_P, -No.4, -No.200	3-5-1	0.939 0.054 0.182	0.964 0.053 0.230	0.901 0.079 0.281
M-8G-M	ω_P, -No.4, TFR	3-17-1	0.969 0.037 0.137	0.962 0.053 0.229	0.904 0.079 0.280
M-9G-M	ω_L, ω_P	2-9-1	0.950 0.064 0.220	0.946 0.069 0.262	0.918 0.068 0.260
M-10G-M	ω_p, -No.4	2-15-1	0.897 0.176 0.280	0.885 0.146 0.381	0.819 0.136 0.367
M-11G-M	-No.4, -No.200	2-5-1	0.939 0.074 0.229	0.962 0.050 0.223	0.912 0.072 0.267
M-12G-M	ω_L, -No.4	2-5-1	0.942 0.061 0.209	0.961 0.054 0.231	0.903 0.079 0.280

The prediction results of modified ω_{opt} are given in Table 5.12. Like in modified γ_{dmax}, using TFR instead of –No.200 does not cause a considerable performance increase when M-2W-M is compared with M-1W-M. As noted from Table 5.12, there is no definite indicator which input variable affects the performance of a model in a positive or negative way. For instance, the performance statistics of the testing subset of both models are almost same when M-3W-M is compared with M-4W-M. Same comparison can be made between M-9W-M and M-11W-M models. As a result, M-11W-M model is considered as the best ANN topology due to the presence of only sieve analysis test results (i.e. –No.4 and –No.200). Figure 5.21 presents the agreement plots both of M-11W-M model. The connection weights and biases of M-11G-M and M-11W-M are summarized in Table 5.13.

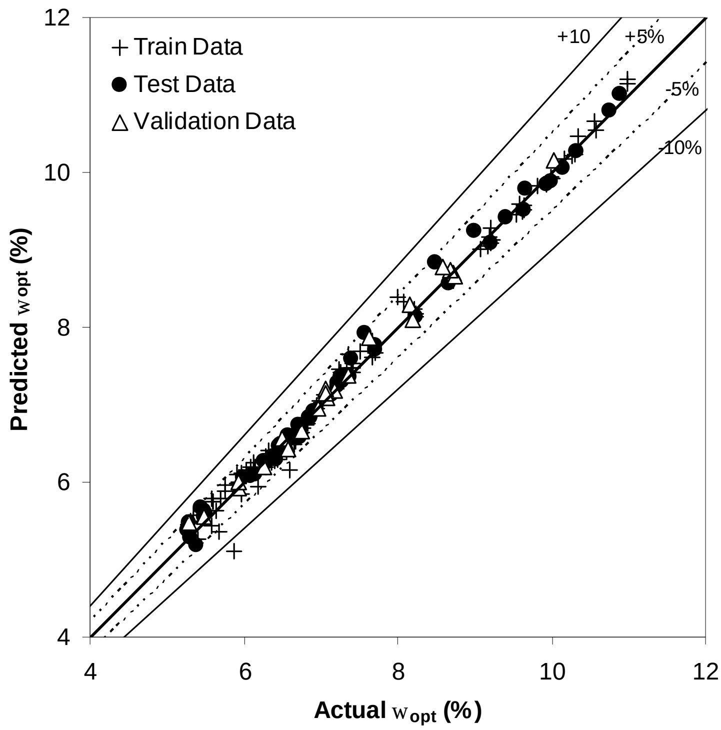

Figure 5.21 Agreement plot of M-11W-M prediction models

Table 5.12 Prediction results of Modified Proctor ANN models for ω_{opt}

Model No.	Model Inputs	Best Topology	Statistical Features		
			Training Data	Testing Data	Validation Data
M-1W-M	ω_L,ω_P,-No.4, -No.200	4-5-1[d]	0.936[a]	0.959	0.913
			0.314[b]	0.287	0.453
			0.470[c]	0.532	0.671
M-2W-M	ω_L,ω_P, -No.4, TFR	4-7-1	0.944	0.957	0.900
			0.357	0.306	0.495
			0.443	0.552	0.703
M-3W-M	ω_L,ω_P, -No.4	3-3-1	0.927	0.959	0.900
			0.211	0.296	0.509
			0.328	0.542	0.711
M-4W-M	ω_L,ω_P, -No.200	3-5-1	0.935	0.960	0.912
			0.330	0.270	0.444
			0.473	0.519	0.666
M-5W-M	ω_L,ω_P, TFR	3-3-1	0.930	0.960	0.914
			0.350	0.265	0.443
			0.450	0.514	0.665
M-6W-M	ω_L, -No.4, -No.200	3-3-1	0.934	0.959	0.904
			0.139	0.275	0.491
			0.288	0.522	0.699
M-7W-M	ω_P, -No.4, -No.200	3-5-1	0.935	0.958	0.912
			0.238	0.287	0.463
			0.398	0.536	0.679
M-8W-M	ω_P, -No.4, TFR	3-3-1	0.931	0.959	0.907
			0.241	0.272	0.476
			0.375	0.521	0.689
M-9W-M	ω_L, ω_P	2-5-1	0.926	0.961	0.911
			0.308	0.278	0.460
			0.491	0.527	0.678
M-10W-M	ω_p, -No.4	2-19-1	0.856	0.815	0.807
			0.734	1.045	0.849
			0.600	1.018	0.918
M-11W-M	-No.4, -No.200	2-3-1	0.935	0.960	0.911
			0.249	0.269	0.469
			0.367	0.518	0.684
M-12W-M	ω_L, -No.4	2-3-1	0.937	0.963	0.912
			0.356	0.252	0.446
			0.428	0.502	0.666

Table 5.13 Weight and bias values of Modified Proctor ANN models of M-11G-M and M-11W-M

Model No.	Hidden Neuron Number	Weight			Bias	
		Input neurons		Output neuron	Hidden layer	Output layer
		-No.4	-No.200	γ_{dmax} [a] ω_{opt}		
M-11G-M	1	-9.4932	-5.2521	0.3218	11.5623	-6.9981
	2	10.4439	-10.3587	0.1883	-3.9571	
	3	0.4600	6.6579	9.1932	1.0760	
	4	1.5601	7.1525	-3.4206	-1.0218	
	5	13.5008	-14.5844	1.4059	3.5333	
M-11W-M	1	-1.4542	11.1347	-2.4711	2.1675	8.5884
	2	89.6665	58.6898	-5.0764	0.3200	
	3	-0.2085	-3.1413	-1.7103	0.9392	

[a] The output neuron of M-11G-M is γ_{dmax} and M-11W-M is ω_{opt}.

5.3.3 Proctor Energy ANN Models

In the past, some researchers tried to correlate γ_{dmax} and ω_{opt} with compaction energy level (Blotz et al., 1998; Gurtug & Sridharan, 2004; Nagaraj et al., 2006; Horpibulsuk et al., 2008; Sivrikaya et al., 2008). In this respect, a neural network was developed by considering compaction energy level (E) as a new feature. For Standard Proctor and Modified Proctor energy levels, this new feature was taken as 593.7 and 2710.5 kJ/m^3, respectively. As it was mentioned before, data set was normalized using min-max normalization method and clustered by means of fuzzy clustering technique. Also, the analysis was performed using the author's experimental results. In order to model Proctor compaction parameters with respect to compaction energy level, a total number of 400 data were used. Half the data are Standard Proctor compaction test results and remaining data are Modified Proctor test results. A total of 246 data were separated for training subset whereas 110 and 44 data were sent to testing and validation subsets, respectively. The prediction results are given in Table 5.14 for estimation of γ_{dmax}. It is revealed from Table 5.14 that the M-6G-E neural networks model is the best prediction model. This decision is reached since (1) there is no further performance improvement occurred with inputting rather than –No.4, –No.200 and E parameters when statistical features of the developed models are checked, (2) only one laboratory test is necessary (i.e. sieve analysis test) for this model. Agreement plot of M-6G-E model is plotted in Figure 5.22.

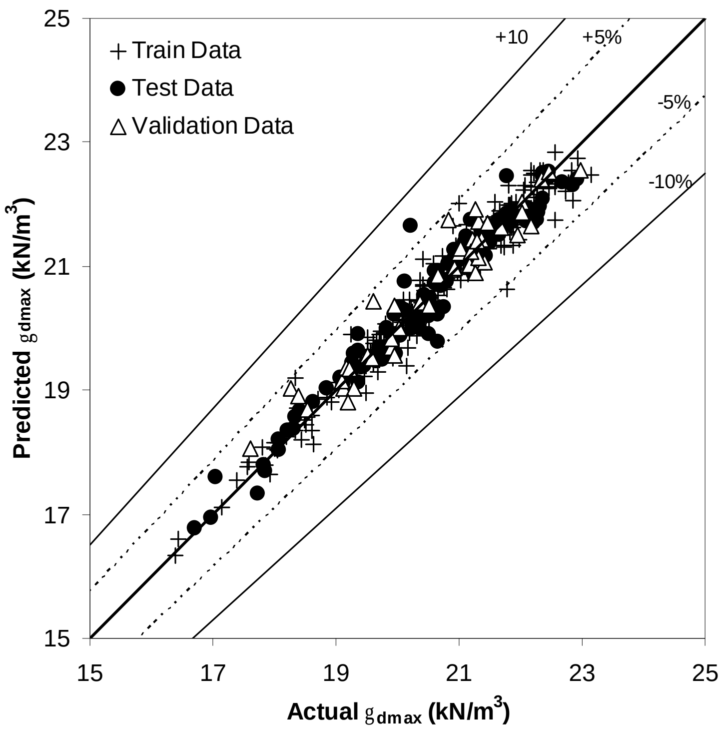

Figure 5.22 Agreement plot of M-6G-E prediction model

Table 5.14 Prediction results of the compaction energy ANN models for γ_{dmax}

Model No.	**Model Inputs**	**Best Topology**	**Statistical Features**		
			Training Data	**Testing Data**	**Validation Data**
M-1G-E	ω_L,ω_P,-No.4, -No.200, E	5-11-1[d]	0.984[a] 0.092[b] 0.212[c]	0.978 0.087 0.295	0.966 0.108 0.329
M-2G-E	ω_L,ω_P, -No.4, TFR, E	5-11-1	0.982 0.106 0.209	0.978 0.085 0.290	0.966 0.107 0.327
M-3G-E	ω_L, -No.4, TFR, E	4-21-1	0.985 0.101 0.219	0.972 0.107 0.325	0.964 0.116 0.340
M-4G-E	ω_P, -No.4, TFR, E	4-13-1	0.984 0.117 0.243	0.977 0.086 0.292	0.966 0.110 0.331
M-5G-E	-No.4, TFR, E	3-19-1	0.978 0.119 0.271	0.975 0.095 0.307	0.960 0.128 0.357
M-6G-E	-No.4,-No.200, E	3-17-1	0.980 0.071 0.186	0.977 0.089 0.298	0.965 0.115 0.338
M-7G-E	ω_L, ω_P, E	3-11-1	0.957 0.163 0.317	0.942 0.221 0.465	0.951 0.157 0.394
M-8G-E	ω_L, -No.4, E	3-15-1	0.979 0.105 0.199	0.974 0.099 0.314	0.959 0.132 0.363
M-9G-E	ω_P, -No.4, E	3-19-1	0.946 0.574 0.594	0.941 0.226 0.475	0.925 0.227 0.475
M-10G-E	ω_L, E	2-11-1	0.910 0.173 0.322	0.931 0.259 0.509	0.888 0.339 0.582
M-11G-E	ω_P, E	2-7-1	0.810 2.174 1.066	0.838 0.585 0.765	0.917 0.281 0.529
M-12G-E	-No.4, E	2-15-1	0.851 1.777 1.125	0.814 0.647 0.805	0.878 0.359 0.599

The average values of ten runs of each ω_{opt} model are summarized in Table 5.15. The M-6W-E model is considered as the best ANN topology to estimate ω_{opt} with same considerations valid for γ_{dmax}. The predicted ω_{opt} values with respect to the actual values are shown in Figure 5.23. The connection weights and biases of M-6G-E and M-6W-E models are given in Table 5.16.

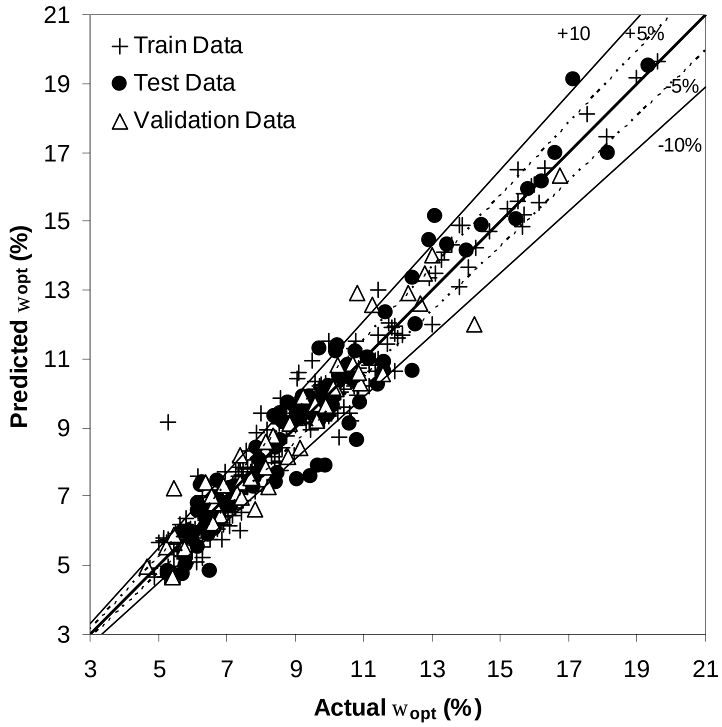

Figure 5.23 Agreement plot of M-6W-E prediction model

Table 5.15 Prediction results of the compaction energy ANN models for ω_{opt}

Model No.	Model Inputs	Best Topology	Statistical Features		
			Training Data	Testing Data	Validation Data
M-1W-E	ω_L,ω_P,-No.4, -No.200, E	5-17-1[d]	0.979[a] 0.529[b] 0.600[c]	0.963 0.643 0.800	0.961 0.545 0.738
M-2W-E	ω_L,ω_P, -No.4, TFR, E	5-19-1	0.979 0.379 0.445	0.963 0.653 0.808	0.959 0.556 0.745
M-3W-E	ω_L, -No.4, TFR, E	4-17-1	0.976 0.455 0.448	0.960 0.711 0.843	0.954 0.623 0.789
M-4W-E	ω_P, -No.4, TFR, E	4-19-1	0.979 0.402 0.530	0.963 0.660 0.811	0.958 0.593 0.769
M-5W-E	-No.4, TFR, E	3-19-1	0.974 0.592 0.639	0.961 0.706 0.838	0.953 0.637 0.798
M-6W-E	-No.4,-No.200, E	3-19-1	0.974 0.578 0.627	0.960 0.697 0.834	0.955 0.619 0.787
M-7W-E	ω_L, ω_P, E	3-9-1	0.954 0.626 0.737	0.953 0.812 0.900	0.946 0.751 0.864
M-8W-E	ω_L, -No.4, E	3-11-1	0.971 0.977 0.834	0.961 0.679 0.824	0.957 0.589 0.767
M-9W-E	ω_P, -No.4, E	3-21-1	0.922 4.070 1.400	0.892 1.798 1.337	0.893 1.443 1.199
M-10W-E	ω_L, E	2-5-1	0.934 0.912 0.858	0.962 0.681 0.825	0.910 1.186 1.089
M-11W-E	ω_P, E	2-11-1	0.801 13.668 2.502	0.804 3.134 1.770	0.884 1.529 1.236
M-12W-E	-No.4, E	2-5-1	0.763 12.644 2.822	0.697 4.582 2.141	0.799 2.526 1.589

Table 5.16 Weight and bias values of Proctor energy ANN models of M-6G-E and M-6W-E

Model No.	Hidden Neuron Number	Weight: Input neurons -No.4	Weight: Input neurons -No.200	Weight: Input neurons E	Weight: Output neuron g_{dmax} [a] w_{opt}	Bias: Hidden layer	Bias: Output layer
	1	-7.7140	12.3532	1.1118	0.4953	5.8534	1.2389
	2	10.5506	2.3314	-8.0332	2.0753	-10.3855	
	3	-12.5382	-2.5314	5.9083	-2.2999	10.1043	
	4	10.4388	0.9175	-4.2328	-3.1826	-8.8346	
	5	-6.5977	-5.2600	5.8644	0.5675	6.8814	
	6	13.4385	-5.4709	1.3883	-0.3768	-4.6777	
	7	-6.8318	3.9184	11.9265	-0.8369	-4.4551	
	8	-8.1315	13.0853	1.3128	0.1657	2.4181	
M-6G-E	9	-3.8547	12.0434	-7.3508	-0.4507	0.2223	
	10	3.0431	-10.5677	-7.5020	0.2797	8.1609	
	11	-0.4314	2.3335	14.6314	1.5777	-9.6053	
	12	-5.1818	-2.8737	-13.0326	0.9046	5.1173	
	13	4.2023	-12.9250	7.7072	0.5298	4.2968	
	14	6.4330	-14.4848	5.5635	-0.3044	2.8532	
	15	2.5731	-11.1722	12.1325	0.2156	4.1864	
	16	12.9506	9.4288	-7.8791	-0.2910	1.4959	
	17	-16.6020	-6.4004	0.1235	-0.5435	6.3609	
	1	-1.3235	11.7187	-1.7876	-1.7330	1.8271	0.5955
	2	-0.7718	-8.4153	-13.2215	1.0655	1.6066	
	3	-18.1338	-0.0626	8.8567	0.7108	12.2165	
	4	-9.3818	-10.4967	-6.1037	0.3468	19.6855	
	5	0.2742	-16.8783	0.1138	-0.7580	1.8785	
	6	-3.0718	8.7836	9.9413	-0.1400	-2.5097	
	7	12.6150	-4.3215	-8.7260	-0.3309	-1.1430	
	8	17.8211	7.2319	1.4307	0.0681	-13.1178	
	9	-4.8392	13.5242	4.6890	-0.2411	-6.5972	
M-6W-E	10	-7.3976	-8.9857	-8.3002	-0.1999	14.6225	
	11	15.1543	-14.9854	-4.3805	1.2784	3.7238	
	12	13.3122	-2.3180	6.4312	0.4267	-8.8262	
	13	11.1860	6.1545	-6.0985	0.5133	-8.0113	
	14	-12.7161	3.5669	10.3620	0.1609	-2.9813	
	15	-3.9260	-6.2825	13.3027	-0.7898	-7.4065	
	16	-0.9452	-10.8452	10.5390	-0.6962	5.3177	
	17	14.7658	-7.4894	-0.3161	3.7913	3.1401	
	18	10.1162	-8.5402	-9.8595	-3.2555	9.7057	
	19	4.3455	-12.9916	8.2369	-0.6919	6.5462	

[a] The output neuron of M-6G-E is γ_{dmax} and M-6W-E is ω_{opt}.

CHAPTER SIX
GENERALIZATION ABILITY OF THE DEVELOPED MODELS

6.1 Overview

Both MLR and ANN models presented in this thesis were developed using experimental test results acquired by the author. It was shown that all of the developed models could predict well both Standard and Modified Proctor compaction characteristics with acceptable error ranges for engineering purposes. The generalization ability of the developed models is discussed in this chapter.

6.1.1 Check of Suitability of Different Data Bases Using Self-Organizing Map

Soils of various compositions and geological origins demonstrate different engineering behavior. It is somehow essential to check if a data belonging to a certain data base is suitable for the developed MLR and ANN models. This may be achieved using the self-organizing map (SOM) technique (Haykin, 1994; Kutlu, 2010). SOM is a type of neural networks trained by unsupervised learning algorithms. SOM is used to visualize the high dimensional data in 2-D map grid. The result obtained through the SOM analysis is the set of weight vectors connecting the high dimensional input vector space and the output map grid. Once the training process is over, the winner SOM units are determined. Based on the winner selection, the weight vectors are updated. The distance between two map units is determined by means of their respective weight vectors. The Unified Distance Matrix (U-matrix) method computes the distance between weight vectors of adjacent map units and provides a good way for visualization of the SOM topology. In this study, the computed U-matrix is visualized using three images: colored image, gray-level image and the “Hill-Valley” landscape. The colored image is a hexagonal grid map scaled with different colors and gives information about the input patterns. In general, lighter color patches indicate location of data which are similar and has less distance. On the other hand, darker color patches indicate location of data having high distance. The gray-level image is used to visualize clusters of the data base. In the literature, the SOM results are also presented in a 3-D landscape. This is called as the “Hill-Valley” landscape visualization of the SOM where the heights of this display represent the distance between the neighbor units. This display has valleys where the map units are close to each other and hills where there are large distances between the adjacent map units. The hills indicate dissimilarities in the input data and height of the hills reveals the degree of dissimilarity of the data. SOM analysis was performed by means of a “SOM-Toolbox” written in MATLAB environment by Vesanto et al. (2000). In the SOM analysis, apart from the author’s experimental test results, results from the comparison data base have also been used. SOM structures were composed of hexagonal topology with 3000 (70x50) neurons. Two different SOM were constructed for visualization of Standard and Modified Proctor data bases. The cluster color codes and corresponding referred literatures used in U-matrix visualization are shown in Table 6.1.

Table 6.1 Cluster color code used in U-matrix visualization

Color	Reference
	Günaydın (2009)
	Sivrikaya (2008)
	Horpibulsuk et al. (2008a)
	Ölmez (2007)
	Sridharan & Nagaraj (2005)
	Engin (2003)
	Yesiller et al. (2000)
	Howell et al. (1997)
	Tinjum et al. (1997)
	Abu-Hassanein et al. (1996)
	Omotosho (1993)
	Al-Khafaji (1993)
	This study

A total number of 471 data (i.e. 271 data from the published literature and 200 data from author’s experimental test) were used to visualize Standard Proctor data base. The U-matrix images of Standard Proctor data are shown in Figure 6.1. The similarity of data is represented by various shades of blue color; conversely, the yellow and red colors indicate the dissimilarity of data. It can be seen that there is a big homogenous blue colored area which indicates the similarity of the data (Figure 6.1a). There is a separate cluster at the bottom right corner of Figure 6.1a. Also, there is a stack of dissimilar data at the upper right corner and in the middle left side of Figure 6.1a. The clusters of data base can be seen in Figure 6.1b. It is evident that all the referred literature data and the data of this study are separated into several clusters (Figure 6.1b). Although they are visualized in different clusters, the U-matrix representation means that these data have a high degree of similarity and it can be concluded that the developed MLR and ANNs models may be used to predict the referred literature data. In order to visualize the SOM map in detail, the hill-valley landscapes image of Standard Proctor data is graphed in Figure 6.1c. The dissimilar data are seen as hills whose color range from yellow to red (Figure 6.1c). The valleys represent similarity of the data.

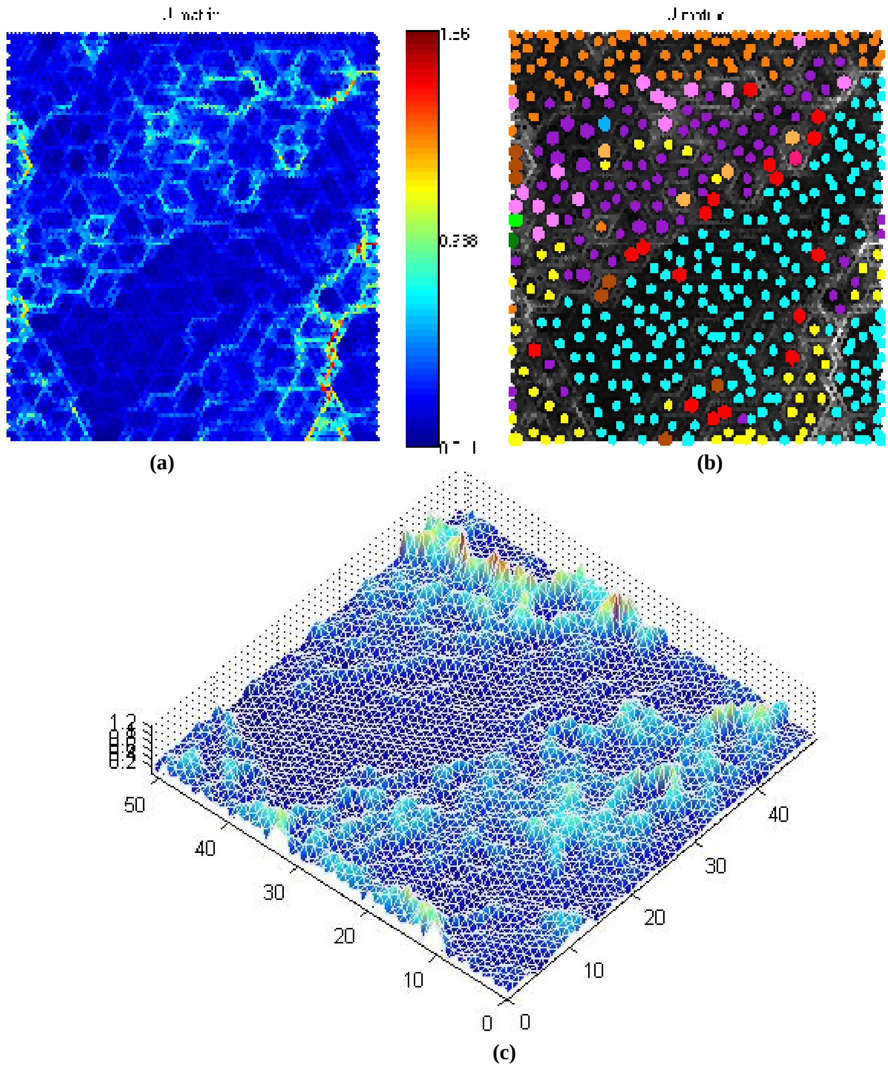

Figure 6.1 U-matrix representation of Standard Proctor SOM network a) colored image, b) gray-level image with colored clusters, c) 3D hill-valley landscape image

A total number of 243 data (i.e. 43 data from the published literature and 200 data from author's experimental test) were used to visualize Modified Proctor compaction. The U-matrix images of Modified Proctor data are shown in Figure 6.2. It is clear from Figure 6.2 that similar conclusions can be drawn for the Modified Proctor data.

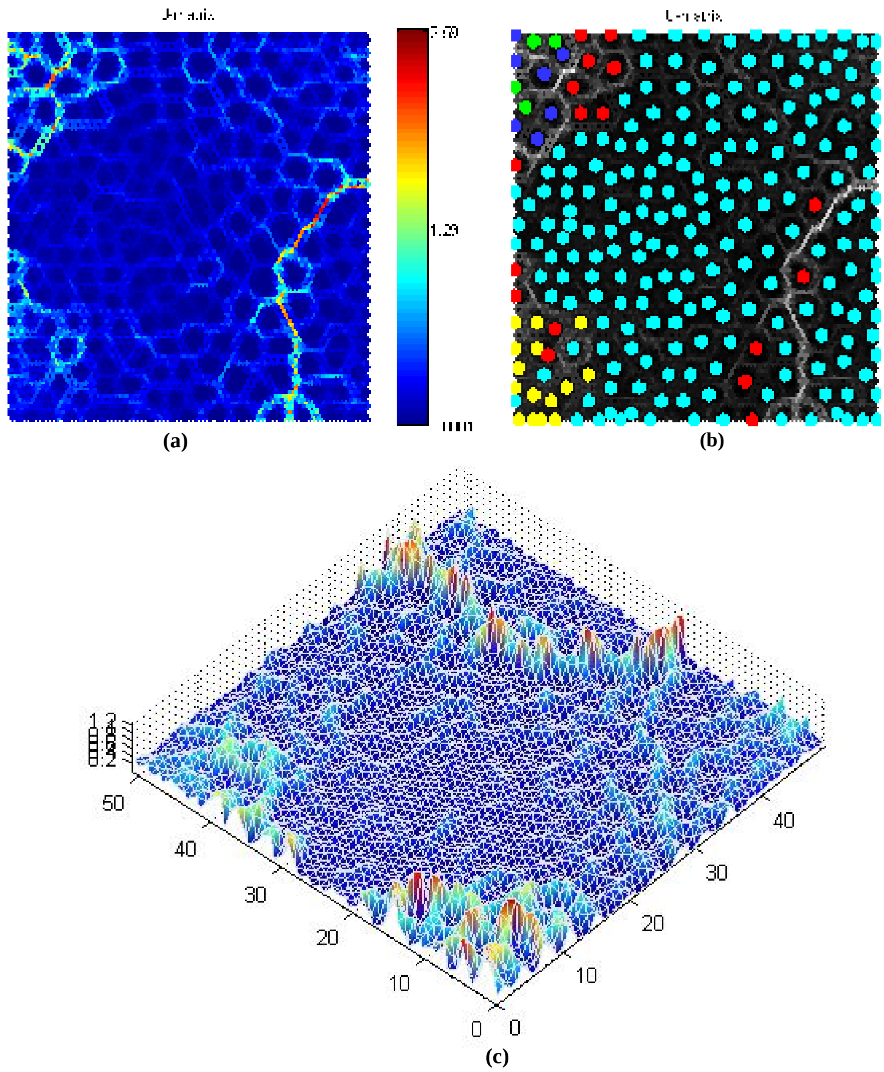

Figure 6.2 U-matrix representation of Modified Proctor SOM network a) colored image, b) gray-level image with colored clusters, c) 3D hill-valley landscape image

The data which were inspected as outlier by means of SOM analysis were removed from the comparison data base. Table 6.2 summarizes the compaction test results acquired from the literature. A total number of 271 Standard Proctor and 43

Modified Proctor compaction test results were used to check the generalization ability of the developed models.

Table 6.2 References of the comparison data base acquired from the published literature

Reference	Standard Proctor	Modified Proctor
Günaydın (2009)	89	-
Sivrikaya (2008)	17	-
Horpibulsuk et al. (2008a)	7	-
Ölmez (2007)	47	15
Sridharan & Nagaraj (2005)	1	-
Engin (2003)	17	17
Yesiller et al. (2000)	1	-
Tinjum et al. (1997)	1	4
Howell et al. (1997)	1	-
Abu-Hassanein et al. (1996)	7	7
Omotosho (1993)	4	-
Al-Khafaji (1993)	79	-
Σ	271	43

6.2 Generalization Ability of the Developed MLR Compaction Models

In order to predict the Standard Proctor compaction characteristics of the comparison data, Equation 5.2 is used for ω_{opt} and Equation 5.3 is used for γ_{dmax}. The predicted ω_{opt} and γ_{dmax} with respect to the actual values are plotted in Figure 6.3a and 6.3b, respectively. It is clear from Figure 6.3a that some of the predicted ω_{opt} are in good agreement with the actual values; however, there are some scattered predictions. There is a considerable scatter in γ_{dmax} values as shown Figure 6.3b. On the other hand, there are unevenly distributed γ_{dmax} values in Figure 6.3b. Particularly at higher values of γ_{dmax}, the model predicts γ_{dmax} higher than the actual value; conversely, the predicted γ_{dmax} values are smaller than the actual values at lower values of γ_{dmax} (Figure 6.3b).

Similarly, the Modified Proctor compaction characteristics of 43 data were calculated using Equation 5.4 for ω_{opt} and Equation 5.5 is used for γ_{dmax}. The scatter diagrams of the predicted and corresponding actual values of both ω_{opt} and γ_{dmax} are shown in Figure 6.4, respectively. The predicted ω_{opt} are in good agreement with the actual values, however, some scattered predictions are still present (Figure 6.4a). Also Figure 6.4a shows that Equation 5.5 generally under estimates ω_{opt}, particularly at small values of ω_{opt}. There is significant scatter in γ_{dmax} data (Figure 6.4b).

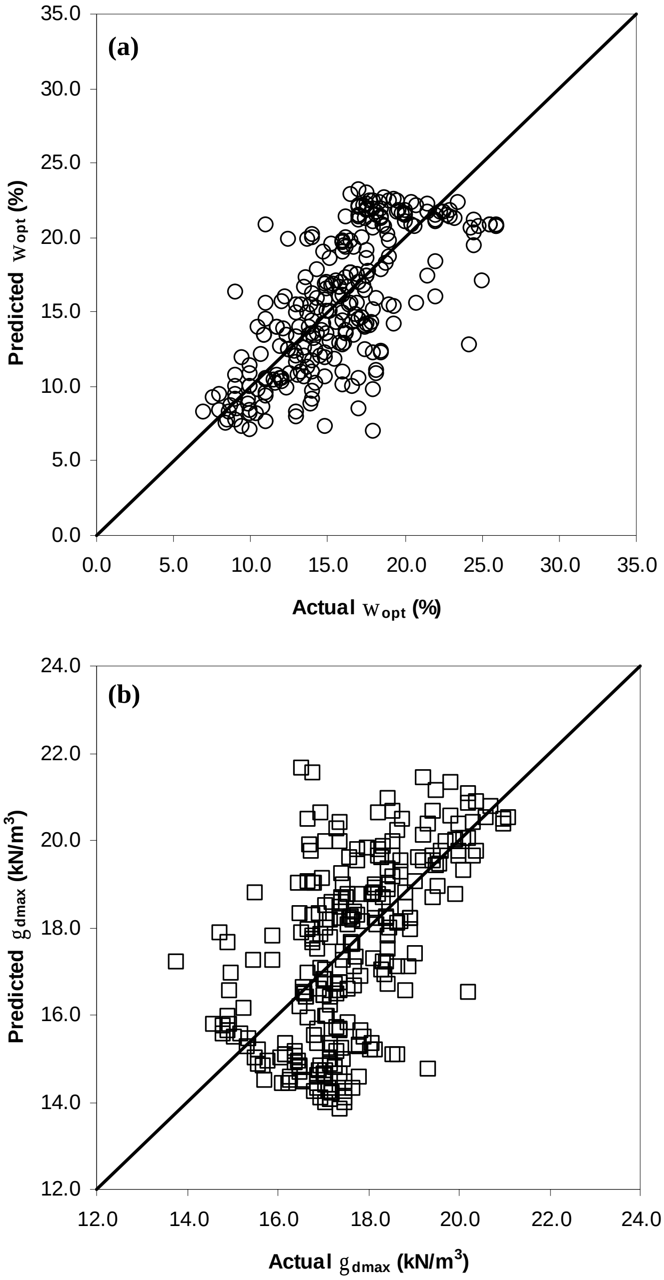

Figure 6.3 Scatter diagram of MLR models predictions for Standard Proctor (a) ω_{opt} and (b) γ_{dmax}

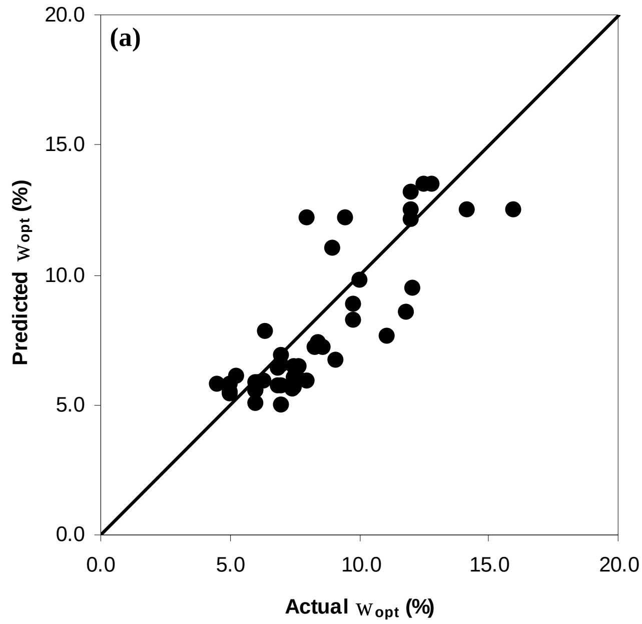

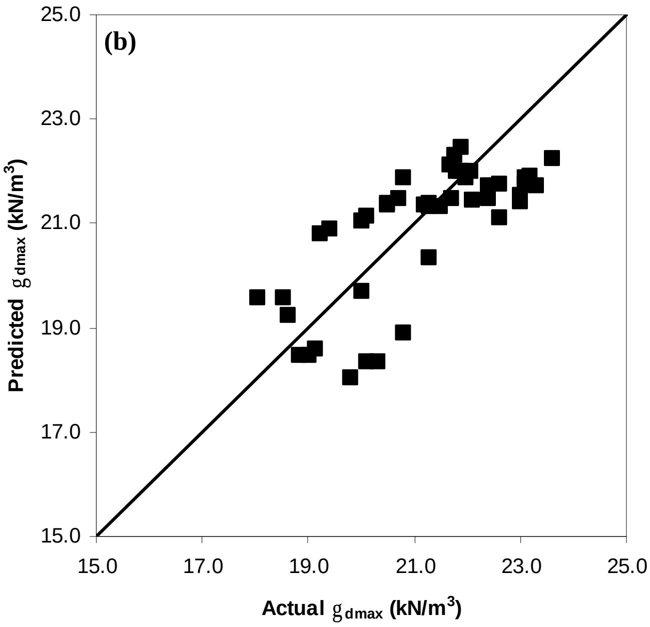

Figure 6.4 Scatter diagram of MLR models predictions for Modified Proctor (a) ω_{opt} and (b) γ_{dmax}

6.3 Generalization Ability of the Developed ANN Compaction Models

Generalization ability of the developed ANN models is checked in a similar manner. For this reason, M-2W-S and M-2G-S neural network models are used to predict the Standard Proctor compaction characteristics of the comparison data. It can be seen from Figure 6.5a that the predicted ω_{opt} values are lower than the actual values. There is a tendency to underestimate ω_{opt} (Figure 6.5a). A similar but reverse trend is also noticed for M-2G-S model (Figure 6.5b). It is evident that the predicted γ_{dmax} values are higher than the actual values as depicted in Figure 6.5b.

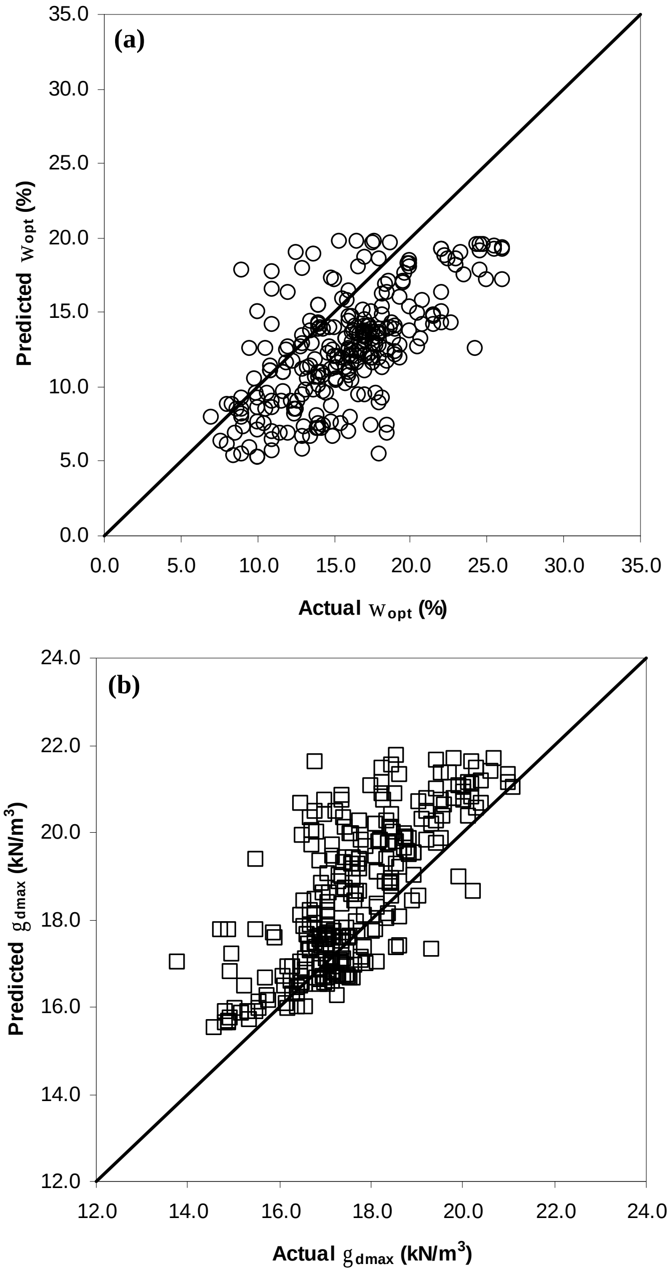

Figure 6.5 Scatter diagram of ANN models predictions for Standard Proctor (a) ω_{opt} and (b) γ_{dmax}

The M-11W-M and M-11G-M models were selected as the best ANN models to predict Modified Proctor characteristics in this thesis. The generalization ability of these models is checked against 43 data. The predicted ω_{opt} values are somehow lower than the actual ones as seen in Figure 6.6a. On the other hand, the predicted γ_{dmax} values are in a good fit with respect to the actual ones with errors acceptable for engineering purposes (Figure 6.6b).

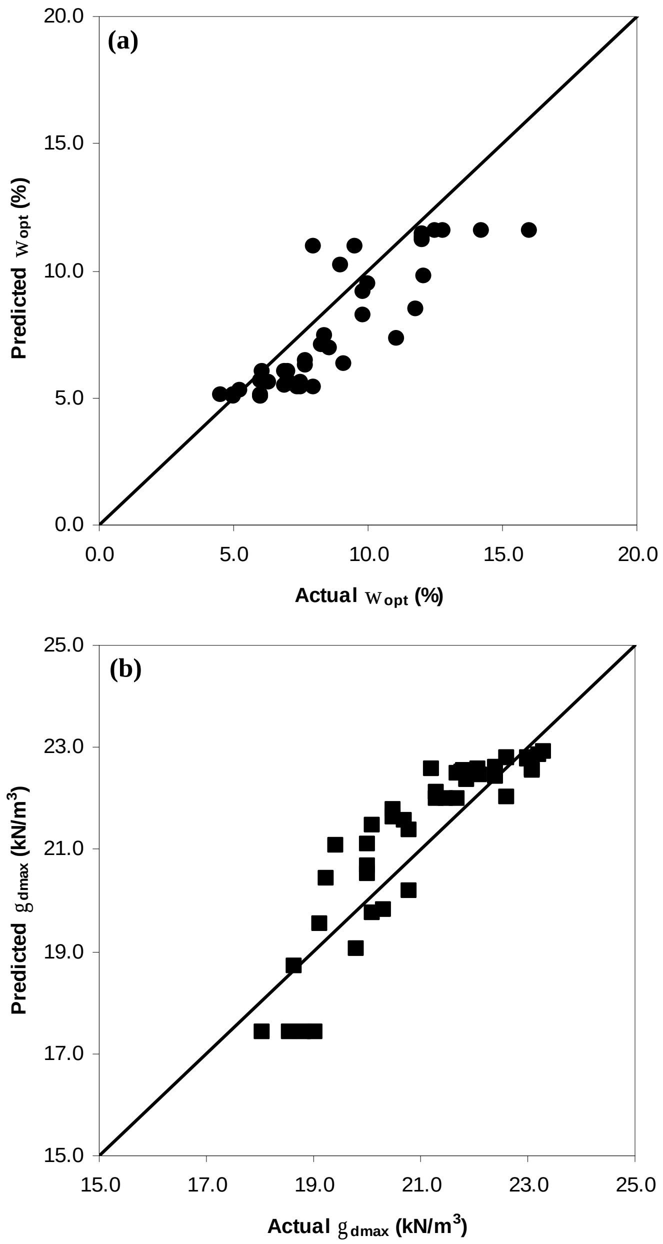

Figure 6.6 Scatter diagram of ANN models predictions for Modified Proctor (a) ω_{opt} and (b) γ_{dmax}

6.4 Discussion of Effect of Automatic Soil Compactor

Effect of the automatic soil compactor was investigated in Section 4.3.3. It is exposed that the difference between the compaction curves obtained using the automatic compactor and by hand is not very significant at Standard Proctor energy level with an exception of negligible increase in ω_{opt} when compacted by hand. However, the automatic compactor has a great effect on compaction curve at Modified Proctor energy level. The modified compaction curve of the automatic compactor moves upward and to the left of the modified compaction curve obtained by hand compaction. The automatic soil compactor makes the soil specimen denser. Hence the modified γ_{dmax} increases and ω_{opt} decreases when soil specimen is compacted by means of the automatic compactor. In addition to the study in Section 4.3.3, influence of the operator fault is also investigated by comparing compaction curves of Mix#195, which are obtained performing a whole compaction test by different operators (Figure 6.7).

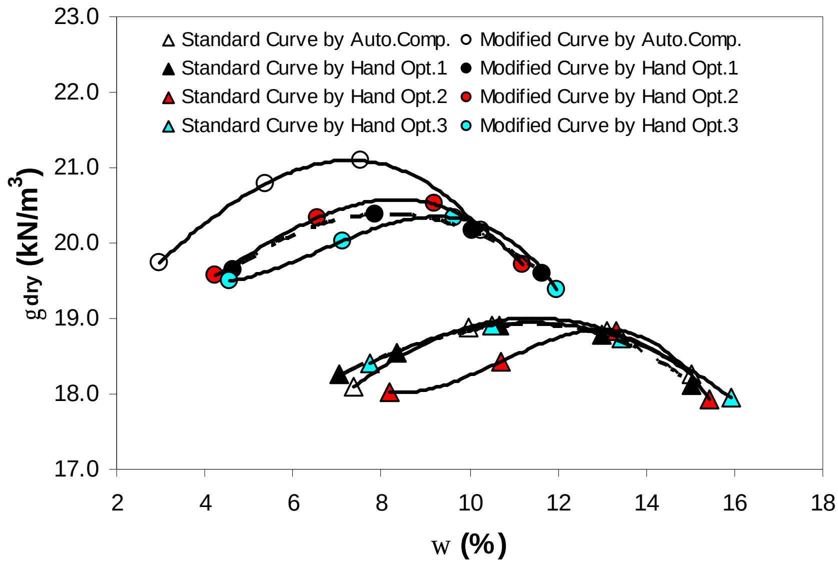

Figure 6.7 Difference between automatic soil compactor and hand operated compaction curves

The compaction test results shown in Figure 6.7 are summarized in Table 6.3. The results reveal that the automatic soil compactor averagely produces ω_{opt} 7.2% lower than that by hand and γ_{dmax} 0.5% larger at Standard Proctor compaction energy level.

Similarly, at Modified Proctor energy level, the automatic soil compactor averagely yields ω_{opt} 22.2% lower than it is obtained by hand and γ_{dmax} 3.5% larger.

Table 6.3 Results of hand operated compaction tests

Compaction Method	**Standard Proctor**		**Modified Proctor**	
	w_{opt} **(%)**	g_{dmax} **(kN/m^3)**	w_{opt} **(%)**	g_{dmax} **(kN/m^3)**
Auto. Soil Comp.*	11.36	18.98	7.04	21.19
Hand Operator-1	11.43	18.91	8.04	20.39
Hand Operator-2	12.92	18.84	8.52	20.54
Hand Operator-3	11.12	18.91	9.25	20.40

* Automatic Soil Compactor

The author of this study is aware that Engin (2003) obtained his compaction data by means of hand compaction equipment. Therefore, the error rate caused by automatic soil compactor could be best checked using his data. The predictions made using the data corrected with respect to the error rate is compared with those obtained using the uncorrected predictions. The comparative scatter diagrams are shown in Figure 6.8 to Figure 6.11. The scatter diagrams of MLR models at Standard Proctor energy level are displayed in Figure 6.8a and Figure 6.8b for ω_{opt} and γ_{dmax}, respectively. It can be seen that there is an improvement at ω_{opt} when the predicted values are corrected with respect to the error rate (Figure 6.8a). However, there is a slight improvement at γ_{dmax}, as shown in Figure 6.8b.

Similarly, the predicted values of Modified MLR models are corrected with the error rates and compared in Figure 6.9. Same trend is observed for compaction characteristics at Modified Proctor energy level. There is improvement in prediction accuracy for the modified ω_{opt} and for the modified γ_{dmax}, as shown in Figure 6.9a and Figure 6.9b, respectively.

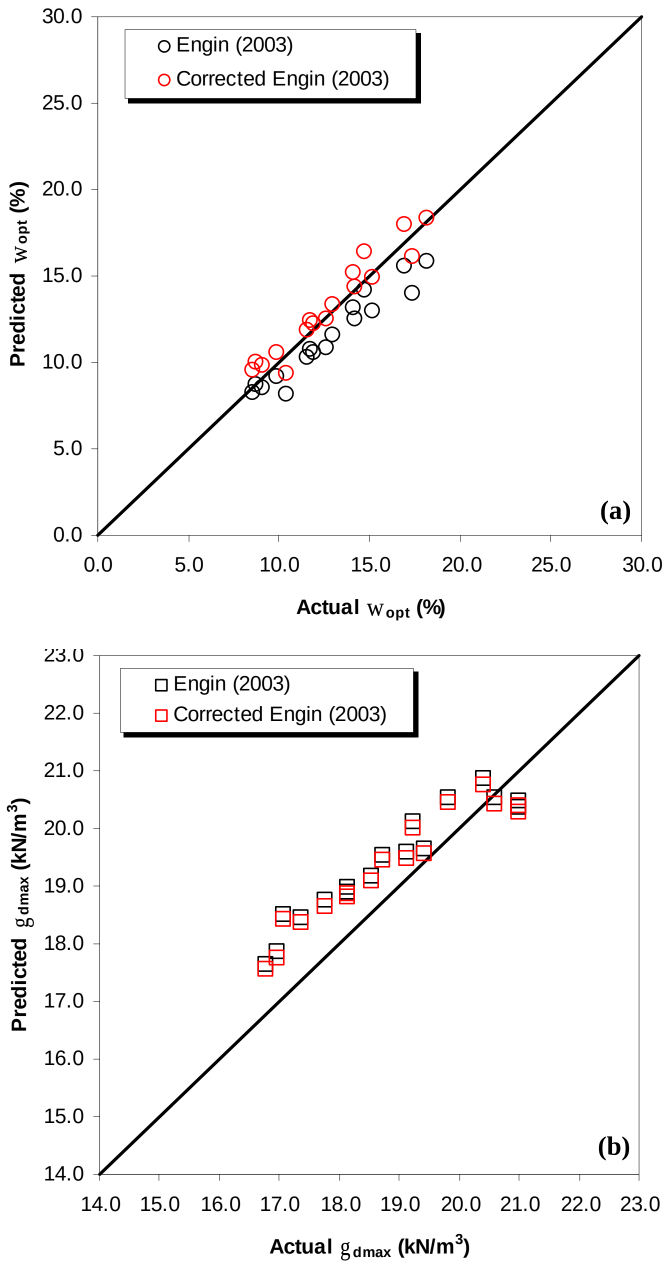

Figure 6.8 Comparative scatter diagrams of MLR models for (a) ω_{opt} and (b) γ_{dmax} at Standard Proctor energy

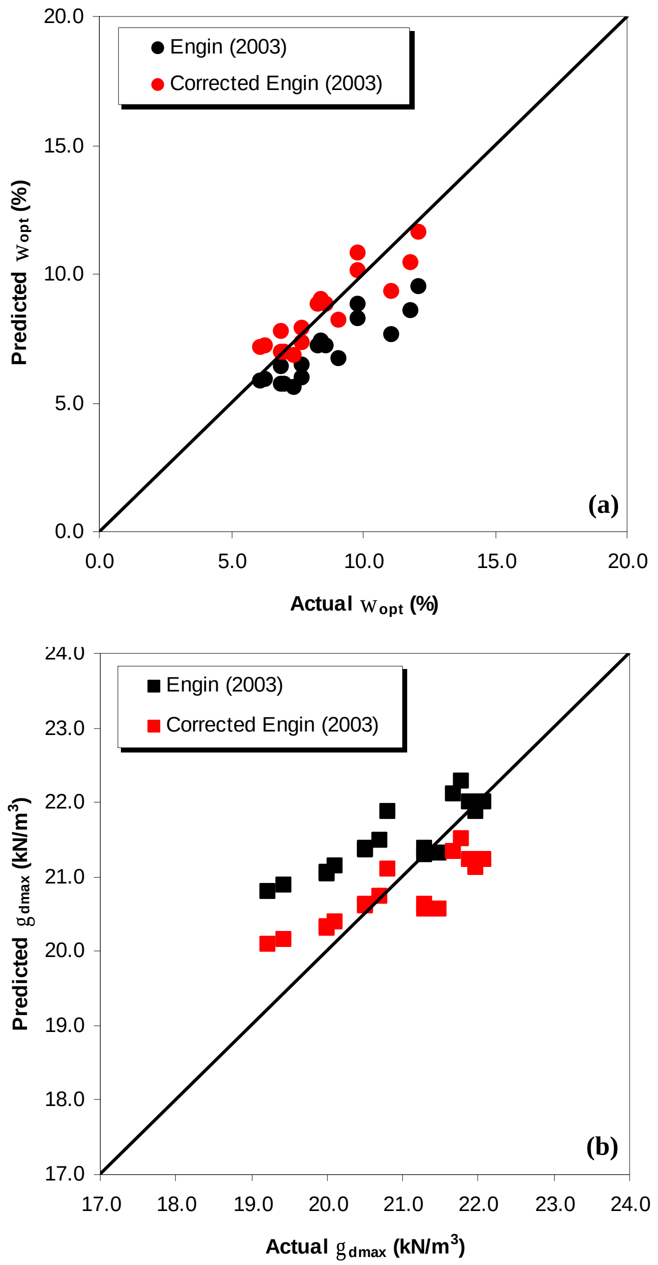

Figure 6.9 Comparative scatter diagrams of MLR models for (a) ω_{opt} and (b) γ_{dmax} at Modified Proctor energy

The influence of automatic soil compactor on developed ANN models is illustrated in Figure 6.10 and Figure 6.11. The predicted and the corrected ω_{opt} values of Engin's data at Standard Proctor energy level are presented in Figure 6.10a. The graph means that the corrected ω_{opt} values, which are arranged with the aforementioned error rate of 7.2%, are in good agreement with the actual values at

Standard Proctor energy level (Figure 6.10a). On the other hand, there is a light improvement for γ_{dmax} at Standard Proctor energy (Figure 6.10b).

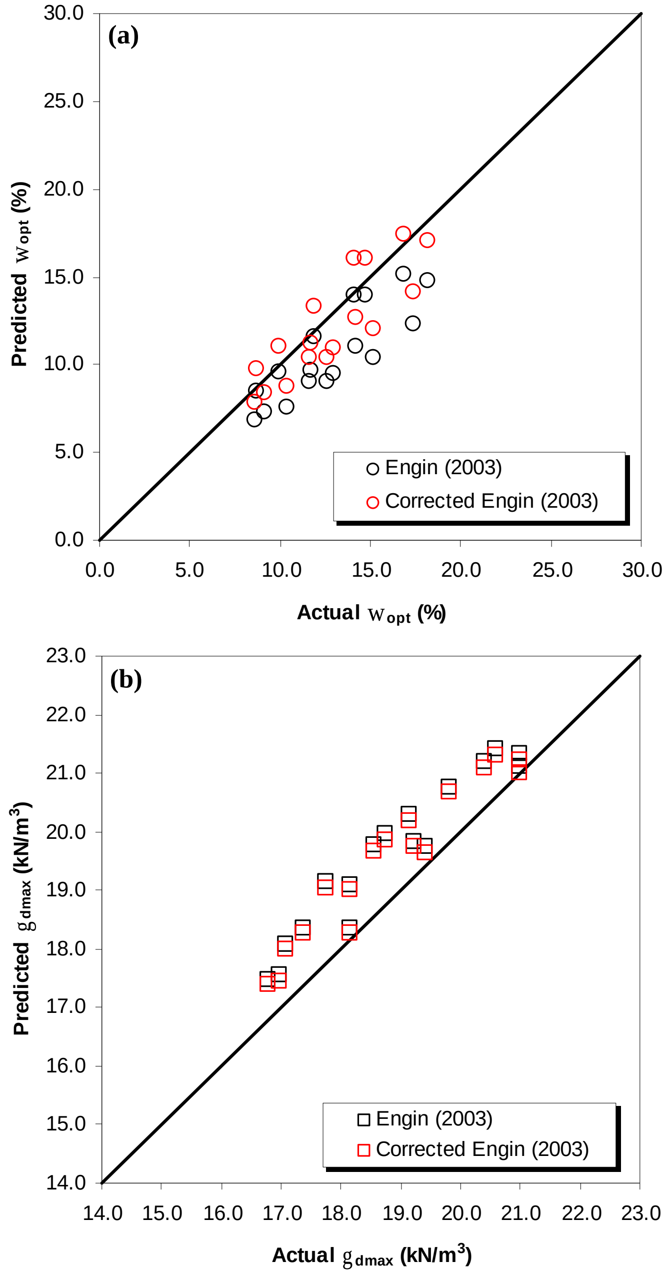

Figure 6.10 Comparative scatter diagrams of ANN models for (a) ω_{opt} and (b) γ_{dmax} at Standard Proctor energy

The comparative scatter diagrams of Modified Proctor ANN prediction models are shown in Figure 6.11. It is seen that corrected values of both ω_{opt} and γ_{dmax} are in good agreement with respect to the actual values.

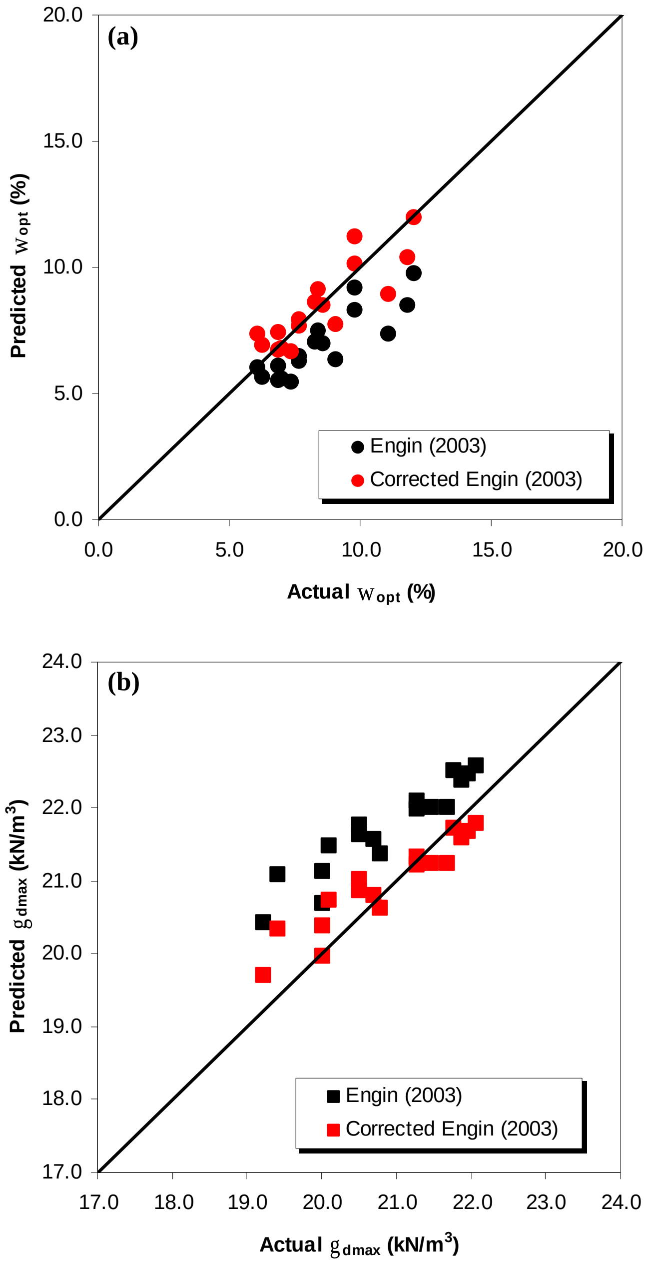

Figure 6.11 Comparative scatter diagrams of ANN models for (a) ω_{opt} and (b) γ_{dmax} at Modified Proctor energy

CHAPTER SEVEN
CONCLUSIONS AND RECOMMENDATOINS

7.1 Conclusions

The overall objective of this research is to predict the compaction characteristics of fill materials using contemporary data mining tools. Therefore, multiple linear regression (MLR) and artificial neural networks (ANN) models which use the basic soil parameters (i.e. liquid and plastic limit, passing percentages of No.4 and No.200 sieves, and transition fine content ratio) were developed to estimate Standard and Modified Proctor compaction characteristics of coarse and fine-grained (c-ϕ) soils. Emphasis was given to ANN methodology since prediction models developed with this technique could better express nonlinear nature of the compaction data. The ANN prediction models work well within the ranges of data used in their development. It should be mentioned that these ranges do not cover high plastic bentonite clays, or tuffa, or deltaic soil types. If it is attempted to predict compaction characteristics of aforementioned soil types, the prediction equations reviewed in the literature may be used. Based on the findings of this thesis, the following conclusions can be drawn:

7.1.1 Compaction Characteristics

- The soil mixtures were compacted by means of an automatic soil compactor machine in this study. In order to investigate effect of the automatic soil compactor, the predetermined soil mixtures were also compacted by hand. The results show that the automatic soil compactor had a considerable effect on compaction curve obtained under Modified Proctor energy level. The modified compaction curve of the tests made using automatic compactor moves to left-upward of the modified compaction curve determined by hand. It is revealed that the automatic soil compactor makes the soil mixtures denser than those compacted by hand. On the other hand, there is no considerable difference between the compaction curves obtained using the automatic compactor and by hand at Standard Proctor energy level.

- As expected, the compaction characteristics of the soil mixtures used in this research change depending on fine content (FC). It is well known that an increase in FC of soils usually results in a decrease in γ_{dmax} causing a corresponding increase of ω_{opt}. However, it is found that γ_{dmax} increases until FC becomes 12%. Beyond this transition value γ_{dmax} decreases steadily as FC increases. A similar but reverse trend is also noticed for the relationship between ω_{opt} and FC.

- In order to better observe transitional behavior of the soil mixtures, two sets of soil samples of which compaction results fall nearby the transition zone were prepared and scanned by means of computed tomography (CT) technique. Although the transition zone can not visually selected in the CT images, the edge to edge contact between gravel particles is more pronounced up to the transition fine content (12%). Beyond this point, the clay particles fill the voids and contribute to the internal contact force chain, and also, start to dominate the compaction behavior of the soil samples. The transitional behavior was also supported by the computed total gravel area of center slice of each CT images. It is found that there is a similar trend with transitional behavior of soil mixtures. The total gravel area of each slice increases to a threshold value and then it starts to decrease.

7.1.2 Multiple Linear Regression Analysis

- Comparison of the existent literature prediction equations shows that they cannot predict well the author's experimental compaction test results with an exception of the Engin(2003)'s prediction equations.
- It is well known that liquid and plastics limits are two important parameters to predict compaction characteristics of fine-grained soil,

however they are not sufficient alone to predict not only coarse-grained soils but also fine-grained soils containing gravel particles.

- It is inferred from the step wise regression modeling that liquid limit, plastic limit and percentage of soils passing through No.200 sieve are three important soil parameters used to predict the compaction characteristics of coarse and fine-grained soils under Standard and Modified Proctor energy levels.

- Compared to the ANN models, the MLR models are not as successful as the ANN models. However, the MLR models estimate the compaction characteristics of coarse and fine-grained soils with acceptable error ranges.

7.1.3 Artificial Neural Networks Analysis

- Although the artificial neural networks modeling technique has undeniable advantage of exploring non-linear relationship of the problem at hand, it is time consuming and requires many iterations to determine the most appropriate network architecture. There is not a clearly defined method for determination of hidden layer number and neuron numbers in the hidden layers. For this reason, the trial-and-error procedure is used to find the best ANN topology.

- The ANNs database is generally separated into training and testing data subsets. The training subset is used to adjust the connection weights of the network. After finalization of the training process, generalization ability of the trained network is evaluated with the testing subset. At this point, a phenomenon called as “overfitting” may exist in the network. An over trained network will memorize the training data causing a marked reduction in generalization ability of the network. Overfitting may be avoided using the cross-validation technique, where a new data subset named as “validation subset” is used. Validation subset controls the performance of the network at each step of training process so that training is stopped early if it attempts to overfit the training data.

- The training subset should cover all pattern ranges in the database. Similarly, the validation subset should be representative of the training subset since it affects the training process by means of its early stopping. Also, the range of testing data should be covered by the training subset because of obtaining perfect predictions. In order not to encounter this problem, the data clustering analysis is performed in this study. It is found that data clustering and division methodologies have a considerable effect on performance of developed networks. In order not to overfit the network, the data base should be divided into three subsets; training, testing and validation. In order to improve the prediction accuracy of ANN models, a clustering method should be used to separate the data. It is found that the best data division methodology is separation of the data according to their membership grades.

- Using different scales of input variables sometimes causes insufficiently converged networks. In order to build the ANN prediction models which are insensitive to units, all input variables and target(s) are normalized in this study. Input variables should be normalized in order to build ANN models which are insensitive to units. Additionally, target variables may be normalized when it is necessary.

- The ANN models predict the compaction characteristics better than the MLR models. In this context, it can be said that the ANN models serve as a more reliable predictive tool for estimating compaction characteristics of data base including both coarse and fine-grained soils.

- Purpose of the developed ANN models is not to invalidate the need for performing whole laboratory compaction test; however, they give reliable predictions about compaction characteristics where there is a lack of time and economical limitations.

7.2 Recommendations

This study confirms that neural networks could be an acceptable alternative instead of performing a complete compaction test. However, several recommendations are offered which will increase the performance of models. Also, some aspects are suggested for further experimental studies as following;

- The developed MLR and ANN models should only be used to predict the compaction characteristics within the input ranges of their development: ω_L (%) = 24.8 - 58.3, ω_P (%) = 15.4 - 26.6, -No.4 (%) = 10.8 - 99.8, -No.200 (%) = 1.6 - 81.6 and TFR = 0.13 - 6.80.

- A transition zone is observed in the vicinity of 12% fine content (FC) in this study. Between 5 and 12% FC, γ_{dmax} increases and above 12% FC it decreases. The trend is reverse for ω_{opt}. This transitional behavior needs to be investigated for various types of soils.

- CT images are used to visualize the transitional behavior. Gravel particles are obviously seen, however, the precision of CT machine is not adequate for visualization of sand and clay particles. Eventually, CT imaging technique will be used as nondestructive technique in geotechnical engineering.

- The differences between manually compacted soils and automatically compacted soils are demonstrated in this study. However, it is suggested that these differences should be determined for various types of soils under different energy levels.

REFERENCES

Abdel-Rahman, A. H. (2008). Predicting compaction of cohesionless soils using ANN. *Ground Improvement, 161*, 3-8, Doi: 10.1680/grim.2008.161.1.3.

Abu-Hassanein, Z.S., Benson,C.H. & Blotz, L.R. (1996). Electrical resistivity of compacted clays. *J. of Geotech. Eng., 122(5)*, 397-406.

Adeli, H. (2001). Neural networks in civil engineering: 1989-2000. *Computer-Aided Civil and Infrastructure Eng., 16*, 126-142.

Al-Khafaji, A. N. (1987). A simple approach to the estimation of soil compaction parameters. *Quarterly Journal of Engineering Geology and Hydrogeology, 20(1),* 15-30.

Arvelo Guerrero, A. M. (2004). Effects of the soil properties on the maximum dry density obtained from the standard proctor test. Master’s thesis, University of Central Florida. Orlando, Florida.

ASTM D 422-63 (1999). Standard test method for particle-size analysis of soils. *Annual Book of ASTM Standards*. American Society for Testing and Materials, Vol 04.08, Philadelphia, USA.

ASTM D 698 (1999). Standard test method for laboratory compaction characteristics of soil using standard effort. *Annual Book of ASTM Standards*. American Society for Testing and Materials, Vol 04.08, Philadelphia, USA.

ASTM D 854-02 (1999). Standard test method for specific gravity of soil solids by water pycnometer. *Annual Book of ASTM Standards*. American Society for Testing and Materials, Vol 04.08, Philadelphia, USA.

ASTM D 1557 (1999). Standard test method for laboratory compaction characteristics of soil using modified effort. *Annual Book of ASTM Standards*. American Society for Testing and Materials, Vol 04.08, Philadelphia, USA.

ASTM D 4318-98 (1999). Standard test method for liquid limit, plastic limit and plasticity index of soils. *Annual Book of ASTM Standards*. American Society for Testing and Materials, Vol 04.08, Philadelphia, USA.

Ashayeri, I. & Yasrebi, S. (2009). Free-swell and swelling pressure of unsaturated compacted clays; Experiments and neural networks modeling. *Geotech.Geol.Eng., 27(1)*, 137-153, DOI 10.1007/s10706-008-9219-y.

Basheer I.A. (2001). Empirical modeling of the compaction curve of cohesive soils. *Can.Geotech. J., 38*, 29-45.

Bezdek, J. C. (1981). *Pattern recognition with fuzzy objective function algorithms.* Plenum Press, New York.

Blotz, L. R., Benson, C. H., & Boutwell, G. P. (1998). Estimating optimum water content and maximum dry unit weight for compacted clays. *Journal of Geotechnical and Geoenvironmental, 124(9)*, 907-912.

Bowden, G.J., Maier, H.R. & Dandy, G.C. (2002). Optimal division of data for neural network models in water resources applications. *Water Resour. Res., 38(2)*, 1-11.

BS 1377-2 (1990). Methods of test for soils for civil engineering purposes. Classification test. *BSI, 2*, London.

Budayan, C., Dikmen, I. & Birgonul, M.T. (2009). Comparing the performance of traditional cluster analysis, self-organizing maps and fuzzy C-means method for strategic grouping. *Expert Systems with Applications, 36*, 11772-11781.

Cetin, H., Fener, M., Soylemez, M. & Gunaydın, O. (2007). Soil structure changes during compaction of a cohesive soil. *Engineering Geology, 92*, 38-48.

Chan, W.T., Chow, Y.K. & Liu, L.F. (1995). Neural networks: An alternative to pile driving formulas. *Computers and Geotechnics, 17*, 135-156.

Das, S. K. & Basudhar P. K. (2009). Utilization of self-organizing map and fuzzy clustering for site characterization using piezocone data. *Comp. and Geotech., 36*, 241-248.

Dulyakarn, P. & Rangsanseri, Y. (2001). Fuzzy c-means clustering using spatial information with application to remote sensing. 22nd Asian Conference on Remote Sensing, 5-9 November, Singapore.

Engin, H. (2003). A laboratory investigation on the correlations of standard and modified compaction test values. Master's thesis, Dokuz Eylul University.

Flood, I. (2006). Next generation artificial neural networks for civil engineering. *J. of Computing in Civil Eng., 20(5)*, pp.305-307.

Garga, V.K. & Madureira, C.J. (1985). Compaction characteristics of river terrace gravel. *J. Geotech. Eng. ASCE, 111(8)*, 987-1007.

Goktepe, A.B. & Sezer, S.A. (2005). Soil clustering by fuzzy c-means algorithm. *Advances in Engineering Software, 36*, 691-698.

Gunaydin, O. (2009). Estimation of soil compaction parameters by using statistical analyses and artificial neural networks. *Environ.Geology, 57*, 203-215, DOI 10.1007/s00254-008-1300-6.

Gurtug, Y. & Sridharan, A. (2002). Prediction of compaction characteristics of fine-grained soils. *Geotechnique*, *52(10),* 761-763.

Gurtug, Y. & Sridharan, A. (2004). Compaction behaviour and prediction of its characteristics of fine grained soils with particular references to compaction energy. *Soil and Foundations, 44(5),* 27-36.

Hagan, M. T., Demuth, H. B. & Beale, M. (1996). *Neural Network Design.* DWS Publishing Company.

Ham, F. M. & Kostanic, I. (2001). *Principles of Neurocomputing for Science & Engineering.* McGraw-Hill Book Co, Singapore.

Hausmann, M. R. (1990). *Engineering Principals of Ground Modifcation*. McGraw-Hill Book Co.

Haykin, S. (1994). *Neural Networks A Comprehensive Foundation.* New Jersey: Prentice-Hall, Inc.

Hilf, J.W. (1956). An investigation of pore water pressures in compacted cohesive soils. *Technical Memorandum 654, U.S. Dep.of the Interior, Bureau of Reclamation, Denver, Colorado.*

Hogentogler, C. A. (1936). Essentials of soil compaction. *Procc. Highway research Board, Nat.Res.Council, Washington, D.C. 309-316.*

Holtz, R.D., & Kovacs, W.D. (1981). *An Introduction to Geotechnical Engineering*. New Jersey: Prentice-Hall, Inc.

Hortibulsuk, S., Katkan, W. & Apichatvullop, A. (2008). An approach for assessment of compaction curves of fine grained soils at various energies using a one point test. *Soils and Foundations, 48(1)*, 115-125.

Howell, J.L., Shackelford, C.D., Amer, N.H., & Stern, R.T. (1997). Compaction of sand-processed clay soil mixtures. *Geotech. Test. J., 20(4),* 443-458.

Joslin, J., G. (1959). Ohio's Typical Moisture-Density Curves. *ASTM STP239,* pp.111-118.

Juang, C.H. & Chen, C.J. (1999). CPT-based liquefaction evaluation using artificial neural networks. *Computer-Aided Civil and Infrastructure Eng., 14 (3),* 221-229.

Juang, C.H., Ni, S.H. & Lu, P.C. (1999). Training artificial neural networks with the aid of fuzzy sets. *Computer-Aided Civil and Infrastructure Eng., 14 (2),* 407-415.

Kiefa, M.A.A (1998). General regression neural networks for driven piles in cohesionless soils. *Geotech. and Geoenvir. Eng., 124 (2)*, 1177-1185.

Kocjancic, R., & Zupan, J. (2000). Modeling of the river flowrate: the influence of the training set selection. *Chemom. Intell. Lab. Syst., 54*, 21-34.

Korfiatis, G., P., & Manikopoulos, C., N. (1982). Correlation of maximum dry density and grain size. *J. of the Geotech. Eng. Division, Proc. of the ASCE, 108 (GT9),* 1171-1176.

Kutlu, Y. (2010). Multi-stage classification of abnormal patterns in EEG and ECG using model-free methods. Ph.D thesis, Dokuz Eylül Universty.

Lambe, T.W. (1958). The engineering behavior of compacted clay. *J. Soil Mech. and Found. Div. ASCE, 84, (SM 2),* Paper No. 1655, 1–34.

Lee, I.M. & Lee, J.H. (1996). Prediction of pile bearing capacity using artificial neural networks. *Computers and Geotechnics, 18 (3)*, 189-200.

MatLab (2009). The language of technical learning. Matworks, Version. R2009b.

Monkul, M. M., & Özden, G. (2007). Compressional behavior clayey sand and transition fines content. *Eng. Geology., 89*, 195-205.

Montgomery, D. C. & Runger, G. C. (2007). *Applied Statistics and Probablity for Engineers (4th ed.)*. John Wiley & Sons, Inc.

Nagaraj, T.S., Lutenegger, A.J., Pandian, N.S. & Manoj, M. (2006). Rapid estimation of compaction parameters for field control. *Geotechnical Testing J., 29 (6)*, 497-506.

Najjar, Y.M. & Basheer, I.A. (1996). Utilizing computational neural networks for evaluating the permeability of compacted clay liners. *Geotech. and Geological Eng., 14*, 193-212.

Najjar, Y.M., Basheer, I.A. & Naouss, W.A. (1996). On the identification of compaction characteristics by neuronets. *Comp. and Geotechnics, 18 (3),* 167-187.

Ölmez, A. (2007). Determination of compaction parameters by means of regression approaches. Master's thesis, Niğde Universty.

Olson, R.E. (1963). Effective stres theory of soil compaction. *J. Soil Mech. and Found. Div., ASCE, 89 (SM2), 27-45*

Omar, M., Shanableh, A., Basma, A. & Barakat, S. (2003). Compaction characteristics of granular soils in United Arab Emirates. *Geotech & Geological Eng., 21,* 283-295.

Omotosho, P.O. (1993). Multi-cyclic influence on standard laboratory compaction of residual soils. *Eng.Geology, 36,* 109-115.

Ören, A. H. (2007). Engineering investigation of zeolite-bentonite mixtures for landfill liner applications. Ph.D thesis, Dokuz Eylül Universty.

Pandian, N.S., Nagaraj, T.S., & Manoj, M. (1997). Re-Examination of compaction characteristics of fine-grained soils. *Geotecnique, 47 (2)*, 363-366.

Pradeep, U., Kurup, M. & Nitin, K.D. (2002). Neural networks for profiling stress history of clays from PCPT data. *J. of Geotech. And Geoenv., 128,* 7,569.

Proctor, R.R., (1933). Fundamental Principles of Compaction. *Eng. News-Rec., 111 (9-10)*, 12-13.

Shahin, M.A., Jaksa, M.B. & Maier, H.R. (2001). Artificial neural network applications in geotechnical engineering. *Australian Geomechanics*, *36 (1),* 49-62.

Shahin, M.A., Maier, H.R. & Jaksa, M.B. (2002). Predicting settlement of shallow foundations using neural networks. *J. of Geotech. And Geoenv. Eng., 128 (9),* 785.

Shahin, M.A., Maier, H.R. & Jaksa, M.B. (2004). Data division for developing neural networks applied to geotechnical engineering. *J.of Computing in Civil Eng., 18 (2),* 105-114.

Shahin, M.A., Jaksa, M.B. & Maier, H.R. (2009). Recent advances and future challenges for artificial neural systems in geotechnical engineering applications. *Advances in Artificial Neural Systems, 2009(308239),*9, doi:10.1155/2009/308239

Shi, J. J. (2002). Clustering technique for evaluating and validating neural network perfromance. *J. of Computing in Civil Eng. , ASCE, 16(2),* 152-184.

Sinha, S.K. & Wang, M.C. (2008). Artificial neural network prediction models for soil compaction and permeability. *Geotech.Geol.Eng., 26,* 47-64.

Sivrikaya, A., Togrol, E., & Kayadelen, C. (2008). Estimating compaction behavior of fine-grained soils based on compaction energy. *Canadian Geotech. J.*, *45*, 877-887.

Sivrikaya, A. (2008). Models of compacted fine-grained soils used as mineral liner for solid waste. *Environ.Geol.*, *53*, 1585-1595.

Sivrikaya, A. & Soycan, T. Y. (2010). Estimation of compaction parameters of fine-grained soils in terms of compaction energy using artificial neural networks. *Int. J. Numer. Anal. Meth. Geomech.,* DOI: 10.1002/nag.981.

Sridharan, A., & Nagaraj, H.B. (2005). Plastic limit and compaction characteristics of fine-grained soils. *Ground Improvement, 9(1),* 17-22.

Thevanayagam, S. (1998). Effect of fines on confining stress on undrained shear strength of silty sands. *Journal of Geotechnical and Geoenvironmental Engineering, ASCE, 124(6),* pp. 479-491

Thevanayagam, S. (2007a). Intergrain contant density indices for granular mixes – i: framework. *Earthquake Engineering and Engineering Vibration, 6(2)*, 123-134.

Thevanayagam, S. (2007b). Intergrain contant density indices for granular mixes – ii: liquefaction resistance. *Earthquake Engineering and Engineering Vibration, 6(2)*, 135-146.

Tinjum, J.M., Benson, C.H., and Blotz, L.R. 1997. Soil water characteristic curves for compacted clays. *J. Geotech. & Geoenviron. Engrg.,* ASCE, *123(11),* 1060–1069.

Toll, D.G. (1996). Artificial intelligence applications in geotechnical engineering. *Electronic J. of Geotechnical Eng.,* Vol. 1, http://www.ejge.com/1996/JourTOC1.htm.

Vesanto, J., Himberg, J., Alhoniemi, E. and Parhankangas, J. (2000). SOM Toolbax for Matlab 5. SOM Toolbox Team, Helsinki Univ. of Technology, FIN-02015 HUT, Finland. http://www.cis.hut.fi/projects/somtoolbox/

Wang, M.C. & Huang, C.C. (1984). Soil compaction and permeability prediction models. *Journal of Environmental Eng., 110(6),* 1063-1083.

Wang, H.B., Xu, W.Y. & Xu, R.C. (2005). Slope stability evaluation using back propagation neural networks. *Eng.Geology, 80,* 302-315.

Wang, K., Wang, B. & Peng, L. (2009). CVAP: Validation for cluster analyses. *Data Science Journal, 8,* 88-93.

Yesiller, N., Miller, C.J., Inci, G., & Yaldo, K. (2000). Desiccation and cracking of three compacted landfill liner soils. *Eng.Geology,* 57, 105-121.